

Development of Electrochemical Biosensors for Clinical Analysis

Dissertation zur Erlangung des Doktorgrades der Naturwissenschaften

(Dr. rer. nat.)

an der Fakultät Chemie und Pharmazie

der Universität Regensburg

Deutschland



vorgelegt von

Franziska Beck

aus Landshut

im Jahr **2022**

Development of Electrochemical Biosensors for Clinical Analysis

Dissertation zur Erlangung des Doktorgrades der Naturwissenschaften

(Dr. rer. nat.)

an der Fakultät Chemie und Pharmazie

der Universität Regensburg

Deutschland



vorgelegt von

Franziska Beck

aus Landshut

im Jahr **2022**

Die vorliegende Dissertation entstand in der Zeit von November 2018 bis Mai 2022 am Institut für Analytische Chemie, Chemo- und Biosensorik der Universität Regensburg.

Die Arbeit wurde angeleitet von Prof. Dr. Antje J. Bäumner.

Promotionsgesuch eingereicht am: 31.05.2022

Kolloquiumstermin: 25.07.2022

Prüfungsausschuss

Vorsitzender: Prof. Dr. Oliver Tepner

Erstgutachterin: Prof. Dr. Antje J. Bäumner

Zweitgutachter: Prof. Dr. Axel Dürkop

Drittprüferin: Prof. Dr. Miriam Breunig

Danksagung

Zuerst würde ich mich gern bei **Prof. Dr. Antje J. Bäumner** bedanken für die Möglichkeit an diesem interessanten Thema zu forschen, ihre kontinuierliche Unterstützung, egal ob forschungsbezogen oder nicht, ihre vielen guten Ideen und unerschütterliche positive Energie, die sogar das ein oder andere Mal auf mich übergesprungen ist. Danke Antje, für viele harmonische, schöne, aber auch produktive und lehrreiche Jahre.

Natürlich will ich mich auch bei **Dr. Carina Horn** und **Roche Diagnostics** für die finanzielle und nicht-finanzielle Unterstützung während meiner ganzen Arbeit bedanken. Auch **Dan Nguyen-Luong**, der bei allen Roche-bezogenen, organisatorischen Problemen mein Ansprechpartner war, möchte ich vielmals danken, dass er mir immer bereitwillig weitergeholfen hat. Danke Carina und Dan, für die angenehme Zusammenarbeit.

Ich möchte mich auch herzlich bei **Prof. Dr. Axel Dürkop** bedanken für die Übernahme der Rolle des Zweitgutachters, **Prof. Dr. Miriam Breunig** für die Übernahme der Rolle der Drittprüferin und **Prof. Dr. Oliver Tepner** als Vorsitzenden der Prüfungskommission. Nochmals vielen Dank auch für die Flexibilität bei der Terminfindung.

Außerdem danke ich **Vanessa Tomanek** für ihre Unterstützung mit dem Erstellen herrlicher Graphiken und Schemata, die bei Weitem professioneller aussehen, als alles, was ich in der Zeit zu Stande bringen könnte. Mercy dir, Vanessa!

Über die letzten Jahre waren **Meike Bauer** und **Simone Rink** meine größte Unterstützung. Danke euch beiden, dass ihr immer für mich da wart, für viele spaßige und lustige Stunden und gute Ratschläge, in, aber auch außerhalb der Uni. Ich bin sehr froh euch beide kennen gelernt zu haben und hoffe auf viele weitere gemeinsame Jahre.

Ich möchte mich auch bei **Mona Meltschoch** bedanken, meiner einzigen Bachelor-Studentin, und meinen Laborkollegen **Arne Behrent** und **Florian Weinzierl** für eine gute Zeit, inspirierende Forschungsdiskussionen, Unterstützung in allen Belangen und einfach nur spaßige Konversationen bedanken. Danke euch Dreien, es ist schön jemanden zu haben, der meinen Humor versteht, und mit dem man zwischendurch auch einfach mal lachen kann, auch wenn manchmal alles zum Weinen ist.

Last, but not least danke ich meiner ganzen **Familie** für ihre fortwährende finanzielle und emotionale Unterstützung während der letzten neun Jahre, was alles erst möglich gemacht hat. Danke Mama, Papa, Susi, Antonia, Julia und alle anderen, dass ihr immer an mich geglaubt habt und zumindest so getan habt, als würde euch Chemie und meine Arbeit interessieren. Und auch meine Omas, die beide unglaublich stolz auf mich sind, ohne sich irgendetwas darunter vorstellen zu können, was ich eigentlich mache. Ich weiß diese bedingungslose Liebe sehr zu schätzen.

Declaration of Collaborations

Most of the theoretical and experimental work presented in this thesis was conducted solely by the author. However, parts of the results were gained in collaboration with other researchers, which are stated in this section in accordance with §8 Abs. 1 Satz 2 Punkt 7 of the "Ordnung zum Erwerb des akademischen Grades eines Doktors der Naturwissenschaften (Dr. rer. Nat.) an der Universität Regensburg vom 18. Juni 2009".

Signaling strategies of silver nanoparticles in optical and electrochemical biosensors: considering their potential for the point-of-care (Chapter 2)

This chapter has been submitted for publication. The literature search and writing of the manuscript draft was done by the author. Antje J. Baeumner revised the manuscript and is corresponding author.

Ag nanoparticles outperform Au nanoparticles for the use as label in electrochemical point-of-care sensors (Chapter 3)

This chapter has been published. Antje J. Baeumner, Carina Horn and the author developed the concept for this work. Antje J. Baeumner and the author planned the experiments. The author did the experimental work and wrote the first draft of the manuscript. Antje J. Baeumner and Carina Horn revised the manuscript. Antje J. Baeumner is corresponding author.

Dry-reagent microfluidic biosensor for simple detection of NT-proBNP via Ag nanoparticles (Chapter 4)

This chapter has been published. Antje J. Baeumner and the author developed the concept for this work. Antje J. Baeumner and the author planned the experiments. The author did the experimental work and wrote the first draft of the manuscript. Antje J. Baeumner and Carina Horn revised the manuscript. Antje J. Baeumner is corresponding author.

Easy electrochemical aggregation assay for quantification of creatinine at the point-of-care (Chapter 5)

This chapter will be further used as part of a manuscript intended for publication. The author developed the concept, performed the experiments, and wrote the chapter. Antje J. Bäumner contributed with strategic discussions and was leader of the project.

Table of Contents

Summary.....	1
Zusammenfassung	3
1 Motivation and Structure of the Thesis.....	5
2 Signaling Strategies of Silver Nanoparticles in Optical and Electrochemical Biosensors: Considering their Potential for the Point-of-Care.....	8
2.1 Introduction.....	10
2.2 Silver Nanoparticles in Optical Biosensors.....	13
2.2.1 SPR-based Biosensors.....	14
2.2.2 Biosensors based on Surface-Enhanced-Raman-Scattering.....	15
2.2.3 Metal-Enhanced Fluorescence-based Biosensors.....	16
2.2.4 Other Fluorescent Sensors.....	17
2.3 Silver Nanoparticles in Electrochemical Biosensors	19
2.3.1 Silver Nanoparticles as Labels.....	19
2.3.2 Silver Nanoparticles for Modification of the Electrode.....	22
2.4 Conclusion.....	23
2.5 References.....	24
3 Ag Nanoparticles Outperform Au Nanoparticles for the Use as Label in Electrochemical Point-of-Care Sensors.....	33
3.1 Introduction.....	35
3.2 Experimental Section.....	37
3.2.1 Materials and Instruments	37
3.2.2 Electrochemical Detection of Gold and Silver Nanoparticles	38
3.2.3 Modification of Silver Nanoparticles.....	39
3.2.4 Performance of the Bioassay.....	39
3.3 Results and Discussion	40

3.3.1	Electrochemical Detection of Metallic Nanoparticles.....	40
3.3.2	Characterization of Modified Silver Nanoparticles.....	42
3.3.3	Comparison of Gold and Silver Nanoparticles as Label in an Electrochemical Sandwich Assay.....	45
3.3.4	Application of AgNPs as Label for NT-proBNP Quantification in Serum.....	47
3.4	Conclusion.....	48
3.5	References.....	49
3.6	Supporting Information.....	53
4	Dry-reagent microfluidic biosensor for simple detection of NT-proBNP via Ag nanoparticles.....	58
4.1	Introduction.....	60
4.2	Experimental Section.....	62
4.2.1	Materials and Instruments.....	62
4.2.2	Modification of Silver Nanoparticles.....	63
4.2.3	Drying of Labeled Probe Antibody.....	63
4.2.4	Fabrication of Flow Chips.....	64
4.2.5	Microfluidic Experiments.....	65
4.3	Results and Discussion.....	66
4.3.1	Development of AB-AgNPs as Dry Reagent for Sensors and Microfluidic Chips.....	66
4.3.2	Development of a Microfluidic Chip for NT-proBNP.....	68
4.3.3	Performance of the Microfluidic Bioassay.....	70
4.3.4	Stability Study.....	73
4.4	Conclusion.....	75
4.5	References.....	76
4.6	Supporting Information.....	79
5	Easy Electrochemical Aggregation Assay for Quantification of Creatinine at the Point-of-Care.....	87

5.1	Introduction	89
5.2	Experimental Section.....	91
5.2.1	Materials and Instruments	91
5.2.2	Modification of Silver Nanoparticles.....	92
5.2.3	Aggregation Assay	92
5.2.4	Development of a Dry Testing Procedure.....	92
5.2.5	Detection of Creatinine in Urine Samples.....	93
5.3	Results and Discussion	93
5.3.1	Optimization of AgNP Modification.....	94
5.3.2	Development and Optimization of a Dry Testing Procedure	95
5.3.3	Dose-Response-Curves in Buffer.....	97
5.3.4	Application for Urine Samples.....	98
5.4	Conclusion.....	100
5.5	References.....	101
5.6	Supporting Information	103
6	Conclusions and Future Perspectives	109
	Curriculum Vitae	112
	List of Publications	114
	Presentations.....	115
	Eidesstattliche Erklärung.....	116

List of Abbreviations and Symbols

In the following, all used abbreviations and symbols, besides the commonly known ones, are explained, while the page number refers to the first appearance in this thesis.

Abbreviation	Meaning	Page
AA	ascorbic acid	17
AB	antibody	34
AB-AgNP	probe AB-modified AgNP or AgNP-labeled probe AB	39
AB-AuNP	probe AB-modified AuNP or AuNP-labeled probe AB	37
AG	antigen	37
AgNC	silver nanocluster	14
AgNP	silver nanoparticle	1
ASV	anodic stripping voltammetry	19
AuNP	gold nanoparticle	1
BNP	brain natriuretic peptide	5
BSA	bovine serum albumin	37
ddH ₂ O	double-distilled water	38
d _H	hydrodynamic diameter	42
DLS	dynamic light scattering	12
DPV	differential pulse voltammetry	2
EDC	1-ethyl-3-(3-dimethylaminopropyl)carbodiimide	45
EDX	energy dispersive X-ray analysis	12
FIA	flow-injection analysis	61
FRET	Foerster resonance energy transfer	14
FTIR	Fourier-transform infrared spectroscopy	12
GO	graphene oxide	22
HCy	homocysteine	91
HEPES	4-(2-hydroxyethyl)-1-piperazineethanesulfonic acid	38
HF	heart failure	2
LFA	lateral flow assay	5

LOD	limit of detection	1
LSV	linear sweep voltammetry	19
MEF	metal-enhanced fluorescence	1
miRNA	micro RNA	15
mNP	metallic nanoparticle	1
NHS	<i>N</i> -hydroxysuccinimide	45
NT-proBNP	<i>N</i> -terminal prohormone brain natriuretic peptide	1
NP	nanoparticle	2
PA	picric acid	2
PA-AgNP	picric acid-modified AgNP	2
PBS	phosphate buffered saline	38
PBST	PBS with Tween20	38
PdI	polydispersity index	42
POC	point-of-care	1
POCT	point-of-care testing	12
proBNP	prohormone brain natriuretic peptide	5
PSA	prostate specific antigen	21
PyBA	pyrene butyric acid	45
R_{CT}	charge-transfer resistance	45
RI	refractive index	14
rt	room temperature	39
SD	standard deviation	2
SEM	scanning electron microscopy	12
SERS	surface-enhanced-Raman-scattering	1
S/N	signal-to-noise ratio	46
SPCE	screen-printed carbon electrode	1
SPR	surface plasmon resonance	1
surin	synthetic urine	2
TEM	transmission electron microscopy	12
WE	working electrode	36
XPS	X-ray photoelectron spectroscopy	12
XRD	X-ray diffraction	12

Summary

In this thesis, the beneficial properties of silver nanoparticles (AgNPs) are employed in the development of electrochemical assays for clinical analysis. AgNPs are the most abundant commercialized nanocompound with a production of 350 t per year. Besides their manifold uses based on their antibacterial, antiviral, antifungal and antimicrobial properties, *e.g.* in coating of medicinal products, they are also employed for various clinical biosensors. While most sensing applications rely on optical detection techniques such as surface plasmon resonance (SPR), surface-enhanced-Raman-scattering (SERS), metal-enhanced fluorescence (MEF) or fluorescence emission, there has been some research in the field of electrochemical biosensors using AgNPs, as well. They are used for modification of the electrode surface or less commonly as labels. The suitability for the use of the respective biosensor at the point-of-care (POC) was assessed carefully based on criteria like ease of handling, storage ability, cost, time consumption and need of sample pretreatment.

Sandwich Immunoassay for NT-proBNP Detection

The first experimental part of this work focuses on the benefit of using AgNPs as electrochemical label, instead of the more commonly employed gold nanoparticles (AuNPs). Using an electrochemical detection strategy with a sequence of oxidation and reduction reactions, lowest limits of detection (LODs) were reached for both metallic nanoparticles (mNPs). When exchanging gold with silver in a simple sandwich immunoassay for the blood biomarker *N*-terminal prohormone brain natriuretic peptide (NT-proBNP) on screen-printed carbon electrodes (SPCEs), the LOD is decreased by a factor of 6, while maintaining the same or better assay reliability and ease of surface functionalization. Moreover, the addition of hydrochloric acid, inevitable for the electrochemical detection of gold due to the high Au stability, is removed. This makes the AgNP assay better suited for POC applications. In order to adjust the procedure better to the needs at the POC, *i.e.* ease of handling and miniaturization, while increasing the analytical performance, this assay was transferred into a microfluidic chip. The chip comprises the SPCE, double-sided adhesive tape with cut out channel design and a PMMA top with in- and outlet as well as a cavity on the inside. This renders it low-cost and easy to produce and enables the integration of all-dried reagents into one chip. The use of a trehalose matrix in combination with a suitable oxygen scavenger stabilizes the AgNPs against oxidation

by air oxygen and renders the chips stable over 18 weeks at 4 °C. With a LOD of 0.26 ng·mL⁻¹ in buffer and 0.56 ng·mL⁻¹ in undiluted human serum, the microfluidic sensor exhibits a sensitivity below the clinically relevant threshold for chronic heart failure (HF) of 1 ng·mL⁻¹. Also, the reproducibility is greatly increased with a mean standard deviation (SD) of 6% in comparison to the standard immunoassay with 15%.

Aggregation Assay for Creatinine Detection

The second experimental part shows the development of an electrochemical aggregation assay for the detection of the renal function biomarker creatinine. In neutral or slightly acidic medium, picric acid (PA) interacts selectively with the tautomeric form of creatinine, while creatinine molecules form hydrogen bonds among each other as well. AgNPs can be functionalized with PA via electrostatic interactions. These picric acid-modified AgNPs (PA-AgNPs) aggregate in the presence of creatinine and the grade of aggregation is a measure for the concentration of the analyte. This system was employed by others in combination with an optical detection. Here, an electrochemical detection via differential pulse voltammetry (DPV) is investigated, which is based on the increasing distance between AgNP and electrode surface upon aggregation. Different nanoparticle (NP) sizes and modifications were tested and 10 nm AgNPs modified with 10 μM PA are ideal for electrochemical detection and show effective aggregation. To render it accessible for POC strategies, the detection was transferred into an all-dried approach without any loss of performance. It was found that the sensitivity can be controlled by changes in the PA-AgNP to sample ratio making the assay easily adjustable to various matrices with different concentration ranges. With a 2:3 ratio, a LOD as low as 76 μM was reached with a mean SD of 12%. This system was also successfully applied in 1:10 diluted synthetic urine (surin) matrix covering a majority of the physiological range (0.4-2 mM in 1:10 diluted surin) without further optimization.

Zusammenfassung

In dieser Dissertation werden die vorteilhaften Eigenschaften von Silbernanopartikeln bei der Entwicklung elektrochemischer Assays für die klinische Analyse genutzt. AgNPs sind die am häufigsten kommerzialisierte Nanoverbindung mit einer Produktion von 350 t pro Jahr. Neben ihren vielfältigen Einsatzmöglichkeiten aufgrund ihrer antibakteriellen, antiviralen, antimykotischen und antimikrobiellen Eigenschaften, z.B. in der Beschichtung von medizinischen Produkten, werden sie auch für verschiedene klinische Biosensoren eingesetzt. Während die meisten Sensoranwendungen auf optischen Detektionstechniken wie SPR, SERS, MEF oder Fluoreszenzemission beruhen, wurde auch auf dem Gebiet der elektrochemischen Biosensoren mit AgNPs geforscht. Sie werden zur Modifikation der Elektrodenoberfläche oder seltener als Marker verwendet. Die Eignung für den Einsatz des jeweiligen Biosensors am Point-of-Care wurde anhand von Kriterien wie einfache Handhabung, Lagerfähigkeit, Kosten, Zeitaufwand und Notwendigkeit der Probenvorbehandlung sorgfältig bewertet.

Sandwich-Immunoassay für die Detektion von NT-proBNP

Der erste experimentelle Teil dieser Arbeit konzentriert sich auf die Vorteile der Verwendung von AgNPs als elektrochemischer Marker anstelle der häufiger verwendeten Goldnanopartikel. Unter Verwendung einer elektrochemischen Nachweisstrategie mit einer Folge von Oxidations- und Reduktionsreaktionen wurden niedrigste Nachweisgrenzen für beide metallischen Nanopartikel erreicht. Beim Austausch von Gold gegen Silber in einem einfachen Sandwich-Immunoassay für den Blutbiomarker NT-proBNP auf siebgedruckten Kohlenstoffelektroden wird der LOD um den Faktor 6 verringert, während die gleiche oder bessere Assay-Zuverlässigkeit und einfache Oberflächenfunktionalisierung beibehalten werden. Außerdem entfällt der für den elektrochemischen Nachweis von Gold aufgrund der hohen Au-Stabilität unumgängliche Zusatz von Salzsäure. Dadurch eignet sich der AgNP-Assay besser für POC-Anwendungen. Um das Verfahren besser an die Bedürfnisse am POC anzupassen, d. h. einfache Handhabung und Miniaturisierung, bei gleichzeitiger Erhöhung der analytischen Leistung, wurde dieser Assay in einen mikrofluidischen Chip überführt. Der Chip besteht aus einer SPCE, doppelseitigem Klebeband mit ausgeschnittenem Kanaldesign und einer PMMA-Oberseite mit Ein- und Auslass sowie einem Hohlraum auf der Innenseite. Dies macht es günstig und einfach herzustellen und ermöglicht die Integration aller getrockneten Reagenzien in einen Chip. Die

Verwendung einer Trehalose-Matrix in Kombination mit einem geeigneten Sauerstofffänger stabilisiert die AgNPs gegen Oxidation durch Luftsauerstoff und macht die Chips über 18 Wochen bei 4 °C stabil. Mit einer LOD von $0,26 \text{ ng}\cdot\text{mL}^{-1}$ in Puffer und $0,56 \text{ ng}\cdot\text{mL}^{-1}$ in unverdünntem Humanserum weist der mikrofluidische Sensor eine Sensitivität unterhalb der klinisch relevanten Schwelle für chronische Herzinsuffizienz von $1 \text{ ng}\cdot\text{mL}^{-1}$ auf. Die Reproduzierbarkeit ist mit einer mittleren Standardabweichung von 6 % im Vergleich zum Standard-Immunoassay mit 15 % stark erhöht.

Aggregations-Assay für die Detektion von Kreatinin

Der zweite experimentelle Teil zeigt die Entwicklung eines elektrochemischen Aggregationsassays zum Nachweis des Nierenfunktions-Biomarkers Kreatinin. In neutralem oder leicht saurem Medium interagiert Pikrinsäure selektiv mit der tautomeren Form von Kreatinin, während Kreatinin-Moleküle auch untereinander Wasserstoffbrückenbindungen eingehen. AgNPs können über elektrostatische Wechselwirkungen mit PA funktionalisiert werden. Diese Pikrinsäure-modifizierten AgNPs aggregieren in Anwesenheit von Kreatinin und der Grad der Aggregation ist ein Maß für die Konzentration des Analyten. Dieses System wurde schon von Anderen in Kombination mit einer optischen Detektion eingesetzt. Hier wird eine elektrochemische Detektion mittels DPV untersucht, die auf dem zunehmenden Abstand zwischen AgNP und Elektrodenoberfläche bei Aggregation basiert. Es wurden verschiedene Nanopartikel-Größen und -Modifikationen getestet, und 10-nm-AgNPs, modifiziert mit 10 μM PA, sind ideal für die elektrochemische Detektion und zeigen eine effektive Aggregation. Um sie für POC-Strategien zugänglich zu machen, wurde die Detektion ohne Performanceverlust in einen All-Dryed-Ansatz überführt. Es wurde festgestellt, dass die Empfindlichkeit durch Änderungen des PA-AgNP-zu-Probe-Verhältnisses gesteuert werden kann, wodurch der Assay leicht an verschiedene Matrices mit unterschiedlichen Konzentrationsbereichen angepasst werden kann. Bei einem Verhältnis von 2:3 wurde ein niedriger LOD von 60 μM mit einer mittleren SD von 16 % erreicht. Dieses System wurde auch ohne weitere Optimierung erfolgreich in einer 1:10 verdünnten Matrix aus synthetischem Urin angewendet, die einen Großteil des physiologischen Bereichs abdeckt (0,4–2 mM in 1:10 verdünntem Surin).

1 Motivation and Structure of the Thesis

This thesis focuses on the development of an electrochemical biosensor for clinical analysis using the inherent instability of silver nanoparticles for efficient signal amplification.

During the COVID-19 pandemic in the last years, sensitive and fast clinical analysis came to the fore. Especially approaches that can be used at the point-of-care with low reagent and sample demand, gained importance. The early diagnosis of most diseases is key to a successful treatment. Primary prevention leads to less incidents, which in consequence increases the quality of medical care for patients with severe courses and with this, the survival rate [1]. The contribution of bioanalytical research in this field is huge, since more sensitive diagnosis platforms with easy testing procedures are required. Due to their unique properties, silver nanoparticles offer strong signal amplification in combination with easy handling and low toxicity.

In **Chapter 2**, the beneficial properties of AgNPs and their current use in biosensing are summarized especially considering their potential for the POC. A major part of assays uses the special optical properties based on the collective oscillation of the conductive electrons induced by visible light, which is called surface plasmon resonance [2]. In contrast to optical detection methods, electrochemical detection offers high miniaturization potential, simplicity, low susceptibility to interferences and the potential for real-time analysis [3]. Moreover, roll-to-roll manufacturing in combination with laser patterning is known to be highly productive and therefore lowers the cost for electrode fabrication [4]. The use of electrode chips instead of lateral flow assays (LFAs) eliminates common problems with the reproducibility of membranes and decreases variability. AgNPs in electrochemistry are used either as label or for the modification of the electrode surface. The main reason, why AgNPs were disregarded by the bioanalytical community for a long time, are toxicity and stability concerns.

The most commonly used metal nanoparticles are gold nanoparticles due to their high biocompatibility and stability, and ease of synthesis and functionalization [5]. Therefore, silver and gold nanoparticles are compared as labels in a standard electrochemical immunoassay in **Chapter 3**. As model analyte, the heart failure biomarker NT-proBNP is utilized. The precursor prohormone brain natriuretic peptide (proBNP) is secreted by myocardial cells upon pressure overload and then cleaved enzymatically forming brain natriuretic peptide (BNP) and

NT-proBNP. While BNP lowers the central venous pressure, NT-proBNP is biologically inert and used to assess the severity of HF [6]. Fast, easy and sensitive quantification of NT-proBNP, which can be ideally performed by the patients themselves in a home setting, is essential for an effective treatment. Due to their greater instability, electrochemical dissolution of AgNPs does not require the addition of hydrochloric acid or application of high potentials like AuNPs. Therefore, the testing procedure is considerably simplified and interferences in biological matrices minimized.

It is key for self-testing to have simple and fast procedures, which can be performed by an untrained patient. Therefore, this principle is implemented into a dry-reagent microfluidic biosensor, which is discussed in **Chapter 4**. Drying of the reagents is a crucial factor for the development of POC sensors. However, since it increases the accessibility of the easily oxidized Ag surface to air oxygen, research in this direction just picked up momentum recently. Microfluidics enable automation as well as the use of low reagent and sample volumes, in the range of a finger prick, and often improve sensitivity, time consumption, cost and reproducibility [7]. While the microfluidic system can be further miniaturized and performance of the test is easy, the set-up and procedure is not yet ready for self-testing of patients. Therefore, a different format, which is suitable for low-cost, sensitive, and easy self-testing is investigated.

The aggregation of AgNPs in presence of an analyte was often employed in the past, especially in combination with optical transduction methods [8, 9]. Usually these assays are easy-to-perform, fast and they were employed for various analytes in a multitude of sample matrices including blood, urine and tap water. However, the sample volume demand for optical detection methods is rather high in order to ensure a sufficient path length. Another limiting factor is the color and turbidity of the sample. Therefore, the development of an electrochemical aggregation assay for creatinine detection is described in **Chapter 5**. Creatinine is a byproduct of muscle and protein metabolism and primarily removed from the bloodstream by glomerular filtration through the kidneys. Increased blood or urine creatinine values can therefore indicate renal problems and are a standard clinical parameter [10]. For patients with previous illnesses, self-testing of creatinine levels can help to track the course of medication or the disease itself. A highly selective surface modification and analyte system is necessary to turn the inherent instability of the AgNP colloid into a useful tool for analyte quantification. In

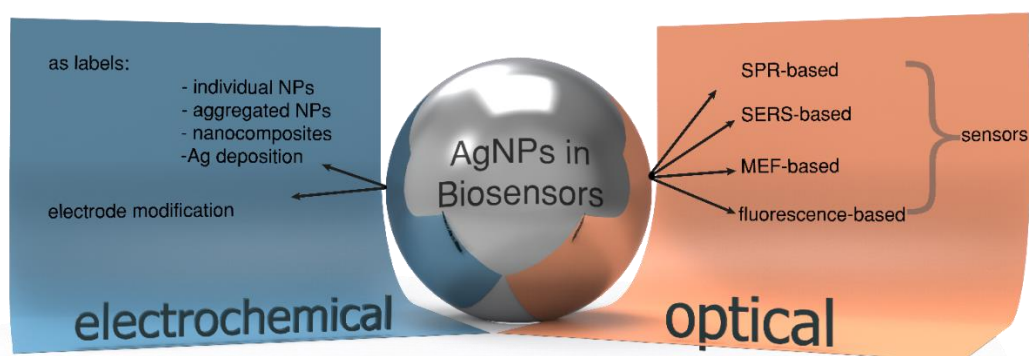
combination with the earlier developed fabrication of dry-reagent sensing chips, this format leads to an easy-to-use, fast, sensitive and selective self-testing device employing picric acid modified-AgNPs as indicators.

References

1. Roger VL. Epidemiology of heart failure. *Circ Res.* 2013;113:646–59. doi:10.1161/CIRCRESAHA.113.300268.
2. Li M, Li R, Li CM, Wu N. Electrochemical and optical biosensors based on nanomaterials and nanostructures: a review. *Front Biosci (Schol Ed).* 2011;3:1308–31. doi:10.2741/228.
3. pichaimuthu K. Silver Nanoparticles Decorated on Graphene Oxide Sheets for Electrochemical Detection of Ascorbic Acid(AA) in Human Urine Sample. *Int. J. Electrochem. Sci.* 2018;7859–69. doi:10.20964/2018.08.16.
4. Lee SH, Lee S. Fabrication and Characterization of Roll-to-Roll Printed Air-Gap Touch Sensors. *Polymers (Basel)* 2019. doi:10.3390/polym11020245.
5. Nanostructured materials in electrochemistry. Weinheim: Wiley-VCH; 2008.
6. Pollok NE, Rabin C, Walgama CT, Smith L, Richards I, Crooks RM. Electrochemical Detection of NT-proBNP Using a Metalloimmunoassay on a Paper Electrode Platform. *ACS Sens.* 2020;5:853–60. doi:10.1021/acssensors.0c00167.
7. Liu Y, Jiang X. Why microfluidics? Merits and trends in chemical synthesis. *Lab Chip.* 2017;17:3960–78. doi:10.1039/C7LC00627F.
8. Diamai S, Negi DPS. Cysteine-stabilized silver nanoparticles as a colorimetric probe for the selective detection of cysteamine. *Spectrochim Acta A Mol Biomol Spectrosc.* 2019;215:203–8. doi:10.1016/j.saa.2019.02.101.
9. Jin F, Li H, Xu D. Enzyme-free fluorescence microarray for determination of hepatitis B virus DNA based on silver nanoparticle aggregates-assisted signal amplification. *Anal Chim Acta.* 2019;1077:297–304. doi:10.1016/j.aca.2019.05.066.
10. Lewis SL, Bucher L, Heitkemper MM, Harding MM, Kwong J, Roberts D. *Medical-Surgical Nursing - E-Book: Assessment and Management of Clinical Problems, Single Volume.* 10th ed.: Mosby; 2016.

2 Signaling Strategies of Silver Nanoparticles in Optical and Electrochemical Biosensors: Considering their Potential for the Point-of-Care

Graphical Abstract



This chapter has been submitted for publication in ACS Sensors on May 23rd 2022.

Author contributions: FB did the literature search and wrote the first draft of the manuscript. AJB revised the manuscript and is corresponding author.

Abstract

Silver nanoparticles have long been overshadowed by gold NPs' success in sensor and point-of-care applications. However, their unique physical, (electro)chemical and optical properties make them excellently suited for such use, as long as their inherent higher instability toward oxidation is controlled. Here, we describe how properties of nanosized Ag (in the range of 1-100 nm) are exploited in optical and electrochemical biosensors providing highly desirable results. Moreover, we critically assess their potential for point-of-care sensors discussing advantages as well as limitations for each detection technique.

Keywords

silver nanoparticles, optical biosensors, electrochemical biosensors, point-of-care, clinical analysis

2.1 Introduction

During the last twenty years, silver nanoparticles gained increasing attention amongst the scientific community due to their unique physico-chemical properties. However, biomedical properties of silver colloids were already exploited by the ancient Greeks and Romans, for example in lotions or unguents [1]. Also, the antimicrobial effect of silver was used to protect vessels from bacterial growth and the food and drinks stored within from spoilage, long before the existence of microbes was found [2]. This effect is based on the interaction of silver ions with thiol type compounds in the vital enzymes and proteins of bacteria. With decreasing size of AgNPs, the surface contact area increases and with this, the antimicrobial effect. In contrast to macro-sized silver, the nanoparticles are able to interact additionally with the cell membrane, which leads to its disruption and subsequent cell death [3]. Nowadays, with a production of 320 t per year AgNPs are the most abundant commercialized nanocompound [4, 5]. They are widely used for example in cosmetics, textiles, medicinal products or water decontamination [6]. In socks for example, they inhibit the development of bad odors [7], while they can improve soft tissue healing in bandages, preventing a bacterial infection [3]. More medical applications include anti-cancer therapy, dentistry [8], the use as antidiabetic agent or vaccine adjuvant [9]. Only a minor part of the produced AgNPs are used in biosensors and serve as signal generation and amplification system instead of enzymes, AuNPs and other nanocontainers. They are efficiently used in combination with optical and electrochemical transduction methods. Aside from their ubiquitous usage, toxicity concerns arose during the last years. It was found that silver nanoparticles play a major role in the generation of reactive oxygen species and oxidative stress in cells. Moreover, they are able to interact with different organs [4]. The toxic effect of AgNPs depends on various factors, *e.g.* size, shape, surface modification, dispersion, concentration, cellular environment *etc.* [10]. Also, the complex mode of action is not fully known and understood, yet. Therefore, assessment of the grade of toxicity is a big challenge and has to be done very carefully.

Due to their general importance, AgNP synthesis (Figure 2.1), surface modification and characterization methods were extensively reviewed before, *e.g.* [6, 8, 9] and many more.

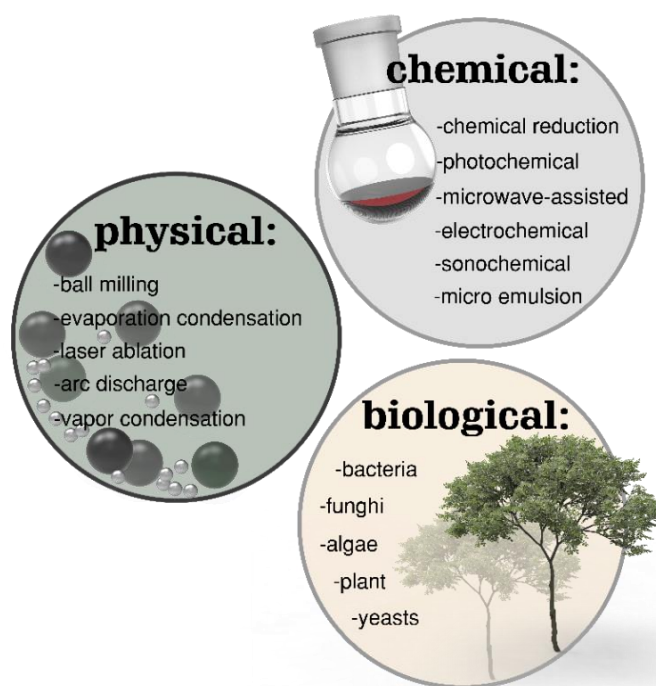


Figure 2.1. Summary of some possible synthesis methods for AgNPs with physical, chemical or biological methods [5, 6].

Nanoparticles can be synthesized in a “top-down” approach. Here, the bulk material is broken down into fine nanoparticles, which are stabilized using colloidal protecting agents. Physical methods like ball milling, evaporation, condensation, laser ablation, arc discharge or vapor condensation are used for this purpose and result usually in nanoparticles in powder form. These methods are fast and easy to scale-up and the resulting nanoparticles are free of hazardous chemicals. However, high energy-consumption, solvent contamination, low yield and a varying size distribution of the nanoparticles are drawbacks of the physical methods. Moreover, dispersing the nanoparticles without aggregation can be challenging. On the other hand, in “bottom-up” approaches a precursor salt, for example AgNO_3 , is reduced forming nuclei via self-assembly, which then grow into nanoparticles. Methods to generate the energy needed for this reduction are photochemical, electrochemical, microwave-assisted, sonochemical, sol-gel processes or reduction in a microemulsion. These “chemical” processes have the advantage of high yield, low-cost, ease-of-production and flexibility in NP shapes and sizes. However, the use of toxic chemicals for reduction leads to inadequate purity of the NPs and is untenable from an environmental point of view. Also, stabilization of the NPs against aggregation and control over their size are challenging and require the use of proper stabilizers. Green or “biological” synthesis of AgNPs overcomes these disadvantages. Here,

natural plants, bacteria, fungi, algae or yeast are used for the reduction of a precursor salt. These methods are environmentally friendly and pollution-free, and avoid harsh conditions like high temperatures, pH or strong reducing agents. Moreover, decreased time-demand, control over shape and size, simple scale-up, high stability, water-solubility, and density make these methods attractive in academia and industry. Post synthesis, AgNPs are characterized employing different methods, *e.g.* dynamic light scattering (DLS), transmission electron microscopy (TEM), scanning electron microscopy (SEM), UV/Vis spectroscopy, energy dispersive X-ray analysis (EDX), Fourier-transform infrared spectroscopy (FTIR), X-ray diffraction (XRD), and X-ray photoelectron spectroscopy (XPS). A detailed insight into these methods is outside the scope of this review, but can be found for example in [11].

In addition to fast, cost-efficient and well-controllable synthesis possibilities, metal nanoparticles offer a flexible, relatively inexpensive platform for signal amplification. They enable real-time detection of biomarkers in small sample volumes with a low LOD and fairly simple procedures [17, 18] and are therefore ideally suited for point-of-care testing (POCT) [19]. Tests used by medical personnel can be observed increasingly on the market [20] and the COVID-19 pandemic has demonstrated that there is an enormous need also for POCT used by patients themselves. In addition to low LODs, other important features need to be addressed including low sample volume demand (especially for blood testing), no additional pipetting, fast response time, low-cost, small size of the detection device, and storage of all chemicals in dry format on chip. Based on the high surface-to-volume ratio of AgNPs, they exhibit special optical and electrochemical properties, which render them ideal for the use in biosensors in combination with different transduction methods [11]. This review will focus on the progress of the use of silver nanoparticles in optical and electrochemical biosensors for clinical diagnostic in the last four years, especially assessing critically their potential for the use at the point-of-care.

2.2 Silver Nanoparticles in Optical Biosensors

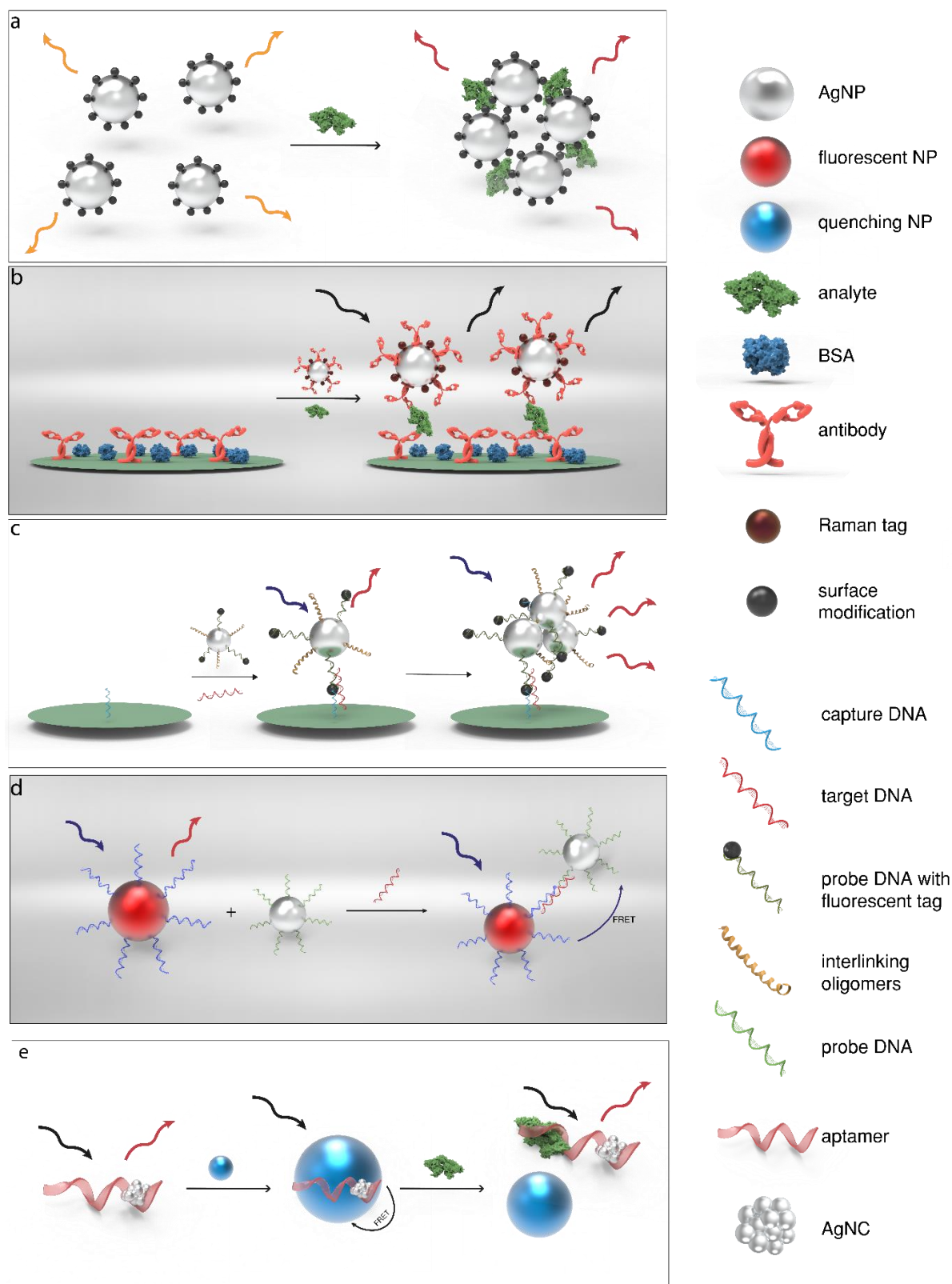


Figure 2.2. Schematic representation of the working principle of various optical biosensors using AgNPs based on (a) SPR, (b) SERS, (c) MEF, (d) FRET or (e) the fluorescent properties of AgNCs.

AgNPs exhibit various special optical properties that can be harnessed for detection by transducers commonly used in biosensors (Figure 2.2). (i) Due to a small band gap, they possess freely moving electrons, which can be excited to a collective oscillation by visible light, a phenomenon called surface plasmon resonance [21]. This leads to a strong absorption in the visible wavelength range, which depends strongly on shape, size and dispersion of the AgNPs [14]. On this basis, various biosensors were developed using the plasmon band shift upon aggregation or changes in the local dielectric constant/ refractive index (RI) due to mere binding to the analyte. (ii) With a high molar extinction coefficient and absorbance in the visible range, AgNPs are considered optimal fluorescence quenchers [22], enabling assay strategies based on Foerster resonance energy transfer (FRET). (iii) AgNPs provoke metal-enhanced fluorescence when in a short distance (5-90 nm) to a fluorophore. They increase the rate of excitation and emission and enable additional electronic configurations of the fluorophore. Therefore quantum yield, photostability and overall sensitivity of the fluorescence sensor is increased [23]. (iv) Moreover, the intrinsic fluorescence of silver nanoclusters (AgNCs) can be used for transduction as also (v) their inherent ability to enhance the Raman-scattering of molecules in spatial proximity of their surface resulting in SERS-based sensors [24].

2.2.1 SPR-based Biosensors

SPR is the collective oscillation of conductive electrons, which originates from acceleration of the electrons by the incident light in combination with restoring forces due to the polarization of particle and environment, and confinement of electrons to dimensions smaller than the wavelength of light [25]. As the SPR band depends on size, shape, interparticle space, surface charge, and nature of the surrounding medium [2], it can be exploited as transduction principle. Biosensors based on Ag nanoarchitected surfaces (*e.g.* nanospheres, nanoholes, nanoarrays *etc.*) measure analyte-dependent refractive index changes [24], whereas those using AgNPs utilize the SPR-band change upon analyte-induced de/aggregation of the silver nanoparticles (Figure 2.2 a). Thus, all molecules that induce aggregation via interaction of functional groups with the AgNP surface ligand, or that change the dielectric environment of the AgNP can be target analytes [26].

Here, silver is superior to other NPs due to its high molar extinction coefficient and narrow SPR-band in the visible region. With decreasing interparticle distance, the plasmonic fields of the individual particles overlap and the absorption shifts to higher wavelength or decreases.

This principle has been employed for years for the detection of various analytes and was reviewed extensively before [2]. It lends itself very well for clinical diagnostics at the POC due to the simple, visual or colorimetric read-out. It has recently been adopted toward the detection of biothiols [27, 28], DNA [29] or small molecules like adenosine [30] where quantification is obtainable through a change of absorption or even absorption ratio on two different wavelengths. Major drawbacks include the high sample volume typically needed for this format, suggesting that finger prick samples are excluded, but urine or saliva are applicable. Probably more important is the urgent need for finely tuned surface modification adapted to not only the analyte but also the desirable matrix. Aggregation of not-well-adjusted AgNPs is mostly influenced by electrolyte concentration or pH, while the presence of biomolecules can inhibit aggregation altogether. Finally, detection in turbid samples is not possible increasing the demand for careful sample preparation strategies. Nonetheless, application in the POC has become a true possibility through the replacement of spectrophotometers via smartphone read-out. This is not trivial due to variations in lighting, in handling by the patient, or in the smartphones themselves. Sophisticated mathematical corrections and internal standards have to be applied and will pave the path forward for AgNP aggregation assays for the POC in the future.

2.2.2 Biosensors based on Surface-Enhanced-Raman-Scattering

Surface-enhanced Raman offers high anti-interference stability due to highly specific fingerprint regions with narrow peaks [31], high multiplexing capabilities, speed, and low background noise [32]. The SERS mechanism is very complex. Researchers agreed on two major contributions to the enhancement of Raman signals: chemical and electromagnetic enhancement. The chemical enhancement, which results from a charge transfer between the Ag nanoparticles and the chemisorbed marker seems to have only minor influence. A stronger influence is attributed to the strong SPR in the local electric field at the AgNP surface in the so-called "hot spots" [24]. SERS can be used in multiple ways, *i.e.* intrinsic and extrinsic. In extrinsic SERS sensing (Figure 2.2 b), modified nanoparticles (SERS-tags) are used as labels [33], such as AgNPs with Raman reporter probe on their surface recently used for the detection of proteins [31], micro RNA (miRNA) [32] and DNA [34]. For intrinsic SERS sensing, the sample is deposited on a SERS active substrate and the Raman signals are recorded [33].

AgNPs are an ideal SERS substrate due to their high optical reflectivity and are typically combined with other materials. Their composition, size, shape and surface roughness influence the SPR band and with it the SERS efficiency of the substrate [24]. Typical material combinations include silicon chips or carbon materials additionally to the AgNPs [35–37]. These approaches offer easy implementation, label-free procedures and little sample preparation. However, data analysis or preparation of a suitable SERS substrate is very challenging. In general, SERS analyses suffer from poor reproducibility and stability of the signal. This makes quantitative SERS difficult, calling for internal standards, a highly ordered substrate, and shielding from external influences [37]. In the last years, this was employed for the detection of glutathione [36], miRNA [35], adenosine triphosphate or even whole bacteria [37]. However, most publications focus mainly on developing new, ultra-sensitive SERS substrates as proof-of-principle, rather than sensor development for clinical applications. The various possible variations of materials and characterization methods make it difficult to compare the published works. Moreover, SERS probe labeling is known to be difficult and the chemicals are rather expensive [38]. Regarding a POC application, there is still a lot of development necessary. The extrinsic sensing seems to have a higher potential to be used for POC, because it can be implemented in already known assays, like PCR assays or lateral flow assays, only with a different detection method [33]. However, with the apparatus necessary for Raman measurements and complex fabrication of SERS active substrate or tags [39], which is time and money consuming, the use of SERS-based sensors for patient self-testing seems to be rather unlikely.

2.2.3 Metal-Enhanced Fluorescence-based Biosensors

Fluorescence is a commonly used transduction technique in biosensors due to its versatility, simplicity, sensitivity, and multiplexing capability. However, high autofluorescence of the samples, as well as low quantum yield and photobleaching of traditional fluorescent labels hinder ultra-sensitive fluorescent detection [2]. These problems can be solved by enhancing the fluorescence via close proximity of the fluorescent dye to a colloidal metal surface. AgNPs are frequently employed here due to their strong SPR, which spans over a broad region of the visible spectrum [40]. The presence of a metal in a small distance (5-90 nm) increases the rate of excitation and emission of the fluorophore and enables additional electronic configurations. Therefore, quantum yield, photostability and after all sensitivity of the sensor is increased [23]. Analogous to the SERS sensors, silver nanoparticles can be used as substrate, for example in

combination with electrospun nanofibers [41], or as colloidal label [40, 42]. For the latter, usually controlled aggregation of the AgNPs is used to increase MEF (Figure 2.2 c). These sensors were employed for example for DNA [40], polysaccharides or enzymes, like heparin and heparinase [42].

Manufacturing of MEF tags and substrates is rather complicated as an exact distance between metal and fluorophore is crucial. If the parties are too close together, the AgNPs quench the emission, while the effect does not appear for too long distances. Finely tuned surfaces are hence of utmost importance [23]. For the use in POC applications, MEF is potentially useful only with special, well-thought-through systems. Furthermore, as the overall signal amplification of the fluorescence is usually rather small, it does not seem to be practical and cost-efficient for the mere amplification of the fluorescence signal. In addition, measurement in biological matrices is difficult, which makes it impossible to use in a self-testing setting without sample preparation. Moreover, the instrumentation and reagents for fluorescence measurements are rather expensive [39].

2.2.4 Other Fluorescent Sensors

Due to their strong and broad absorbance properties, AgNPs are ideal fluorescence quenchers [22]. This process takes place via FRET, a non-radiative, distance-dependent energy transfer via dipole-dipole interactions [24]. Since nanospheres possess an anisotropic shape, they do not have a defined dipole moment. Therefore, energy transfer can take place in any orientation and the efficiency of FRET increases. In the last years, AgNPs were employed as quencher in combination with various other fluorescent nanomaterials like metal-organic frameworks [43], carbon dots [44] or silica nanoparticles [45]. These FRET sensors can either be employed for analytes, which are able to cross-link donor and acceptor (Figure 2.2 d), like miRNA [43], or analytes, which are able to reduce Ag^+ and form the quenching AgNPs in situ, *e.g.* ascorbic acid (AA) [44] or dopamine [45]. These sensors can be developed in "turn-on" or "turn-off" mode. However, the AgNPs as quenchers are rarely employed for clinical analytes, and rather for environmental mercury monitoring. This method has true potential for future POC development due to its simplicity, sensitivity, rapidity and the various combination possibilities of materials and methods. However, most published work is still in the proof-of-principle stage, trying to fully understand mechanisms and influencing factors, rather than adapting specific assays to the POC.

A tiny subtype of AgNPs has seen special attention in recent years. These Ag nanoclusters are made of several to tens of atoms resulting in a size in the range of the Fermi wavelength of electrons. This gives rise to new interesting features [46], while they do not suffer from the usual limitations of organic fluorophores such as narrow excitation profiles, photobleaching, and non-symmetrical emission spectra. Instead, AgNCs possess an emission varying between blue and the near-IR depending on the size of the cluster, which makes them ideal for multiplexing [24]. They have a high quantum yield, narrow photoluminescence bands, and excellent biocompatibility [47]. Also, their simple synthesis protocol is usually performed by reduction of a silver salt in presence of a DNA template. Most recent sensing examples include RNA or miRNA detection [46, 48], ELISAs [49] or dopamine [50]. Often such approaches are also combined with FRET (Figure 2.2 e). Also, the combination of the DNA-templated synthesis with aptamers was done, for example for the cancer biomarkers carcinoembryonic antigen and alpha-fetoprotein [47]. Unfortunately, many assays rely on the in-situ synthesis of the AgNCs, which is not possible considering a POC, self-testing approach due to multi-step addition of chemicals. However, if their long-term stability can be confirmed, they could have a big potential replacing traditional, organic fluorophore markers.

2.3 Silver Nanoparticles in Electrochemical Biosensors

Electrochemical biosensors are often preferred over optical ones, since they show high sensitivity, cost-effectiveness, simplicity, low susceptibility to interferences and the potential for real-time analysis, which is particularly interesting for clinical analysis of biological fluids [51–53]. Simultaneously, they have a higher potential for miniaturization, because no optical components or minimum path lengths are needed [54, 55]. Therefore, sensors with electrochemical detection are frequently used in food quality monitoring, biomedical research, clinical diagnostic, and environmental monitoring [18]. AgNPs are of special interest as they have the highest conductivity of all metals, high electrochemical activity, *i.e.* low oxidation potential and high electron transfer rates, and catalytic activity towards certain analytes [56, 57]. This chapter is divided into the use of AgNPs as label and the use for modification of the electrode. In both cases, the use of silver nanoparticles leads to an amplified signal.

2.3.1 Silver Nanoparticles as Labels

The characteristic Ag/AgCl solid-state reaction of AgNPs is used for their quantification when used as label. Oxidation of Ag is directly monitored via voltammetric methods, like linear sweep voltammetry (LSV), square wave voltammetry (SWV) or differential pulse voltammetry. AgNPs are also dissolved for sensitive detection via anodic stripping voltammetry (ASV) [56]. Due to their high electrochemical activity, the oxidation and reduction are possible using a low potential and without the use of additional hazardous chemicals. This minimizes the potential interferences and ensures a reaction outside of the potential region, where water electrolysis or the electrochemical reaction of dissolved oxygen occurs. Together with relatively sharp peaks and thus precise and sensitive detection [58], AgNPs are highly advantageous as label in electrochemical sensors in comparison to for example gold nanoparticles or quantum dots and are used employing four overall strategies (Figure 2.3).

Signaling Strategies of Silver Nanoparticles in Optical and Electrochemical Biosensors: Considering their Potential for the Point-of-Care

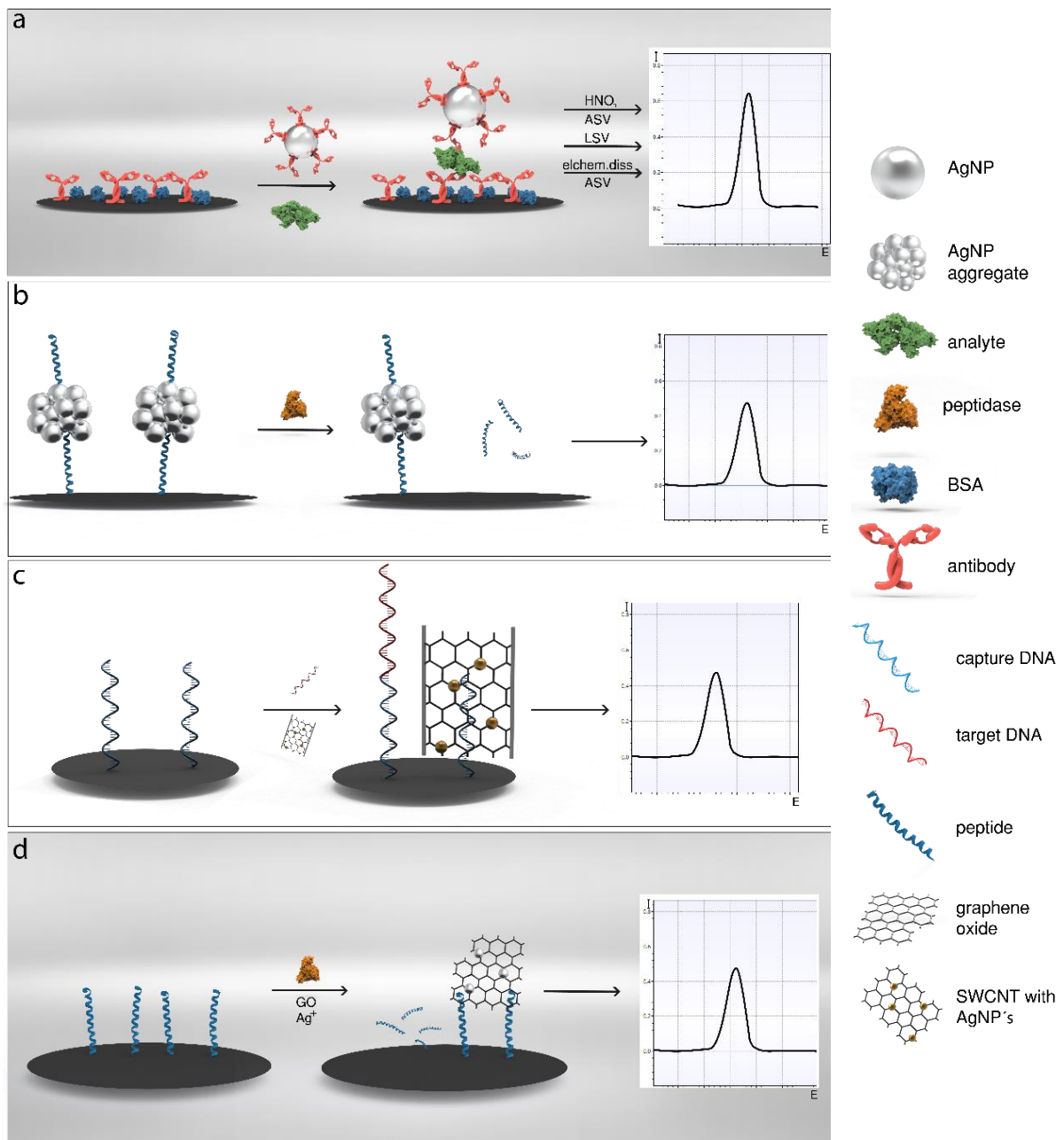


Figure 2.3. Schematic representation of a bioassay using (a) individual AgNPs with chemical dissolution, direct LSV and electrochemical dissolution, (b) AgNP aggregates or (c) nanocomposites as electrochemical label or (d) in situ synthesis of AgNPs.

2.3.1.1 Individual AgNPs

One individual AgNP consists of thousands of silver atoms. This provides considerable signal-amplification compared to the use of single molecule labels (Figure 2.3 a). Traditionally, AgNPs were dissolved using strong acids like HNO_3 , preconcentrated on the transducer by reduction and then oxidatively stripped off the surface [51, 55]. This method is very sensitive, since the chemical treatment dissolves the whole particle, can potentially clean the electrode, and ASV is known to be used for trace analysis. Still, as the chemical dissolution uses harsh chemicals, is

time-consuming, and can be the origin of mistakes, its application is very limited [59]. With regard to POC application, the further addition of solutions makes it most problematic. Overcoming these limitations, a number of researchers monitor directly the oxidation of the Ag in KCl electrolyte via LSV [39, 53, 54]. This procedure was used for a variety of clinical analytes, *e.g.* prostate specific antigen (PSA) [54], enzyme activity [53] or DNA [39]. It offers fast and simple procedures. Since no external dissolution step is necessary, these assays can be performed in a one-step fashion and even potentially transferred to a desirable chip-based approach.

Further improvements have been accomplished through various electrochemical dissolution strategies [60, 61], which then combined preconcentration and stripping analysis with the simple LSV and enable the detection of lower abundant analytes. Challenges occur when the AgNPs need to be modified with biorecognition elements as these may hinder the electrochemical conversion for electrochemical dissolution or direct detection. Also, such modifications are often performed solely by adsorption, which may interfere with long-time storage. Most obvious, researchers must provide a strategy to prevent Ag oxidation by air oxygen to enable reliable detection and storage of their labels, which is too often not considered in published works.

2.3.1.2 AgNP Aggregates and Nanocomposites

To increase the number of abundant AgNPs, individual nanoparticles are bridged with small molecules. These aggregates are then used analogous to the individual nanoparticles as labels increasing the overall signal amplification (Figure 2.3 b). This was used for example for enzyme activity [62, 63] or PSA [64]. For the same analyte PSA, the researchers were able to perform a considerably more sensitive detection using AgNP aggregates as labels instead of individual AgNPs ($0.11 \text{ pg}\cdot\text{mL}^{-1}$ vs. $33 \text{ fg}\cdot\text{mL}^{-1}$). It is not clear, how larger AgNP may provide the same amplification power, however. Also, the AgNP aggregation has to be precisely controlled resulting in complicated experimental procedures, questioning the strategy for POC and self-testing applications. Specifically, AgNP aggregation can vary with biological matrix components which likely makes any one-step procedure impossible.

Alternatively, a multitude of AgNPs can be generated through nanocomposites (Figure 2.3 c). Here, several nanostructures, like nanofibers [65], carbon nanotubes [66] or -cubes [67], are loaded with AgNPs for signal generation and amplification. Especially the carbon

nanocomposites are easy to synthesize due to the natural affinity of Ag^+ ions to carboxyl and carbonyl groups. The advantages of both materials can be combined and various analytes can be detected ranging from whole cells [65] to small molecules like miRNA [66]. These successful approaches have to be viewed separate from many publications with AgNP nanocomposites where the second nanomaterial seems to have no purpose. For POC applications, there are no specific limitations to the use of nanocomposites as long as the synthesis and assay can be performed in a fast and cost-effective way and the nanocomposites exhibit sufficient stability.

2.3.1.3 Promoted Reduction of Ag^+ and Silver Deposition

In these assays, a precursor silver salt is reduced to produce metallic AgNPs. This can be promoted for example by reducing nanomaterials, such as graphene oxide (GO) [68], C_{60} -AuNPs [69] or hydrazine modified AuNPs [70], and is effectively an in situ synthesis of nanocomposites (Figure 2.3 d).

Due to further addition of solutions in the experimental procedure, these methods are difficult for a POC self-testing procedure and the publications shown so far do not convince with lower limits of detection or sensitivities in comparison to the standard AgNP nanocomposites. The same holds true with AgNP in situ synthesis based on biomolecules like DNA [71, 72] or alkaline phosphatase [73] albeit the integration of such molecules into assays has a long tradition and may therefore be advantageous. Still, it is not suitable for a self-testing approach, because the addition of reagent solutions after sample addition cannot be circumvented and sometimes long reaction times are needed.

2.3.2 Silver Nanoparticles for Modification of the Electrode

AgNPs are used just like other metal NPs to increase the active electrode area, and also to provide additional reactivity to simplify or enhance the oxidation or reduction of an analyte (Figure 2.4). For example, a glassy-carbon electrode was modified using eco-friendly synthesized mucilage-AgNPs to enable the detection of glucose in human blood samples [74]. By covering the electrode with AgNPs, the mass transport to the surface increases due to convergent rather than linear diffusion. Moreover, more exposed crystal planes in comparison to the bulk material can lead to current improvement and covering a low-cost electrode, like screen-printed carbon electrode, with only a fraction of the expensive metal is highly cost-efficient in comparison to using a silver electrode [75]. Furthermore, the superior electroanalytical properties of AgNPs enable inexpensive electrodes to interact with analytes

at low potentials. This was for example used for the detection of hydrogen peroxide [76] or ascorbic acid [52].

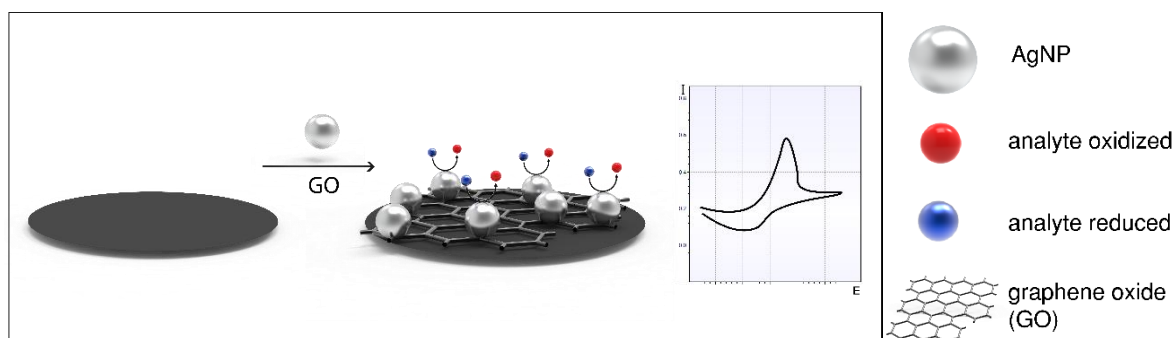


Figure 2.4. Schematic representation of an electrode modification designed to facilitate the oxidation of an analyte molecule.

Maduraiveeran *et al.* used AgNP to interact with the redox active center of proteins enabling direct electron transfer and facilitating the enzyme immobilization, which otherwise would often denature on the plain electrode surface. It is also assumed that AgNPs can form a microenvironment that is similar to the native one for redox enzymes. Other researchers used the AgNPs instead of redox mediators and benefited simultaneously from better electron transfer and larger surface area. The modification of electrodes with AgNPs is usually done via electrodeposition, which is low-cost, highly productive, and readily adaptable [57]. However, the building of such composite electrodes increases the complexity of redox reactions happening on the surface which gives rise to measuring artifacts, and selectivity and specificity issues [50]. If these issues can be solved, and the detection works also in biological media, this method would indeed be good for a POC self-testing approach.

2.4 Conclusion

Long overlooked, AgNPs find increasing interest in optical and electrochemical biosensors, however barely any sophisticated POC self-testing approaches are published, yet. The main reason, why AgNPs were disregarded for a long time, are stability and toxicity concerns. The highly active Ag is easily oxidized by air oxygen, especially in dried form, which makes it difficult to implement in self-testing strips or disks. Drying in a protective matrix with oxygen scavenger can be a solution for this problem, as well as smart surface modifications of the AgNPs themselves. Some publications start addressing this issue, but more attention needs to be spent to find long-term and smart solutions. Often mentioned are worries about the toxic effect

Ag⁺ ions can have on biomolecules which would result in a destruction of the important, adjacent biorecognition element. However, considering the many successful strategies published, these properties are well-controllable and tailorable by specific synthetic procedures. While by now even green synthesis strategies are well-documented, to-date it must be concluded that more well-executed and complete investigations are needed to fully understand AgNPs and their properties in order to enable their use in the POC field.

Overall, electrochemical detection through AgNPs shows many advantages over optical methods, but even here, their experimental procedures are often too complicated to adapt for POC testing and more innovation is needed to overcome multi-step processes. Often, long incubation times and the need for elevated assay temperatures hinder the use in self-testing. Therefore, different formats have to be employed to use the highly beneficial properties of AgNPs to their full extend. Yet, most nanoparticle research is focused on new compositions or combinations of materials to develop ultra-sensitive sensors rather than facilitating the experimental procedures and finding a real application for the existing materials and developing this further.

In general, when exploring the exciting field of sensors for the POC, definitions for certain terms, like "point-of-care", "(bio)sensors", or "sample pretreatment", do not follow the same guidelines and are often enough interpreted according to the authors' opinions. This makes an assessment of the real potential for POC self-testing devices more complicated. Considering the exciting examples described here, it can be concluded though that AgNPs are the long overseen nanoparticle that has a great potential as signal generator and signal amplification system due to its unique nature.

2.5 References

1. Beyene HD, Werkneh AA, Bezabh HK, Ambaye TG. Synthesis paradigm and applications of silver nanoparticles (AgNPs), a review. *Sustainable Materials and Technologies*. 2017;13:18–23. doi:10.1016/j.susmat.2017.08.001.
2. Loiseau A, Asila V, Boitel-Aullen G, Lam M, Salmain M, Boujday S. Silver-Based Plasmonic Nanoparticles for and Their Use in Biosensing. *Biosensors (Basel)* 2019. doi:10.3390/bios9020078.

3. Marin S, Vlasceanu GM, Tiplea RE, Bucur IR, Lemnaru M, Marin MM, Grumezescu AM. Applications and toxicity of silver nanoparticles: a recent review. *Curr Top Med Chem*. 2015;15:1596–604. doi:10.2174/1568026615666150414142209.
4. Flores-López LZ, Espinoza-Gómez H, Somanathan R. Silver nanoparticles: Electron transfer, reactive oxygen species, oxidative stress, beneficial and toxicological effects. Mini review. *J Appl Toxicol*. 2019;39:16–26. doi:10.1002/jat.3654.
5. Siddiqi KS, Husen A, Rao RAK. A review on biosynthesis of silver nanoparticles and their biocidal properties. *J Nanobiotechnology*. 2018;16:14. doi:10.1186/s12951-018-0334-5.
6. Rafique M, Sadaf I, Rafique MS, Tahir MB. A review on green synthesis of silver nanoparticles and their applications. *Artif Cells Nanomed Biotechnol*. 2017;45:1272–91. doi:10.1080/21691401.2016.1241792.
7. Benn TM, Westerhoff P. Nanoparticle silver released into water from commercially available sock fabrics. *Environ Sci Technol*. 2008;42:4133–9. doi:10.1021/es7032718.
8. Kaur P, Luthra R. Silver nanoparticles in dentistry: An emerging trend. *SRM J Res Dent Sci*. 2016;7:162. doi:10.4103/0976-433X.188808.
9. Xu L, Wang Y-Y, Huang J, Chen C-Y, Wang Z-X, Xie H. Silver nanoparticles: Synthesis, medical applications and biosafety. *Theranostics*. 2020;10:8996–9031. doi:10.7150/thno.45413.
10. Durán N, Silveira CP, Durán M, Martinez DST. Silver nanoparticle protein corona and toxicity: a mini-review. *J Nanobiotechnology*. 2015;13:55. doi:10.1186/s12951-015-0114-4.
11. Zhang X-F, Liu Z-G, Shen W, Gurunathan S. Silver Nanoparticles: Synthesis, Characterization, Properties, Applications, and Therapeutic Approaches. *Int J Mol Sci* 2016. doi:10.3390/ijms17091534.
12. Bhakta SA, Evans E, Benavidez TE, Garcia CD. Protein adsorption onto nanomaterials for the development of biosensors and analytical devices: a review. *Anal Chim Acta*. 2015;872:7–25. doi:10.1016/j.aca.2014.10.031.
13. Rawat M. A review on green synthesis and characterization of silver nanoparticles and their applications: a green nanoworld. *WJPPS*. 2016:730–62. doi:10.20959/wjpps20167-7227.

14. Fahmy HM, Mosleh AM, Elghany AA, Shams-Eldin E, Abu Serea ES, Ali SA, Shalan AE. Coated silver nanoparticles: synthesis, cytotoxicity, and optical properties. *RSC Adv.* 2019;9:20118–36. doi:10.1039/c9ra02907a.
15. Tarannum N, Divya D, Gautam YK. Facile green synthesis and applications of silver nanoparticles: a state-of-the-art review. *RSC Adv.* 2019;9:34926–48. doi:10.1039/c9ra04164h.
16. Kaabipour S, Hemmati S. A review on the green and sustainable synthesis of silver nanoparticles and one-dimensional silver nanostructures. *Beilstein J Nanotechnol.* 2021;12:102–36. doi:10.3762/bjnano.12.9.
17. Du H, Li Z, Wang Y, Yang Q, Wu W. Nanomaterial-based Optical Biosensors for the Detection of Foodborne Bacteria. *Food Reviews International.* 2020:1–30. doi:10.1080/87559129.2020.1740733.
18. Xia N, Wang X, Zhou B, Wu Y, Mao W, Liu L. Electrochemical Detection of Amyloid- β Oligomers Based on the Signal Amplification of a Network of Silver Nanoparticles. *ACS Appl Mater Interfaces.* 2016;8:19303–11. doi:10.1021/acsami.6b05423.
19. Lippa PB. *POCT - Patientennahe Labordiagnostik.* 2nd ed. Berlin, Heidelberg: Springer Berlin / Heidelberg; 2012.
20. Vashist SK. *Point-of-Care Diagnostics: Recent Advances and Trends.* Biosensors (Basel) 2017. doi:10.3390/bios7040062.
21. Guo X. Surface plasmon resonance based biosensor technique: a review. *J Biophotonics.* 2012;5:483–501. doi:10.1002/jbio.201200015.
22. Ghosh D, Chattopadhyay N. Gold and silver nanoparticles based superquenching of fluorescence: A review. *Journal of Luminescence.* 2015;160:223–32. doi:10.1016/j.jlumin.2014.12.018.
23. Jeong Y, Kook Y-M, Lee K, Koh W-G. Metal enhanced fluorescence (MEF) for biosensors: General approaches and a review of recent developments. *Biosens Bioelectron.* 2018;111:102–16. doi:10.1016/j.bios.2018.04.007.
24. Li M, Li R, Li CM, Wu N. Electrochemical and optical biosensors based on nanomaterials and nanostructures: a review. *Front Biosci (Schol Ed).* 2011;3:1308–31. doi:10.2741/228.

25. Ravindran A, Chandran P, Khan SS. Biofunctionalized silver nanoparticles: advances and prospects. *Colloids Surf B Biointerfaces*. 2013;105:342–52. doi:10.1016/j.colsurfb.2012.07.036.
26. Yu L, Li N. Noble Metal Nanoparticles-Based Colorimetric Biosensor for Visual Quantification: A Mini Review. *Chemosensors*. 2019;7:53. doi:10.3390/chemosensors7040053.
27. Diamai S, Negi DPS. Cysteine-stabilized silver nanoparticles as a colorimetric probe for the selective detection of cysteamine. *Spectrochim Acta A Mol Biomol Spectrosc*. 2019;215:203–8. doi:10.1016/j.saa.2019.02.101.
28. Thomas A, Sivasankaran U, Kumar KG. Biothiols induced colour change of silver nanoparticles: A colorimetric sensing strategy. *Spectrochim Acta A Mol Biomol Spectrosc*. 2018;188:113–9. doi:10.1016/j.saa.2017.06.040.
29. Ma X, Miao P. Silver nanoparticle@DNA tetrahedron-based colorimetric detection of HIV-related DNA with cascade strand displacement amplification. *J Mater Chem B*. 2019;7:2608–12. doi:10.1039/c9tb00274j.
30. Yousefi S, Saraji M. Optical aptasensor based on silver nanoparticles for the colorimetric detection of adenosine. *Spectrochim Acta A Mol Biomol Spectrosc*. 2019;213:1–5. doi:10.1016/j.saa.2019.01.036.
31. Zhao P, Li H-X, Li D-W, Hou Y-J, Mao L, Yang M, Wang Y. A SERS nano-tag-based magnetic-separation strategy for highly sensitive immunoassay in unprocessed whole blood. *Talanta*. 2019;198:527–33. doi:10.1016/j.talanta.2019.02.040.
32. Pang Y, Wang C, Lu L, Wang C, Sun Z, Xiao R. Dual-SERS biosensor for one-step detection of microRNAs in exosome and residual plasma of blood samples for diagnosing pancreatic cancer. *Biosens Bioelectron*. 2019;130:204–13. doi:10.1016/j.bios.2019.01.039.
33. Quarin S, Strobbia P. Recent Advances Towards Point-Of-Care Applications of Surface-Enhanced Raman Scattering Sensing. *Front Chem*. 2021;9:714113. doi:10.3389/fchem.2021.714113.
34. Macdonald D, Smith E, Faulds K, Graham D. DNA detection by SERS: hybridisation parameters and the potential for asymmetric PCR. *Analyst*. 2020;145:1871–7. doi:10.1039/c9an01732a.

35. Chen J, Wu Y, Fu C, Cao H, Tan X, Shi W, Wu Z. Ratiometric SERS biosensor for sensitive and reproducible detection of microRNA based on mismatched catalytic hairpin assembly. *Biosens Bioelectron.* 2019;143:111619. doi:10.1016/j.bios.2019.111619.
36. Bu Y, Zhu G, Li S, Qi R, Bhave G, Zhang D, et al. Silver-Nanoparticle-Embedded Porous Silicon Disks Enabled SERS Signal Amplification for Selective Glutathione Detection. *ACS Appl Nano Mater.* 2018;1:410–7. doi:10.1021/acsanm.7b00290.
37. Meng X, Wang H, Chen N, Ding P, Shi H, Zhai X, et al. A Graphene-Silver Nanoparticle-Silicon Sandwich SERS Chip for Quantitative Detection of Molecules and Capture, Discrimination, and Inactivation of Bacteria. *Anal Chem.* 2018;90:5646–53. doi:10.1021/acs.analchem.7b05139.
38. He Y, Yang X, Yuan R, Chai Y. A novel ratiometric SERS biosensor with one Raman probe for ultrasensitive microRNA detection based on DNA hydrogel amplification. *J Mater Chem B.* 2019;7:2643–7. doi:10.1039/C8TB02894J.
39. Chai H, Miao P. Bipedal DNA Walker Based Electrochemical Genosensing Strategy. *Anal Chem.* 2019;91:4953–7. doi:10.1021/acs.analchem.9b01118.
40. Jin F, Li H, Xu D. Enzyme-free fluorescence microarray for determination of hepatitis B virus DNA based on silver nanoparticle aggregates-assisted signal amplification. *Anal Chim Acta.* 2019;1077:297–304. doi:10.1016/j.aca.2019.05.066.
41. Yun BJ, Kwon JE, Lee K, Koh W-G. Highly sensitive metal-enhanced fluorescence biosensor prepared on electrospun fibers decorated with silica-coated silver nanoparticles. *Sensors and Actuators B: Chemical.* 2019;284:140–7. doi:10.1016/j.snb.2018.12.096.
42. Li J, Xu J, Guo W, Zhong W, Li Q, Tan L, Shang L. Ratiometric fluorescence sensors for heparin and heparinase based on enhanced excimer emission of perylene probe induced by cationic silver nanoparticles. *Sensors and Actuators B: Chemical.* 2020;305:127422. doi:10.1016/j.snb.2019.127422.
43. Afzalnia A, Mirzaee M. Ultrasensitive Fluorescent miRNA Biosensor Based on a "Sandwich" Oligonucleotide Hybridization and Fluorescence Resonance Energy Transfer Process Using an Ln(III)-MOF and Ag Nanoparticles for Early Cancer Diagnosis: Application of

Central Composite Design. *ACS Appl Mater Interfaces*. 2020;12:16076–87. doi:10.1021/acsami.0c00891.

44. Liu J, Wang L, Bao H. A novel fluorescent probe for ascorbic acid based on seed-mediated growth of silver nanoparticles quenching of carbon dots fluorescence. *Anal Bioanal Chem*. 2019;411:877–83. doi:10.1007/s00216-018-1505-9.

45. Lu Q, Chen X, Liu D, Wu C, Liu M, Li H, et al. Synergistic electron transfer effect-based signal amplification strategy for the ultrasensitive detection of dopamine. *Talanta*. 2018;182:428–32. doi:10.1016/j.talanta.2018.01.068.

46. Jiang Y, Ma X, Shao X, Wang M, Jiang Y, Miao P. Chameleon silver nanoclusters for ratiometric sensing of miRNA. *Sensors and Actuators B: Chemical*. 2019;297:126788. doi:10.1016/j.snb.2019.126788.

47. Jiang Y, Tang Y, Miao P. Polydopamine nanosphere@silver nanoclusters for fluorescence detection of multiplex tumor markers. *Nanoscale*. 2019;11:8119–23. doi:10.1039/C9NR01307E.

48. Shen F, Cheng Y, Xie Y, Yu H, Yao W, Li H-W, et al. DNA-silver nanocluster probe for norovirus RNA detection based on changes in secondary structure of nucleic acids. *Anal Biochem*. 2019;583:113365. doi:10.1016/j.ab.2019.113365.

49. Wang C, Xing K, Zhang G, Yuan M, Xu S, Liu D, et al. Novel ELISA based on fluorescent quenching of DNA-stabilized silver nanoclusters for detecting *E. coli* O157:H7. *Food Chem*. 2019;281:91–6. doi:10.1016/j.foodchem.2018.12.079.

50. Del Bonis-O'Donnell JT, Thakrar A, Hirschberg JW, Vong D, Queenan BN, Fygenson DK, Pennathur S. DNA-Stabilized Silver Nanoclusters as Specific, Ratiometric Fluorescent Dopamine Sensors. *ACS Chem Neurosci*. 2018;9:849–57. doi:10.1021/acschemneuro.7b00444.

51. Yazdanparast S, Benvidi A, Banaei M, Nikukar H, Tezerjani MD, Azimzadeh M. Dual-aptamer based electrochemical sandwich biosensor for MCF-7 human breast cancer cells using silver nanoparticle labels and a poly(glutamic acid)/MWNT nanocomposite. *Mikrochim Acta*. 2018;185:405. doi:10.1007/s00604-018-2918-z.

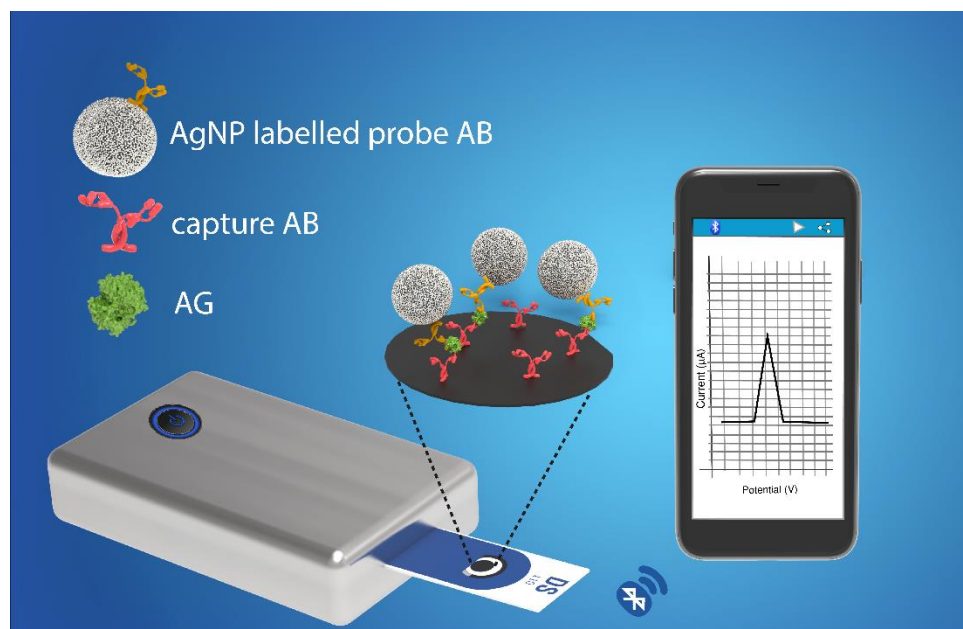
52. pichaimuthu K. Silver Nanoparticles Decorated on Graphene Oxide Sheets for Electrochemical Detection of Ascorbic Acid(AA) in Human Urine Sample. *Int. J. Electrochem. Sci.* 2018;7859–69. doi:10.20964/2018.08.16.
53. Miao X, Wang Y, Gu Z, Mao D, Ning L, Cao Y. Cucurbit[8]uril-assisted peptide assembly for feasible electrochemical assay of histone acetyltransferase activity. *Anal Bioanal Chem.* 2018;411:387–93. doi:10.1007/s00216-018-1445-4.
54. Miao P, Jiang Y, Wang Y, Yin J, Tang Y. An electrochemical approach capable of prostate specific antigen assay in human serum based on exonuclease-aided target recycling amplification. *Sensors and Actuators B: Chemical.* 2018;257:1021–6. doi:10.1016/j.snb.2017.11.064.
55. Abbaspour A, Norouz-Sarvestani F, Noori A, Soltani N. Aptamer-conjugated silver nanoparticles for electrochemical dual-aptamer-based sandwich detection of staphylococcus aureus. *Biosens Bioelectron.* 2015;68:149–55. doi:10.1016/j.bios.2014.12.040.
56. Yu C-X. Electrochemical Biosensors with Silver Nanoparticles as Signal Labels. *Int. J. Electrochem. Sci.* 2020;3869–90. doi:10.20964/2020.05.53.
57. Chen S, Yuan R, Chai Y, Hu F. Electrochemical sensing of hydrogen peroxide using metal nanoparticles: a review. *Microchim Acta.* 2013;180:15–32. doi:10.1007/s00604-012-0904-4.
58. Song W, Li H, Liang H, Qiang W, Xu D. Disposable electrochemical aptasensor array by using in situ DNA hybridization inducing silver nanoparticles aggregate for signal amplification. *Anal Chem.* 2014;86:2775–83. doi:10.1021/ac500011k.
59. Geagea R, Aubert P-H, Banet P, Sanson N. Signal enhancement of electrochemical biosensors via direct electrochemical oxidation of silver nanoparticle labels coated with zwitterionic polymers. *Chem Commun (Camb).* 2015;51:402–5. doi:10.1039/c4cc07474b.
60. Beck F, Horn C, Baeumner AJ. Ag nanoparticles outperform Au nanoparticles for the use as label in electrochemical point-of-care sensors. *Anal Bioanal Chem.* 2022;414:475–83. doi:10.1007/s00216-021-03288-6.
61. Pollok NE, Rabin C, Walgama CT, Smith L, Richards I, Crooks RM. Electrochemical Detection of NT-proBNP Using a Metalloimmunoassay on a Paper Electrode Platform. *ACS Sens.* 2020;5:853–60. doi:10.1021/acssensors.0c00167.

62. Cheng W, Ma J, Kong D, Zhang Z, Khan A, Yi C, et al. One step electrochemical detection for matrix metalloproteinase 2 based on anodic stripping of silver nanoparticles mediated by host-guest interactions. *Sensors and Actuators B: Chemical*. 2021;330:129379. doi:10.1016/j.snb.2020.129379.
63. Song S, Hu X, Li H, Zhao J, Koh K, Chen H. Guests involved CB[8] capped silver nanoparticles as a means of electrochemical signal enhancement for sensitive detection of Caspase-3. *Sensors and Actuators B: Chemical*. 2018;274:54–9. doi:10.1016/j.snb.2018.07.143.
64. Chen X, Wang Y, Zhang J, Zhang Y. DNA concatemer-silver nanoparticles as a signal probe for electrochemical prostate-specific antigen detection. *Analyst*. 2019;144:6313–20. doi:10.1039/c9an01484e.
65. Tang Y, Dai Y, Huang X, Li L, Han B, Cao Y, Zhao J. Self-Assembling Peptide-Based Multifunctional Nanofibers for Electrochemical Identification of Breast Cancer Stem-like Cells. *Anal Chem*. 2019;91:7531–7. doi:10.1021/acs.analchem.8b05359.
66. Asadzadeh-Firouzabadi A, Zare HR. Preparation and application of AgNPs/SWCNTs nanohybrid as an electroactive label for sensitive detection of miRNA related to lung cancer. *Sensors and Actuators B: Chemical*. 2018;260:824–31. doi:10.1016/j.snb.2017.12.195.
67. Gao J, Jia M, Xu Y, Zheng J, Shao N, Zhao M. Prereduction-promoted enhanced growth of silver nanoparticles for ultrasensitive colorimetric detection of alkaline phosphatase and carbohydrate antigen 125. *Talanta*. 2018;189:129–36. doi:10.1016/j.talanta.2018.06.064.
68. Meng F, Sun H, Huang Y, Tang Y, Chen Q, Miao P. Peptide cleavage-based electrochemical biosensor coupling graphene oxide and silver nanoparticles. *Anal Chim Acta*. 2019;1047:45–51. doi:10.1016/j.aca.2018.09.053.
69. Chen P, Wang T, Zheng X, Tian D, Xia F, Zhou C. An ultrasensitive electrochemical immunosensor based on C₆₀-modified polyamidoamine dendrimers and Au NPs for co-catalytic silver deposition. *New J. Chem*. 2018;42:4653–60. doi:10.1039/C8NJ00059J.
70. Shamsipur M, Emami M, Farzin L, Saber R. A sandwich-type electrochemical immunosensor based on in situ silver deposition for determination of serum level of HER2 in breast cancer patients. *Biosens Bioelectron*. 2018;103:54–61. doi:10.1016/j.bios.2017.12.022.

71. Sun H, Kong J, Wang Q, Liu Q, Zhang X. Dual Signal Amplification by eATRP and DNA-Templated Silver Nanoparticles for Ultrasensitive Electrochemical Detection of Nucleic Acids. *ACS Appl Mater Interfaces*. 2019;11:27568–73. doi:10.1021/acsami.9b08037.
72. Sun H, Xu W, Liu B, Liu Q, Wang Q, Li L, et al. Ultrasensitive Detection of DNA via SI-eRAFT and in Situ Metalization Dual-Signal Amplification. *Anal Chem*. 2019;91:9198–205. doi:10.1021/acs.analchem.9b01961.
73. Marques RCB, Costa-Rama E, Viswanathan S, Nouws HPA, Costa-García A, Delerue-Matos C, González-García MB. Voltammetric immunosensor for the simultaneous analysis of the breast cancer biomarkers CA 15-3 and HER2-ECD. *Sensors and Actuators B: Chemical*. 2018;255:918–25. doi:10.1016/j.snb.2017.08.107.
74. Khalifa Z, Zahran M, A-H Zahran M, Azzem MA. Mucilage-capped silver nanoparticles for glucose electrochemical sensing and fuel cell applications. *RSC Adv*. 2020;10:37675–82. doi:10.1039/d0ra07359h.
75. Campbell FW, Compton RG. The use of nanoparticles in electroanalysis: an updated review. *Anal Bioanal Chem*. 2010;396:241–59. doi:10.1007/s00216-009-3063-7.
76. Maduraiveeran G, Kundu M, Sasidharan M. Electrochemical detection of hydrogen peroxide based on silver nanoparticles via amplified electron transfer process. *J Mater Sci*. 2018;53:8328–38. doi:10.1007/s10853-018-2141-7.

3 Ag Nanoparticles Outperform Au Nanoparticles for the Use as Label in Electrochemical Point-of-Care Sensors

Graphical Abstract



This chapter has been published.

Franziska Beck, Carina Horn, and Antje J. Baeumner, *Anal. Bioanal. Chem.* 2022, 414, 475 - 483.

DOI: <https://doi.org/10.1007/s00216-021-03288-6>.

Author contributions: AJB, CH and FB developed the concept for this work. AJB and FB planned the experiments. FB did the experimental work and wrote the first draft of the manuscript. AJB and CH revised the manuscript. AJB is corresponding author.

Abstract

Electrochemical immunosensors enable rapid analyte quantification in small sample volumes, and have been demonstrated to provide high sensitivity and selectivity, simple miniaturization and easy sensor production strategies. As a point-of-care format, user-friendliness is equally important and most often not combinable with high sensitivity. As such, we demonstrate here that a sequence of metal oxidation and reduction, followed by stripping via DPV provides lowest limits of detection within a 2 min automatic measurement. Exchanging gold nanoparticles, which dominate in the development of POC sensors, with silver nanoparticles, not only better sensitivity was obtained, but more importantly, the assay protocol could be simplified to match POC requirements. Specifically, we studied both nanoparticles as reporter labels in a sandwich immunoassay with the blood protein biomarker NT-proBNP. For both kinds of nanoparticles, the dose-response curves easily covered the $\text{ng}\cdot\text{mL}^{-1}$ range. Mean SD of all measurements of 17% ($n\geq 4$) and a limit of detection of $26\text{ ng}\cdot\text{mL}^{-1}$ were achieved using AuNPs, but their detection requires addition of HCl, which is impossible in a POC format. In contrast, since AgNPs are electrochemically less stable they enabled a simplified assay protocol and provided even lower LODs of $4.0\text{ ng}\cdot\text{mL}^{-1}$ in buffer and $4.7\text{ ng}\cdot\text{mL}^{-1}$ in human serum while maintaining the same or even better assay reliability, storage stability, and easy antibody (AB) immobilization protocols. Thus, in direct comparison, AgNPs clearly outperform AuNPs in desirable POC electrochemical assays and should gain much more attention in the future development of such biosensors.

Keywords

electrochemical biosensor, silver nanoparticle, gold nanoparticle, blood analysis, DPV

3.1 Introduction

Recent advances in modern medicine present new challenges for immunoassays and sensors. A fast detection of certain biomarkers in an ultra-low concentration range is crucial for an early diagnosis, which should also lead to increased patient survival rate [1, 2]. The use of low sample volumes of biological fluids like blood is desirable to accelerate the whole testing procedure. Moreover, a reliable target quantification should be striven to assess the severity of the disease and adapt the medication appropriately [3]. Simultaneously, reproducibility, selectivity, easy handling, and low-cost of the device have to be preserved [4]. Electrochemical detection lends itself very well for this cause. The biological recognition element is coupled to an electrical transducer, which translates the binding event into an electrical signal [1]. This makes it a rapid and simple detection method [5]. The instrumentation is rather inexpensive and can be easily miniaturized towards a portable point-of-care device [4]. Commonly, the measurements are performed in an amperometric or potentiometric fashion, while amperometric biosensors are often more attractive due to their good sensitivity, accuracy and wide linear range [1]. Another advantage of electrochemical detection over *e.g.* optical sensors is that the measurements can be performed in a small volume (few microliters) and eventually in turbid and colored samples without the need of prior purification [4]. As marker in immunoassays radioactive, fluorescent, bio- and chemiluminescent probes or enzymes are usually used. Since the 1970s also the use of metal-based labels in so called "metalloimmunoassays" is reported to overcome disadvantages of these common markers [6]. The use of metallic nanoparticles with a size between 10 and 50 nm for example got increasing attention over the past years [7]. The physical, electrical, and optical properties are highly different from those of the bulk metal and they can be tailored by synthesis and chemical or biological modifications [8]. Due to the high surface-to-volume ratio, mNPs are able to catalyze reactions and accelerate the electron transfer rate efficiently [2]. Through using nanoparticles in an electrochemical biosensor, the loading of the electrode with electroactive species increases drastically compared to a single molecule label. This leads to an enormous amplification of current signal [5, 9]. Amplification power of mNPs is similar to the best enzyme labels, but don't require timed signal recording and are not prone to denaturing during storage [10]. Moreover, electrochemical biosensors using mNPs show high multiplexing capabilities due to the diversity of modifications and metals, which could be used [5]. Most often reported metal nanoparticle labels are gold

nanoparticles due to their unique optical, catalytic, and electronic properties [8]. Their excellent biocompatibility renders them highly useful for immunocytochemistry and cell biology [11]. Moreover, they can be easily synthesized and modified and show great colloidal stability. Most assays exploit their optical properties, but in the 2000s also electrochemical immuno, and DNA sensing gained increasing attention [11]. First procedures included a chemical dissolution of gold in a HBr/Br₂ solution, an accumulation on the electrode and stripping analysis [4]. These approaches proved to be very sensitive. However, using this highly toxic solution is not favorable and supplementary steps are always time consuming and prone to errors [9]. Therefore, alternative approaches with direct electrochemical dissolution were developed. Pumera *et al.* for example applied a three-step analysis consisting of adsorption of the AuNPs on the electrode surface, oxidative dissolution in presence of HCl and reverse electroreduction [11]. Most electrochemical assays reported in literature describing AuNPs as label are used for the quantification of DNA [7, 12]. Immunoassays are more challenging due to the higher complexity of proteins, the absence of amplification technologies like PCR and the stronger non-specific binding to solid supports [7]. Although a combination of gold and silver has already been quite common in the beginning of the 2000s [13, 14], the replacement of gold with silver tags was only suggested recently. Its greater electrochemical activity leads to well-defined, sharp reduction peaks. Moreover, dissolution of the silver nanoparticles is easier than for gold. Chemical dissolution is possible with the less oxidative and toxic nitric acid or MnO₄⁻ [10, 15]. Yet, even more interesting, electrochemical dissolution takes place at a smaller potential and without addition of hydrochloric acid [16]. Meanwhile, some DNA assays using AgNP tags for electrochemical analysis have been described [10, 17]. Szymanski *et al.* demonstrated protein quantification in 2010, where the AgNPs are detached chemically and pipetted separately onto an electrode for subsequent detection [18]. The Crooks working group has been using AgNP labels for the detection of various analytes, including NT-proBNP, for numerous years. However, they perform a microtiter plate assay and subsequently transfer the sandwich complex onto a paper-based device for quantification using magnetic beads for immobilization of the complex on the working electrode (WE) and galvanic exchange as detection principle [19–22]. All of these proof-of-principle assays confirmed that an actual biosensor strategy should be feasible. Hence, a biosensor concept was studied here with AgNPs and AuNPs as direct labels for sandwich assays. Important design aspects were the ability to

perform the assay directly on the transducer, *i.e.* a screen-printed electrode, and the minimization of assay steps (Figure 3.1).

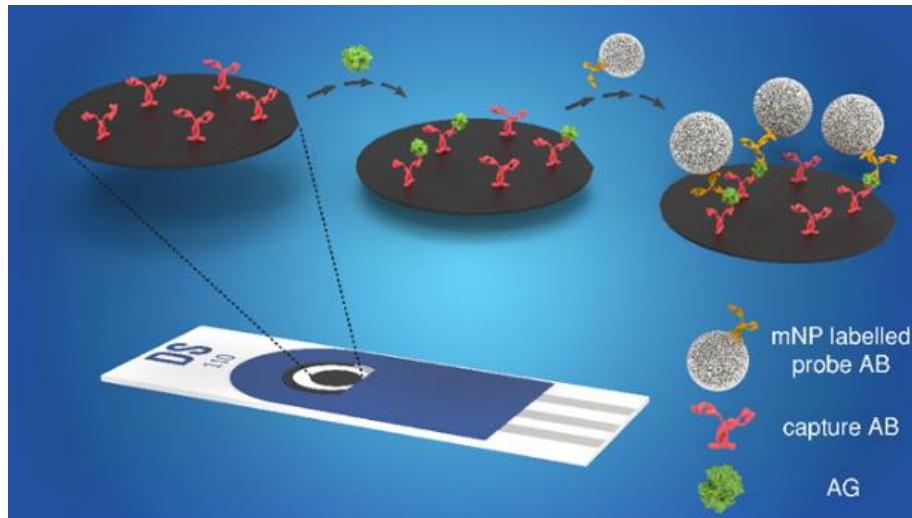


Figure 3.1. Schematic (not to scale) illustration of the assay principle for an electrochemical biosensor on a DropSens screen-printed carbon electrode.

Considering the ubiquitous use of AuNPs and the emerging use of AgNPs, these two labels were compared with respect to sensitivity, reproducibility and ease of handling. Furthermore, it was shown that a sequence of metal oxidation, reduction followed by stripping via differential pulse voltammetry [2, 8] is highly suitable for a biosensor concept providing desirable low limits of detection.

3.2 Experimental Section

3.2.1 Materials and Instruments

The biotinylated capture antibody (polyclonal proBNP sheep-IgG-biotin), antigen (AG, NT-proBNP (1-76) amid) in buffer or human serum, probe antibody (monoclonal NTproBNP mouse-IgG) and probe antibody-modified gold nanoparticles (AB-AuNPs) were provided by Roche Diagnostics GmbH, Mannheim, Germany. Citrate capped silver nanospheres ($d=50$ nm, 0.022 mg·mL⁻¹) were purchased from nanoComposix (www.nanocomposix.com). Hydrochloric acid (HCl, 0.1 M, 1 M), sodium chloride (NaCl, *p.a.*), disodium hydrogen phosphate (Na₂HPO₄·2 H₂O, *p.a.*) and potassium dihydrogen phosphate (KH₂PO₄, *p.a.*) were ordered from Merck (www.merckmillipore.com). Bovine serum albumin (BSA, >96%) and Tween 20 (>97%) were supplied from Sigma Aldrich (www.sigmaaldrich.com). Potassium chloride (KCl, *p.a.*) was

obtained from Roth (www.carlroth.com). 4-(2-hydroxyethyl)-1-piperazineethanesulfonic acid (HEPES, $\geq 99\%$) was acquired from VWR (de.vwr.com) and sodium hydroxide (NaOH, 1 M) was bought from Labochem international (www.labochem.de).

HEPES buffer consisted of 10 mM HEPES in double-distilled water (ddH₂O) and was adjusted to a pH of 7.4. HEPES blocking buffer was prepared by addition of 0.1% (w/v) BSA to this HEPES buffer. Phosphate buffered saline (PBS) consisted of 137 mM NaCl, 2.7 mM KCl, 38 mM Na₂HPO₄·2 H₂O and 12 mM KH₂PO₄ in dd H₂O with a pH of 7.4. For PBST washing buffer 0.05% (w/v) Tween 20 were added to this PBS. PBS blocking buffer was prepared by addition of 1% (w/v) BSA to the PBS.

All electrochemical measurements were performed using screen-printed carbon electrodes bare (DRP-110) or with streptavidin coated working electrode (DRP-110STR, both: Metrohm AG, www.dropsens.com) and an EmStat blue potentiostat with corresponding software (PalmSens, www.palmsens.com). For nanoparticle modification, the ThermoMixer comfort (Eppendorf, online-shop.eppendorf.de) was used. A Plate reader Synergy Neo2 Hybrid Multi-Mode Reader from Bio-Tek Instruments (BioTek Instruments Inc., www.biotek.de), a Malvern Zetasizer Nano-ZS (www.malvern.com) and a 120 kV Philips CM12 (www.fei.com) transmission electron microscope were employed for characterization of the modified AgNPs.

3.2.2 Electrochemical Detection of Gold and Silver Nanoparticles

For the electrochemical detection of both metallic nanoparticles (gold and silver), 10 μ L of the variously concentrated NP solutions (diluted in 10 mM HEPES buffer, pH 7.4) were dried on top of the working electrode of the SPCE (DRP-110). Immediately afterwards, 50 μ L of 0.1 M HCl for the gold measurement or 0.1 M KCl for silver respectively, were added and the electrochemical measurement was started. The measurement procedure consisted of a pretreatment and the actual differential pulse voltammetry. For gold nanoparticles, a voltage of 1.25 V was applied for 60 s, then DPV was performed from 1.25 V to 0 V with $t_{\text{puls}}=50$ ms, $E_{\text{step}}=10$ mV, $E_{\text{pulse}}=80$ mV, and scan rate= 20 mV·s⁻¹. For silver nanoparticles an equivalent, but slightly different procedure was used. As pretreatment, a voltage of 1.25 V was applied for 60 s, then -0.8 V for 30 s. The DPV was recorded from -0.25 V to 0.25 V with same settings.

3.2.3 Modification of Silver Nanoparticles

For the AgNP modification, a modified procedure of Szymanski *et al.* [23] was utilized. A volume of 1 mL of AgNP stock solution ($0.02 \text{ mg}\cdot\text{mL}^{-1}$) was centrifuged for 10 min at 10,000 g. The supernatant was discarded and the pellet resuspended in 1 mL 10 mM HEPES (pH 7.4) with different amount of probe antibody. After incubation at room temperature (rt) with gentle mixing (350 rpm) for 2 h in the dark, the nanoparticles were centrifuged once again for 10 min at 10,000 g. The supernatant was discarded and the pellet resuspended in 1 mL 10 mM HEPES (pH 7.4) or HEPES blocking buffer (10 mM HEPES+0.1% (w/v) BSA, pH 7.4). For characterization of those particles, UV/Vis measurements were performed first. Four AgNP solutions, modified with 1, 5, 10 and 20 μg AB in 10 mM HEPES (pH 7.4) were adjusted to the same concentration (according to maximum absorbance). Then, 200 μL of each solution were pipetted into a transparent 96 well microtiter plate (Greiner, shop.gbo.com) and the maximum absorbance at 340 nm was measured. After addition of 50 μL 2 M NaCl and mixing for 2 min, the maximum absorbance was measured once again. Four additional AgNP solutions were modified with 1, 5, 10 and 20 μg AB in HEPES blocking buffer (10 mM HEPES+0.1% (w/v) BSA, pH 7.4). These blocked probe AB-modified AgNPs (AB-AgNPs) were used for all further experiments. The characterization was completed by dynamic light scattering measurements at 25 °C in disposable PMMA cuvettes (semi-micro), TEM imaging and the performance of the bioassay with 100 $\text{ng}\cdot\text{mL}^{-1}$ antigen (in 50 mM PBS, pH 7.4) concentration.

3.2.4 Performance of the Bioassay

Prior to use, the SPCEs (DRP-110STR) were washed three times with 50 μL 50 mM PBS buffer (pH 7.4). For capture AB immobilization, 10 μL biotinylated capture AB ($25 \mu\text{g}\cdot\text{mL}^{-1}$ in 50 mM PBS, pH 7.4) were pipetted onto the working electrode. After incubation in water-saturated atmosphere for 1 h at room temperature, the solution was removed and the electrode was washed three times with 50 μL PBST (50 mM PBS+0.05% (w/v) Tween 20, pH 7.4). After drying under nitrogen flow to prevent uncontrolled spreading of the next liquid on the electrode, blocking of the electrode was performed with 10 μL PBS blocking buffer (50 mM PBS+1% (w/v) BSA, pH 7.4) with analogue incubation, washing and drying. This was followed by incubation for 1 h at room temperature with 10 μL AG ($0\text{--}3000 \text{ ng}\cdot\text{mL}^{-1}$ in 50 mM PBS, pH 7.4). After washing and drying as described above, the WE was incubated for 1 h at room temperature with 10 μL mNP-labeled probe AB ($7.1 \text{ ng}\cdot\text{mL}^{-1}$ AuNP-tagged probe AB or $20 \mu\text{g}\cdot\text{mL}^{-1}$ probe

AB-modified AgNP in 10 mM HEPES, pH 7.4). Due to different concentration data given by the manufacturer, dilutions of AB-AuNP and AB-AgNP cannot be given in a consistent form. However, this dissimilar approach did not interfere with assay optimizations. Afterwards, the electrodes were washed three times with 50 μ L PBST (50 mM PBS+0.05% (w/v) Tween 20, pH 7.4), 50 mM PBS (pH 7.4) and ddH₂O, respectively. Directly prior to the electrochemical measurement, the electrode was dried under nitrogen flow and the three-electrode area was covered with 50 μ L of a 0.1 M HCl or KCl, respectively. The electrochemical measurement was performed as described in section 3.2.2.

3.3 Results and Discussion

3.3.1 Electrochemical Detection of Metallic Nanoparticles

For the electrochemical detection of both kinds of metallic nanoparticles, already published procedures were slightly adjusted. For the user, sensitive AuNP detection is a two-step process, sensitive detection of AgNP can be a simple one-step process. The electroanalytical strategy is in both cases a sequence of oxidation and reduction reactions designed to optimize the detection efficacy for the respective metal. The processes on the electrode surface are shown in Figure 3.2. The gold nanoparticle detection (a) was discussed in more detail by La Escosura-Muñiz *et al.* [8]. Through the biochemical reaction, the AuNPs are immobilized on the working electrode of the SPCE. After addition of hydrochloric acid by the user, the particles dissolve upon oxidation at 1.25 V. Hereby, a gold chlorido complex forms near the electrode surface. The reduction of bound Au³⁺ ions at 0.25 V is monitored by DPV. The hydrochloric acid is inevitable for the initial oxidation of the very stable AuNPs, because the complex is only formed at a pH around one.

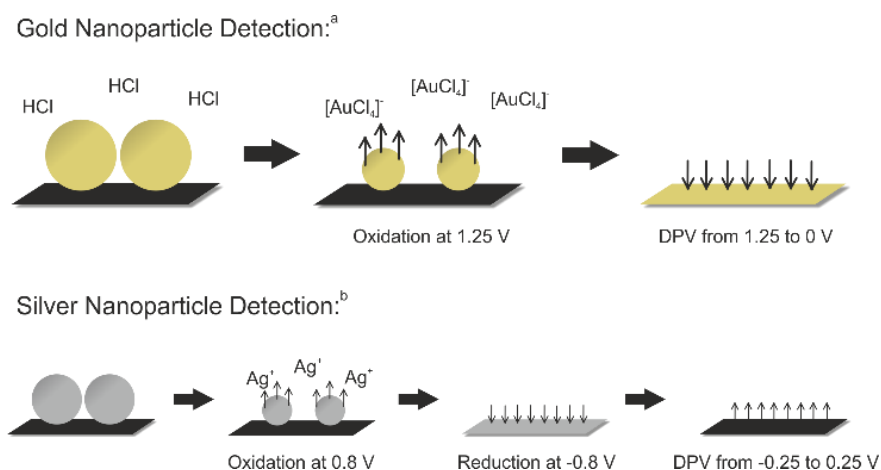


Figure 3.2. Schematic (not to scale) representation of electrochemical detection of AuNPs and AgNPs at a SPCE. (a) AuNP detection is performed in a two-step process: After immobilization of the AuNPs on top of the carbon working electrode through the biochemical reaction, HCl is added and the AuNPs are dissolved via oxidation at 1.25 V, forming a gold chlorido complex. The following reduction of Au^{3+} ions near the surface is measured by DPV from 1.25 to 0 V. (b) AgNPs detection can be performed in a one-step process. After immobilization of the AgNPs on the carbon working electrode surface through the biochemical reaction, a mere sequence of varying potentials leads to their sensitive quantification: the AgNPs are oxidized in presence of KCl at 1.25 V and AgCl precipitates immediately on the surface. Then, the Ag^+ ions are reduced at -0.8 V upon formation of a silver layer. The following oxidation is monitored by DPV from -0.25 to 0.25 V. (Note, KCl was added here as a separate reagent, but can be used as a dried reagent in a final sensor set-up)

For the silver nanoparticle detection (Figure 3.2 b) an equivalent but slightly more complex approach was used [2]. Here, the AgNPs dissolve by oxidation at 1.25 V after immobilization through the biochemical reaction. Due to the higher instability of silver compared to gold, already 0.8 V would be enough to oxidize the bare nanoparticles. However, the presence of proteins on the NP surface requires a higher potential to clean the NP surface and thus get a measurable DPV signal. The Ag^+ ions then form an AgCl precipitate on the electrode surface with the present chloride, which hinders the diffusion away from the electrode surface [5]. This is followed by a reduction at -0.8 V to form a silver layer, which penetrates into the pores of the electrode material. Then, the oxidation around 0.025 V is monitored by DPV. The additional pretreatment step renders the electrochemical detection considerably more sensitive and sharper peaks are obtained [18]. The main advantage of silver over gold is that no addition of hydrochloric acid is needed due to its higher chemical instability. While in this proof-of-principle, KCl was added separately, it can be used as a dry reagent in the final test enabling the one-step analysis in the future.

As proof of concept, differential pulse voltammetry was performed with both different mNPs. A concentration dependence of peak area and height was found (Figure S3.1). Due to marginal smaller errors, the peak area was used for all following data evaluation. The plot of peak area against NP concentration shows the same course for both metals and is shown exemplary for AgNPs in the supplementary information (Figure S3.2). First, the signal increases linearly with the amount of NP on the surface, while a constant value is reached after saturation of the electrode surface. This shows that the DPV detection method can be used for both, gold and silver nanoparticles.

3.3.2 Characterization of Modified Silver Nanoparticles

Purchased silver nanoparticles were modified with different amounts of probe AB to find the optimal loading density. UV/Vis analysis was performed to prove the passive adsorption of AB to AgNPs worked and see the stabilizing effect of the proteins [2]. In high ionic strength media, bare NPs tend to aggregate and in consequence, their color changes from yellow to transparent. For the different modifications (with 1 to 20 $\mu\text{g}\cdot\text{mL}^{-1}$ probe AB), the maximum absorbance after addition of 2 M NaCl was divided by the original maximum value. Non-blocked particles had to be used for this study, since AB-AgNPs would not show any signal change after blocking. The ratio of both maxima, shown in Figure 3.3 a, reaches one when 10 μg AB are used in the modification and stays constant for higher amounts. This means, that a minimum modification concentration of 10 $\mu\text{g}\cdot\text{mL}^{-1}$ is needed to preserve the NPs from agglomeration, *i.e.* to cover the NP surface completely. In the DLS measurements (Figure 3.3 b) it can be seen that the hydrodynamic diameter (d_H) and Polydispersity Index (Pdl) decrease until a constant value of around 75 nm and 0.160, respectively, are reached for AB-AgNPs modified with 10 μg of probe AB. A complete coverage of the surface with ABs decreases the overall size and increases uniformity, because less BSA adheres to the nanoparticle during blocking. The d_H increases by about 25 nm compared to the bare NPs (52 nm, given by the manufacturer) due to protein uptake.

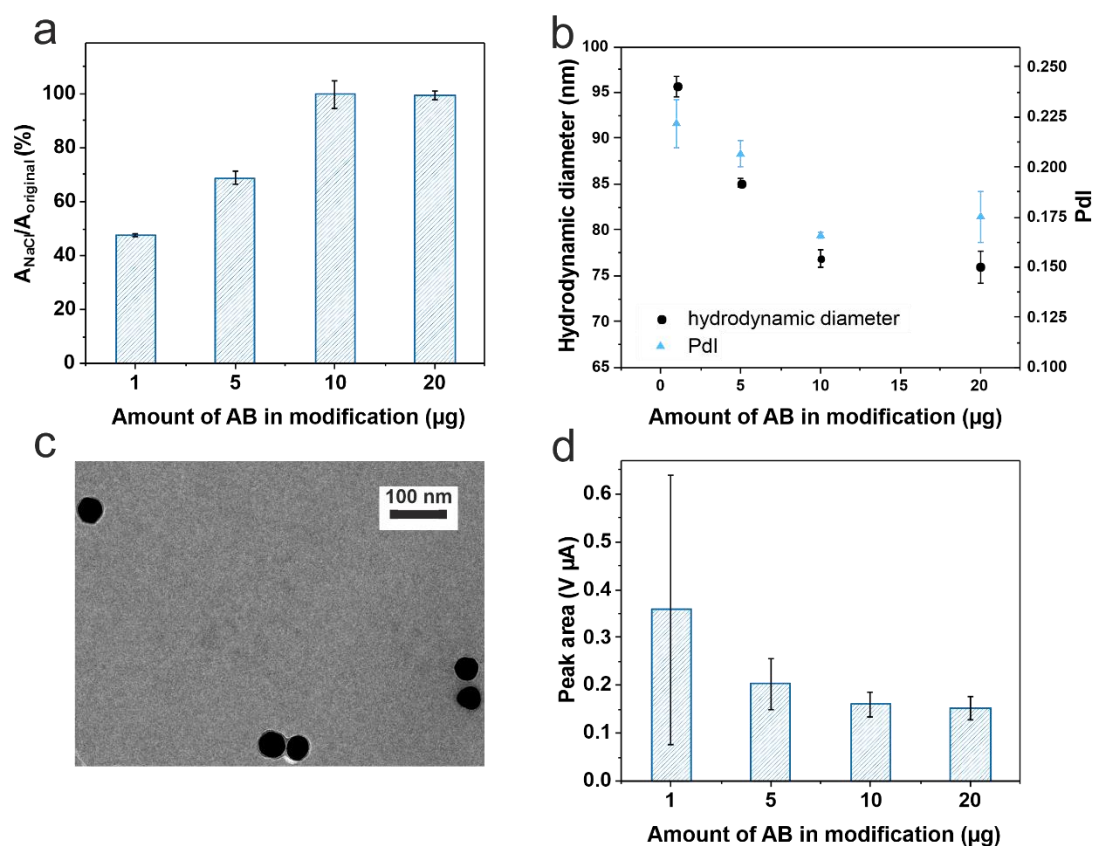


Figure 3.3. (a) Plot of the ratio of maximum absorbance in presence of 2 M NaCl to the maximum absorbance of the pure AgNP solution against the amount of probe AB used in the modification process. Non-blocked AB-AgNPs were used for this measurement. Error bars represent mean values $\pm 1\sigma$ and were calculated based on three parallel measurements ($n=3$). (b) Change of hydrodynamic diameter (black) and PDI (blue) of blocked AB-AgNPs with changing amount of probe AB. Error bars represent mean values $\pm 1\sigma$ and were calculated based on three parallel measurements ($n=3$). (c) Exemplary TEM image of the blocked AB-AgNP modified with 10 μg probe AB, scale bar represents 100 nm. (d) Plot of peak area of the bioassay using a constant AG concentration of 100 $\text{ng}\cdot\text{mL}^{-1}$ against the amount of probe AB used in the modification process of AgNPs. Error bars represent mean values $\pm 1\sigma$ and were calculated based on three parallel measurements on three different SPCEs ($n=3$).

The TEM images (Figure 3.3 c) show that the AgNP core size is not affected by the modification procedure and no aggregates are formed. The differently modified AB-AgNPs were then used in the bioassay with a constant AG concentration of 100 $\text{ng}\cdot\text{mL}^{-1}$ (Figure 3.3 d). With increasing amount of probe AB, the peak area decreases slightly, but the standard deviations show a huge improvement. This proposes an increased uniformity of the NPs with increasing surface coverage. In the following, AgNPs modified with 10 μg probe AB were used, since their surface is completely covered and they show excellent uniformity.

Since silver nanoparticles are known to be quite unstable due to aggregation and oxidation, a stability study was performed next. DLS measurements and the bioassay with a constant AG concentration were performed over eight weeks after modification (Figure 3.4). The hydrodynamic diameter and Pdl decrease minimally within the first days after modification (a). This drop of d_H by 8 to 10 nm in the first days can be seen for blocked and non-blocked AB-AgNPs (Figure S3.3 a). Both AB-AgNPs reach a constant hydrodynamic diameter after ten days. This matches the theoretical value, which was estimated based on the hydrodynamic diameter of probe AB [24] $d_H(AB) \approx 10$ nm and nanoparticle $d_H(AgNP) \approx 52$ nm as follows:

$$d_H(AB - AgNP) = d_H(AgNP) + 2 \cdot d_H(AB) = 72 \text{ nm} \quad (3.1)$$

Since BSA blocks vacancies on the particle surface and is smaller than the AB [25], its presence does not influence the hydrodynamic diameter. Control AgNPs in HEPES blocking buffer (10 mM HEPES+0.1% (w/v) BSA) showed a significantly smaller hydrodynamic diameter of around 65 nm directly after modification, which did not change in the course of ten days (Figure S3.4). This suggests that the decrease of hydrodynamic diameter is due to the slow release of loosely attached antibody on the particle until a stable layer is formed. In absence of antibodies, this equilibrium is reached considerably faster. However, the modified nanoparticles are stable against aggregation for at least two months.

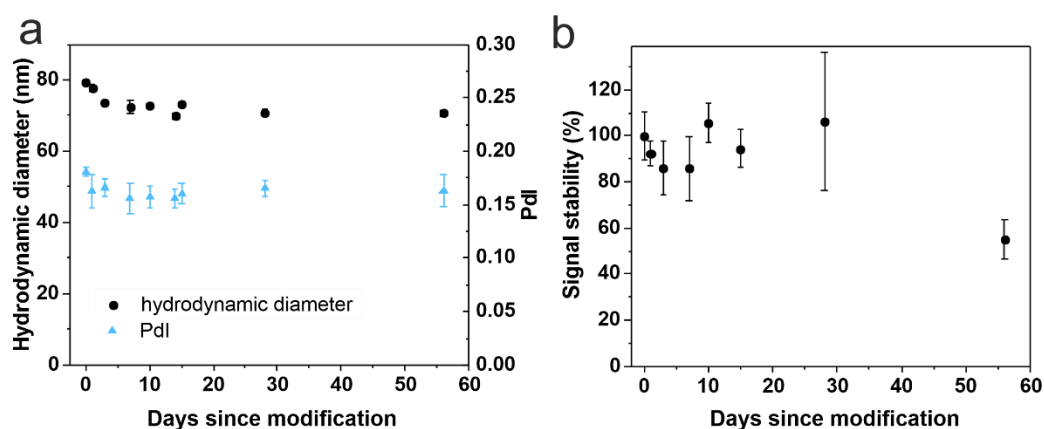


Figure 3.4. (a) Change of hydrodynamic diameter (black) and Pdl (blue) of AB-AgNPs (modified with $10 \mu\text{g}$ AB, blocked with BSA) over 56 days after modification. Error bars represent mean values $\pm 1\sigma$ and were calculated based on three parallel measurements ($n=3$). (b) Stability of the electrochemical signal of the bioassay using a constant AG concentration of $100 \text{ ng}\cdot\text{mL}^{-1}$ over 56 days. Peak area was normalized to the signal right after the modification. Error bars represent mean values $\pm 1\sigma$ and were calculated based on three parallel measurements on three different SPCEs ($n=3$).

Application of the prepared and stored AB-AgNPs in the bioassay (Figure 3.4 b) shows the stability of the AB-AgNP against oxidation by air oxygen as well as the functionality of the tagged probe ABs, since a constant signal can only be obtained if both are intact. Specifically, signals do not change within the margin of error observed for a period of 4 weeks. At day 30, large error bars were obtained. It could obviously be a manual handling error; however, it is more likely that this indicates the beginning of the AB-AgNP degradation. This reduces the uniformity of the labeled probe AB, and higher signal variation occurs. With progressing deterioration, the uniformity of the particles increases again and the error bar decreases. After eight weeks, the peak area drops to 50% of the original value. This indicates that the overall assay and signal enhancement strategy is rugged, but for final application, further studies are needed to increase the storage stability of the particles. The short-term stability of non-blocked AB-AgNPs was also tested (Figure S3.3 b). For short-term stability, blocking with BSA made no significant difference. However, to optimize long-term stability and avoid any unspecific binding in the final application, the blocked AB-AgNPs were used for all further measurements.

3.3.3 Comparison of Gold and Silver Nanoparticles as Label in an Electrochemical Sandwich Assay

To be able to compare both mNP labels a sandwich assay was developed in the following (Figure 3.1). The used antibodies (biotinylated polyclonal capture AB and AuNP-labeled monoclonal probe AB) are included in a commercially available NT-proBNP test by Roche Diagnostics [26]. The same probe AB was used for the modification of AgNPs. Therefore, the specificity and binding efficacy of this AB pair was adopted without further tests. First, different techniques to immobilize the AG on the working electrode were tested using AuNPs (Figure S3.5 a). No gold signal at 0.25 V was obtained neither for a direct adsorption of the AG, nor for a covalent binding of the capture AB using 1-Ethyl-3-(3-dimethylaminopropyl)-carbodiimide (EDC)/*N*-hydroxysuccinimid (NHS) chemistry. Adsorption processes are highly dependent on the protein-electrode combination, which is used. In this case, the AG was washed away even after incubation overnight, since the interaction was too weak. The covalent AB immobilization was monitored via impedance measurements (Figure S3.6): The charge-transfer resistance (R_{CT} , intercept with x-axis) increases after addition of pyrene butyric acid (PyBA, red), which was used as anchor moiety, due to coverage of the electrode surface. The R_{CT} increased even further, after binding of capture AB in the last step (blue). In the negative

control (green), pure buffer was added and no change of the impedance spectrum was seen. This shows that the covalent AB immobilization itself was successful. The absence of a gold signal could be due to the blocking of the electrode by the PyBA and the increased distance between NP label and electrode surface. Thus, a third approach exploiting streptavidin/biotin binding on purchased streptavidin-functionalized electrodes (DRP-110STR) was performed. The streptavidin is not coated on top of the electrode, but rather included in the conductive material. With this method, the AG was bound to the electrode and the presence of gold nanoparticles was measured at 0.25 V due to decreased NP-electrode distance and blocking of the electrode. In the next step, the capture AB concentration was varied and an optimal concentration of $25 \mu\text{g}\cdot\text{mL}^{-1}$ was found (Figure S3.5 b). The working electrode seems to be completely covered and further increasing the capture AB concentration did not change the signal. Moreover, different dilutions of the purchased AuNP-tagged probe AB solutions were used for the bioassay (Figure S3.7). Due to a drastically higher signal, the probe ABs were used in a 1:10 dilution. Using the AuNP solution without any dilution worsened the signal-to-noise ratio (S/N) due to an increase in background. The AB-AgNP solution was used without further dilution. With these optimized parameters, the bioassay was performed using AuNPs and AgNPs as label. Prior to addition of a new solution, the electrodes were dried under nitrogen flow. Since denaturation of biomolecules upon drying is a commonly known problem [27], control experiments without drying in between all assay steps were carried out (Figure S3.8). The electrochemical signal decreases by around 40% with drying steps included. However, the relative error was reduced from 17% to 7% due to prevention of uncontrolled spreading of the solution on the electrode. In order to optimize reproducibility of the assay, drying was included in the assay procedure for all shown experiments. For both labels, the bioassay was performed using various AG concentrations. Exemplary differential pulse voltammograms are shown in Figure S3.9. The silver peaks (b) have a considerably smaller full-width at half maximum compared to gold (a), which is due to the additional step in the detection. Moreover, the signal of the electrochemically more active silver arises at a ten-time smaller potential. This is always beneficial considering interferences in biological samples.

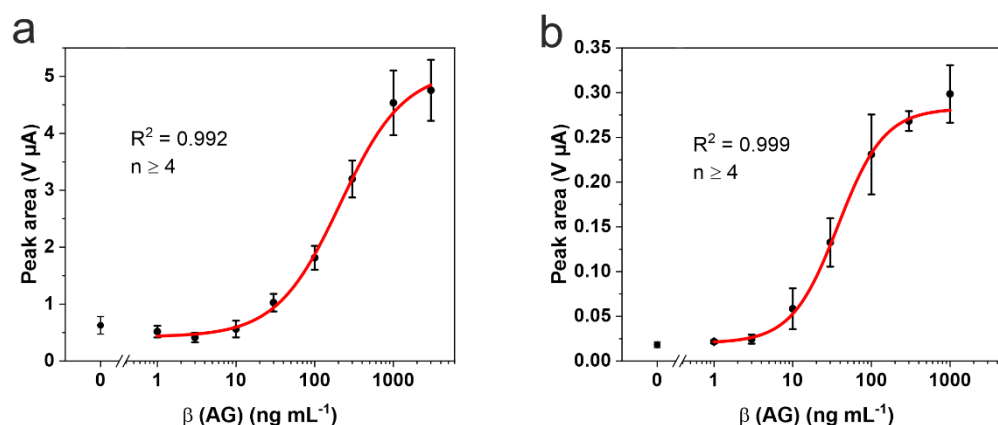


Figure 3.5. Plot of peak area against logarithm of antigen concentration with logistic fit (red line) and corresponding parameters for (a) gold and (b) silver nanoparticles as label in the proof-of-principle bioassay. Standard deviations were calculated based on five parallel measurements on five different SPCEs, while outliers were removed after Q-test (confidence interval 95%). Error bars represent mean values $\pm 1\sigma$ ($n \geq 4$).

In the plot of the peak area against logarithm of AG concentration, a sigmoidal binding curve can be seen for both labels (Figure 3.5). The limit of detection was calculated using the logistic fit parameter for the lower border $A1$ and the standard deviation of the blind $SD(blind)$:

$$LOD = A1 + 3 \cdot SD(blind) \quad (3.2)$$

A concentration value of $26 \text{ ng} \cdot \text{mL}^{-1}$ was calculated based on the logistic fit for AuNPs. This was improved by a factor of six by the use of AgNPs, which show a LOD of $4.0 \text{ ng} \cdot \text{mL}^{-1}$. For both labels, the mean error of all measurements is 17% and the dynamic range extends over nearly two orders of magnitude. The bioassay using gold is easy to perform and provides reliable results. However, the addition of hydrochloric acid is cumbersome considering a future POC application. The AgNP assay shows an overall better analytical performance accompanied with the increased simplicity as no acid is needed. Since Cl^- is contained in blood plasma (97 to 107 mM [28]) or can be stored within the sensor as dry reagent, no second user-step is needed rendering it to the far more favorable POC format.

3.3.4 Application of AgNPs as Label for NT-proBNP Quantification in Serum

Finally, demonstrating its applicability in a complex biological matrix, the AgNP bioassay was tested with real serum samples, specifically analyses were performed in human serum samples, spiked with different amounts of NT-proBNP (Figure 3.6).

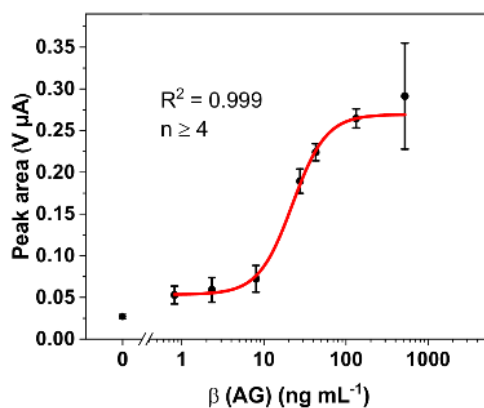


Figure 3.6. Plot of peak area against logarithm of antigen concentration in spiked human serum samples with logistic fit (red line) and corresponding parameters. Standard deviations were calculated based on five parallel measurements on five different SPCEs, while outliers were removed after Q-test (confidence interval 95%). Error bars represent mean values $\pm 1\sigma$ ($n \geq 4$).

Most of the parameters are similar to those of the silver bioassay in buffer: the curve shape and with it, the dynamic range. The calculated LOD of $4.7 \text{ ng}\cdot\text{mL}^{-1}$ is marginally higher due to background adsorption of serum proteins. However, due to an overlap of error bars of lowest concentrations, the practical LOD should be around $10 \text{ ng}\cdot\text{mL}^{-1}$. The mean error of 15% is even slightly better. Physicians use a threshold of $1 \text{ ng}\cdot\text{mL}^{-1}$ NT-proBNP in blood to assess severity of heart failure and risk of hospitalization [29]. This study shows that a one-step biosensor assay based on AgNPs has the potential to serve in this diagnostic setting and furthermore that AgNPs can be used to detect a marker six times more sensitive than AuNPs using the same assay principle and setup.

3.4 Conclusion

Two bioassays with metal nanoparticles for signal enhancement were investigated with respect to their applicability towards point-of-care sensing. In the case of AuNPs, these excel due to an excellent analyte concentration range, *i.e.* from 25 to $1000 \text{ ng}\cdot\text{mL}^{-1}$ with very good S/N. Moreover, it is well-known that gold nanoparticles are easy to modify and stable over a longer period of time [30]. However, due to their greater electrochemical activity, AgNPs provide a six-times more sensitive assay. Most importantly, the AgNP bioassay is significantly simpler and hence more adaptable to a POC setting as no further addition of any solution is necessary once it is used in a biological sample. Of importance here is also the long-term storage stability of the probe antibody-modified AgNPs. Due to its many advantages, the use of AgNPs in

research increased drastically over the last years. Recently, researchers use it for surface modification and labeling in optical sensing, for example via SERS [31] or UV/Vis analysis [32], as well as in electrochemical sensing [33, 34]. This supports our finding that they are highly promising and can lead the way into a new generation of mNP sensors.

3.5 References

1. Wang J. Electrochemical biosensors: towards point-of-care cancer diagnostics. *Biosens Bioelectron.* 2006;21:1887–92. doi:10.1016/j.bios.2005.10.027.
2. Hao N, Li H, Long Y, Zhang L, Zhao X, Xu D, Chen H-Y. An electrochemical immunosensing method based on silver nanoparticles. *Journal of Electroanalytical Chemistry.* 2011;656:50–4. doi:10.1016/j.jelechem.2011.01.029.
3. Sepunaru L, Plowman BJ, Sokolov SV, Young NP, Compton RG. Rapid electrochemical detection of single influenza viruses tagged with silver nanoparticles. *Chem Sci.* 2016;7:3892–9. doi:10.1039/c6sc00412a.
4. Dequaire M, Degrand C, Limoges B. An electrochemical metalloimmunoassay based on a colloidal gold label. *Anal Chem.* 2000;72:5521–8. doi:10.1021/ac000781m.
5. Ting BP, Zhang J, Gao Z, Ying JY. A DNA biosensor based on the detection of doxorubicin-conjugated Ag nanoparticle labels using solid-state voltammetry. *Biosens Bioelectron.* 2009;25:282–7. doi:10.1016/j.bios.2009.07.005.
6. Cais M, Dani S, Eden Y, Gandolfi O, Horn M, Isaacs EE, et al. Metalloimmunoassay. *Nature.* 1977;270:534–5. doi:10.1038/270534a0.
7. Wang J. Nanomaterial-based electrochemical biosensors. *Analyst.* 2005;130:421–6. doi:10.1039/b414248a.
8. La Escosura-Muñiz A de, Parolo C, Maran F, Mekoçi A. Size-dependent direct electrochemical detection of gold nanoparticles: application in magnetoimmunoassays. *Nanoscale.* 2011;3:3350–6. doi:10.1039/c1nr10377f.
9. Geagea R, Aubert P-H, Banet P, Sanson N. Signal enhancement of electrochemical biosensors via direct electrochemical oxidation of silver nanoparticle labels coated with zwitterionic polymers. *Chem Commun (Camb).* 2015;51:402–5. doi:10.1039/c4cc07474b.
10. Cai H, Xu Y, Zhu N, He P, Fang Y. An electrochemical DNA hybridization detection assay based on a silver nanoparticle label. *Analyst.* 2002;127:803–8. doi:10.1039/b200555g.

11. Pumera M, Aldavert M, Mills C, Merkoçi A, Alegret S. Direct voltammetric determination of gold nanoparticles using graphite-epoxy composite electrode. *Electrochimica Acta*. 2005;50:3702–7. doi:10.1016/j.electacta.2005.01.035.
12. Karadeniz H, Erdem A, Caliskan A, Pereira CM, Pereira EM, Ribeiro JA. Electrochemical sensing of silver tags labelled DNA immobilized onto disposable graphite electrodes. *Electrochemistry Communications*. 2007;9:2167–73. doi:10.1016/j.elecom.2007.05.016.
13. Wang J, Polsky R, Xu D. Silver-Enhanced Colloidal Gold Electrochemical Stripping Detection of DNA Hybridization. *Langmuir*. 2001;17:5739–41. doi:10.1021/la011002f.
14. Taton TA, Mirkin CA, Letsinger RL. Scanometric DNA array detection with nanoparticle probes. *Science*. 2000;289:1757–60. doi:10.1126/science.289.5485.1757.
15. Li X, Scida K, Crooks RM. Detection of hepatitis B virus DNA with a paper electrochemical sensor. *Anal Chem*. 2015;87:9009–15. doi:10.1021/acs.analchem.5b02210.
16. Zhang J, Ting BP, Jana NR, Gao Z, Ying JY. Ultrasensitive electrochemical DNA biosensors based on the detection of a highly characteristic solid-state process. *Small*. 2009;5:1414–7. doi:10.1002/sml.200900073.
17. Kashefi-Kheyraadi L, Mehrgardi MA. Aptamer-conjugated silver nanoparticles for electrochemical detection of adenosine triphosphate. *Biosens Bioelectron*. 2012;37:94–8. doi:10.1016/j.bios.2012.04.045.
18. Szymanski M, Turner AP, Porter R. Electrochemical Dissolution of Silver Nanoparticles and Its Application in Metalloimmunoassay. *Electroanalysis*. 2010;22:191–8. doi:10.1002/elan.200900275.
19. Pollok NE, Rabin C, Walgama CT, Smith L, Richards I, Crooks RM. Electrochemical Detection of NT-proBNP Using a Metalloimmunoassay on a Paper Electrode Platform. *ACS Sens*. 2020;5:853–60. doi:10.1021/acssensors.0c00167.
20. Cunningham JC, Kogan MR, Tsai Y-J, Luo L, Richards I, Crooks RM. Paper-Based Sensor for Electrochemical Detection of Silver Nanoparticle Labels by Galvanic Exchange. *ACS Sens*. 2016;1:40–7. doi:10.1021/acssensors.5b00051.
21. Degregory PR, Tapia J, Wong T, Villa J, Richards I, Crooks RM. Managing Heart Failure at Home With Point-of-Care Diagnostics. *IEEE J Transl Eng Health Med*. 2017;5:2800206. doi:10.1109/JTEHM.2017.2740920.

22. Degregory PR, Tsai Y-J, Scida K, Richards I, Crooks RM. Quantitative electrochemical metalloimmunoassay for TFF3 in urine using a paper analytical device. *Analyst*. 2016;141:1734–44. doi:10.1039/c5an02386f.
23. Szymanski MS, Porter RA. Preparation and quality control of silver nanoparticle-antibody conjugate for use in electrochemical immunoassays. *J Immunol Methods*. 2013;387:262–9. doi:10.1016/j.jim.2012.11.003.
24. Mizutani N, Korposh S, Selyanchyn R, Wakamatsu S, Lee S-W. Application of a Quartz Crystal Microbalance (QCM) Twin Sensor for Selective Label-free Immunoassay to Simultaneous Antigen-antibody Reactions. *Sensors & Transducers Journal*. 2012;137:1–9.
25. Adel A, Nadia M, Mohamed O, Abdelhafidh G. Study of thermally and chemically unfolded conformations of bovine serum albumin by means of dynamic light scattering. *Materials Science and Engineering: C*. 2008;28:594–600. doi:10.1016/j.msec.2007.10.004.
26. Bertsch T, Dikkeschei B, Gurr E, Hayen W, Jørgensen B, Lotz J, et al. Development and calibration of a new point-of-care test for the determination of NT-proBNP in whole blood. *Clin Lab*. 2007;53:423–31.
27. Mensink MA, Frijlink HW, van der Voort Maarschalk K, Hinrichs WLJ. How sugars protect proteins in the solid state and during drying (review): Mechanisms of stabilization in relation to stress conditions. *Eur J Pharm Biopharm*. 2017;114:288–95. doi:10.1016/j.ejpb.2017.01.024.
28. Pfortmueller CA, Uehlinger D, Haehling S von, Schefold JC. Serum chloride levels in critical illness-the hidden story. *Intensive Care Med Exp*. 2018;6:10. doi:10.1186/s40635-018-0174-5.
29. Kim H-N, Januzzi JL. Natriuretic peptide testing in heart failure. *Circulation*. 2011;123:2015–9. doi:10.1161/CIRCULATIONAHA.110.979500.
30. Parak WJ, Gerion D, Pellegrino T, Zanchet D, Micheel C, Williams SC, et al. Biological applications of colloidal nanocrystals. *Langmuir*. 2003;14:R15-R27. doi:10.1088/0957-4484/14/7/201.
31. Zhao Y, Yamaguchi Y, Ni Y, Li M, Dou X. A SERS-based capillary sensor for the detection of mercury ions in environmental water. *Spectrochim Acta A Mol Biomol Spectrosc*. 2020;233:118193. doi:10.1016/j.saa.2020.118193.

32. Sheini A. Colorimetric aggregation assay based on array of gold and silver nanoparticles for simultaneous analysis of aflatoxins, ochratoxin and zearalenone by using chemometric analysis and paper based analytical devices. *Mikrochim Acta*. 2020;187:167. doi:10.1007/s00604-020-4147-5.
33. Vidal JC, Torrero D, Menés S, La Fuente A de, Castillo JR. Voltammetric sensing of silver nanoparticles on electrodes modified with selective ligands by using covalent and electropolymerization procedures. Discrimination between silver(I) and metallic silver. *Mikrochim Acta*. 2020;187:183. doi:10.1007/s00604-020-4139-5.
34. Bampakos D, Tsamis C, Kaltsas G. Multi-parameter paper sensor fabricated by inkjet-printed silver nanoparticle ink and PEDOT:PSS. *Microelectronic Engineering*. 2020;225:111266. doi:10.1016/j.mee.2020.111266.

3.6 Supporting Information

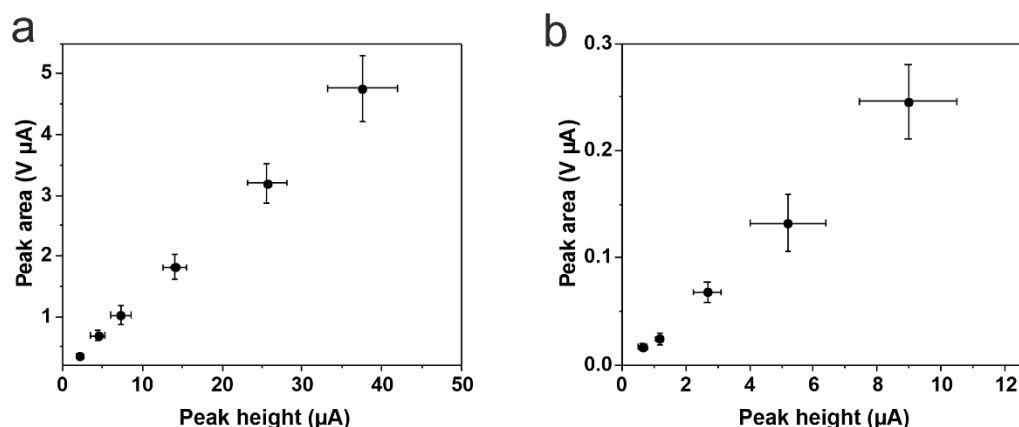


Figure S3.1. Correlation of peak height and area for the bioassay with (a) AuNPs and (b) AgNPs. Standard deviations of peak area and peak height were calculated based on five parallel measurements on five different SPCEs, while outliers were removed after Q-test (confidence interval 90%). Error bars represent mean values $\pm 1\sigma$ ($n \geq 4$). Each data point correlates to one AG concentration.

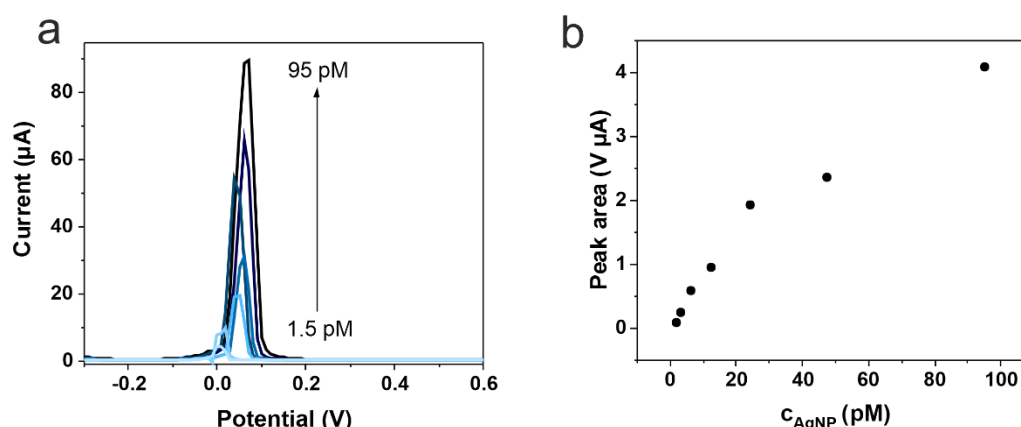


Figure S3.2. (a) Exemplary differential pulse voltammograms of differently concentrated AgNP solutions (1.5–95 pM, light blue to dark blue) dried on top of the WE of the SPCE DRP-110 without pretreatment and (b) plot of peak area against AgNP concentration. After drying of 10 μL AgNPs on the WE and addition of 50 μL of 0.3 M KCl, the following measurement parameters were applied: $E_{\text{step}}=10$ mV, $E_{\text{pulse}}=50$ mV, $t_{\text{puls}}=50$ ms, scan rate= 20 mV·s⁻¹. Since these were first try-outs, only single measurements were performed.

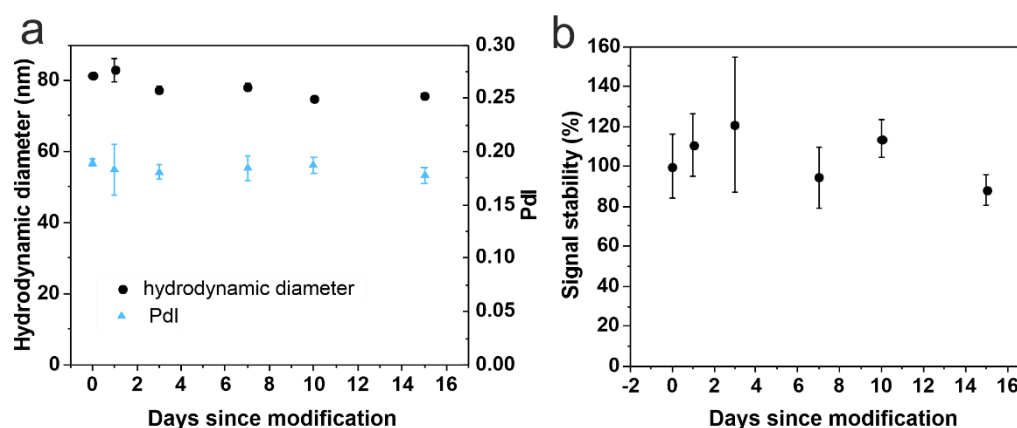


Figure S3.3. (a) Change of hydrodynamic diameter (black) and Pdl (blue) of non-blocked AB-AgNPs (modified with 10 μg AB in 10 mM HEPES, pH 7.4) over 16 days after modification. Error bars represent mean values $\pm 1\sigma$ ($n=3$). (b) Peak area of the bioassay using a constant AG concentration of 100 $\text{ng}\cdot\text{mL}^{-1}$ (in 50 mM PBS, pH 7.4) over 16 days. Error bars represent mean values $\pm 1\sigma$ and were calculated based on three parallel measurements on three different SPCEs ($n=3$).

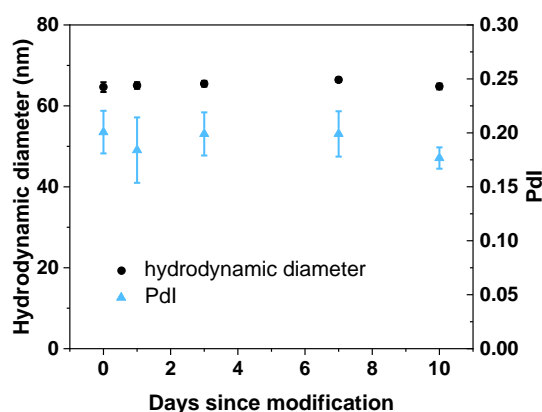


Figure S3.4. Change of hydrodynamic diameter (black) and Pdl (blue) of control AgNPs in HEPES blocking buffer (10 mM HEPES+0.1% (w/v) BSA, pH 7.4), prepared using the standard modification procedure described in the main part without AB, over 10 days after modification. Standard deviations were calculated based on three parallel measurements. Error bars represent mean values $\pm 1\sigma$ ($n=3$).

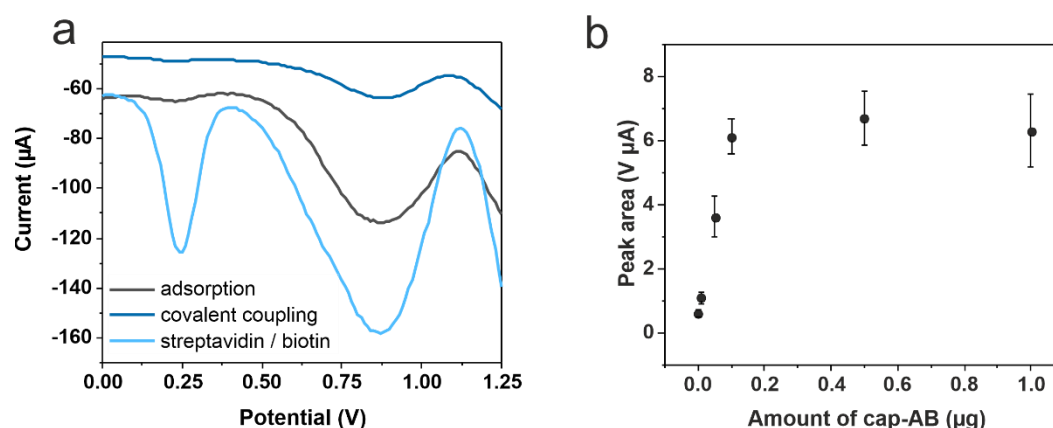


Figure S3.5. (a) Exemplary differential pulse voltammograms of different immobilization techniques for the sandwich labeled with AuNPs on the working electrode: adsorption means adsorption of the AG ($10 \mu\text{L}$, $1000 \text{ ng}\cdot\text{mL}^{-1}$ in 50 mM PBS, pH 7.4) overnight at $4 \text{ }^\circ\text{C}$ on the bare DropSens electrode (DRP-110). Covalent coupling was performed via incubating the WE of the DRP-110 with $2 \mu\text{L}$ pyrene butyric acid (5 mM in DMSO) for 1 h at rt, washing and incubating with $10 \mu\text{L}$ EDC/NHS ($10 \text{ mM}/25 \text{ mM}$ in 50 mM MES buffer, pH 6.0) for 1 h at rt. After washing, the WE was incubated with $10 \mu\text{L}$ capture AB ($50 \mu\text{g}\cdot\text{mL}^{-1}$ in 50 mM PBS, pH 7.4) for 2 h at rt. For streptavidin/biotin binding the streptavidin-coated WE of the SPCE (DRP-110STR) was incubated with the biontynylated capture AB ($10 \mu\text{L}$, $50 \mu\text{g}\cdot\text{mL}^{-1}$ in 50 mM PBS, pH 7.4) for 1 h at rt. Covalently and streptavidin/biotin modified electrodes were then incubated with AG ($10 \mu\text{L}$, $1000 \text{ ng}\cdot\text{mL}^{-1}$ in 50 mM PBS, pH 7.4) and AuNP-tagged probe AB ($7.1 \text{ ng}\cdot\text{mL}^{-1}$ in 50 mM HEPES, pH 7.4). (b) Plot of peak area of the AuNP bioassay against the amount of capture AB (cap-AB), used for the immobilization via streptavidin/biotin binding, measured with $1000 \text{ ng}\cdot\text{mL}^{-1}$ AG concentration in 50 mM PBS, pH 7.4. Error bars represent mean values $\pm 1\sigma$ and were calculated using three parallel measurements ($n=3$).

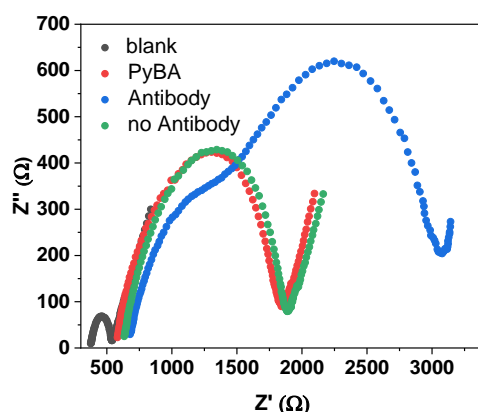


Figure S3.6. Exemplary impedance spectra of the DRP-110 electrodes in different stages of the covalent AB immobilization after washing with 50 mM PBS (pH 7.4). Covalent coupling was performed via incubating the WE of the DRP-110 with 2 μL pyrene butyric acid (PyBA, 5 mM in DMSO) for 1 h at rt, washing and incubating with 10 μL EDC/NHS (10 mM/25 mM in 50 mM MES buffer, pH 6.0) for 1 h at rt. After washing, the WE was incubated with 10 μL capture AB (150 $\mu\text{g}\cdot\text{mL}^{-1}$ in 50 mM PBS, pH 7.4) for 2 h at rt. Washing was performed three times with 50 μL of the corresponding buffer of the next step. Shown are the bare DRP-110 electrodes (blank, black), after incubation with PyBA (red) and afterwards direct covalent immobilization of antibody (blue) or after incubation with buffer as control (green). Impedance spectra were recorded in a two-electrode setup with 50 μL ferri-/ferrocyanide solution (10 mM of both substances in 100 mM phosphate buffer+100 mM KCl, pH 7.4) as mediator, $E_{AC}=5$ mV, from 0.1 Hz to 100 kHz. This data shows, that the immobilization via covering the electrode with pyrene butyric acid (PyBA, red) increases the charge-transfer resistance (R_{CT}). After activation with EDC/NHS and incubation with the capture AB (blue) R_{CT} increases significantly, while the control (green) showed no change. This leads to the assumption, that the covalent AB immobilization was successful.

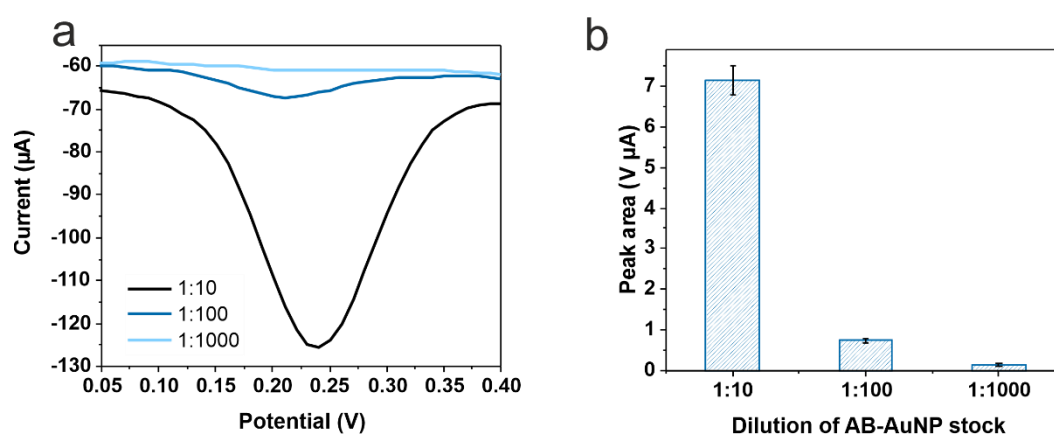


Figure S3.7. (a) Exemplary differential pulse voltammograms using different dilutions (1:10 to 1:1000, dark blue to light blue) of the AuNP-labeled probe AB (AB-AuNP, 70.8 $\text{ng}\cdot\text{mL}^{-1}$ in 50 mM HEPES, pH 7.4) in the bioassay with 1000 $\text{ng}\cdot\text{mL}^{-1}$ AG (in 50 mM PBS, pH 7.4) and (b) plot of the corresponding peak area against dilution of probe AB-AuNP stock. Error bars represent mean values $\pm 1\sigma$ and were calculated based on three parallel measurements ($n=3$).

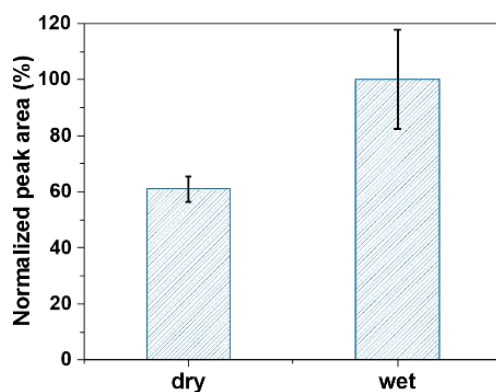


Figure S3.8. Comparison of peak area after performance of the bioassay using a constant AG concentration of $100 \text{ ng}\cdot\text{mL}^{-1}$ (in 50 mM PBS, pH 7.4) and AB-AgNPs ($20 \mu\text{g}\cdot\text{mL}^{-1}$ in 10 mM HEPES, pH 7.4) as described in the main text (dry) and without any drying of the electrode (wet). Peak area was normalized to the dry data. Error bars represent mean values $\pm 1\sigma$, which were calculated based on three measurements on separate DRP-110STR electrodes ($n=3$).

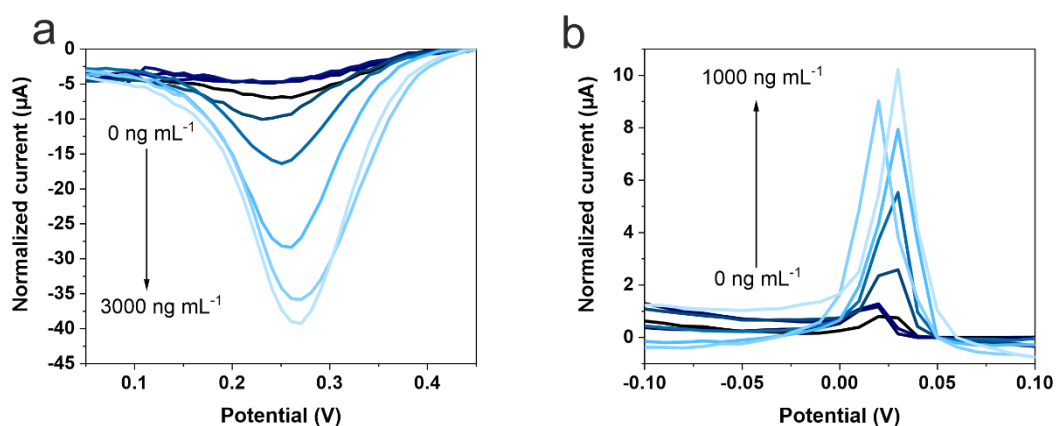
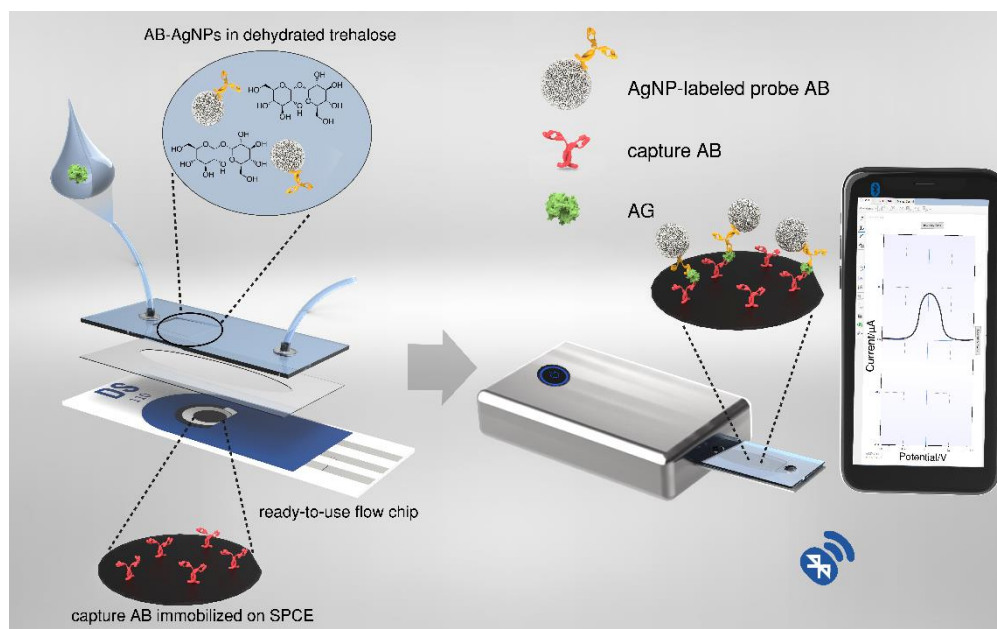


Figure S3.9. Exemplary differential pulse voltammograms of the bioassay using (a) gold and (b) silver nanoparticle-labeled probe AB for differently concentrated AG solutions (increasing from deep to light blue), current normalized with respect to the baseline.

4 Dry-reagent microfluidic biosensor for simple detection of NT-proBNP via Ag nanoparticles

Graphical Abstract



This chapter has been published.

Franziska Beck, Carina Horn, and Antje J. Baeumner, *Anal. Chim. Acta.* **2022**, 1191, 339375. DOI: <https://doi.org/10.1016/j.aca.2021.339375>.

Author contributions: AJB and FB developed the concept for this work. AJB and FB planned the experiments. FB did the experimental work and wrote the first draft of the manuscript. AJB and CH revised the manuscript. AJB is corresponding author.

Abstract

The diagnosis of many diseases requires monitoring of biomarker levels over a period of time instead of assessing their concentration only once. For example, in case of heart failure determination, the levels of NT-proBNP in blood vary so strongly amongst individuals, that the current procedure of one-time measurement in combination with clinical examination does not allow for accurate assessment of disease severity and progression. Our microfluidic biosensor addresses key characteristics of desirable home-tests, which include low limits of detection, small sample volume (less than 10 μL), simple detection strategies, and ready-to-go all-dried long-term stable reagents. Here, electrochemically superior silver nanoparticles were dried directly within the microfluidic channel in a matrix of trehalose sugar doped with Na_2SO_3 as oxygen scavenger. This successfully prevented AgNP oxidation and enabled dry and ready-to-use storage for at least 18 weeks. Based on this, laser-cut flow chips were developed containing all bioassay reagents needed in a ready-to-go dry format. An oxidation-reduction stripping voltammetry strategy was used for highly sensitive quantification of the AgNPs as electrochemical label. This microfluidic biosensor demonstrated limits of detection for NT-proBNP of $0.57 \text{ ng}\cdot\text{mL}^{-1}$ with a mean error of 6% ($n \geq 3$) in undiluted human serum, which is below the clinically relevant cut-off of 1 ng mL^{-1} . This practical approach has the potential to substitute commonly used lateral flow assays for various biomarkers, as it offers low patient sample volumes hence supporting simple finger-prick strategies well-known also for other electrochemical biosensors, and independence from the notorious variability in fleece fabrication.

Keywords

electrochemical biosensor, silver nanoparticle, microfluidic, blood analysis, differential pulse voltammetry

4.1 Introduction

Heart failure is a "global pandemic affecting at least 26 million people worldwide" with rising tendency [1]. The American Heart Association defines HF as "a complex clinical syndrome that can result from any structural or functional cardiac disorder that impairs the ability of the ventricle to fill or eject blood" [2]. In terms of diagnosis, clinical examinations dominate and are often paired with a detection of the HF marker NT-proBNP. The precursor propeptide proBNP is secreted due to myocardial wall stress upon volume or pressure overload. It is cleaved enzymatically forming BNP and NT-proBNP and both peptides are released into the blood stream. While BNP lowers the cardiac output and central venous pressure, NT-proBNP is biologically inert [3]. Although both peptides are initially present in equal concentrations, the NT-proBNP level is higher, since it is solely cleared passively from the circulation (half-life of 120 min vs. 20 min, respectively). Therefore, NT-proBNP concentration in blood is commonly used instead of BNP as measure for severity and progression of HF [4]. The combination of one-time measurements of NT-proBNP with clinical examination is challenging [5], as this is not a definite evidence for HF, and its level depends additionally on age, gender, race, disease, severity, comorbidities, and medication [3]. Therefore, it is difficult to assess one certain cut-off value, which is true for every patient, which makes a quantification of NT-proBNP concentration in blood necessary [6]. Up to now, the prognostically meaningful threshold used by physicians for chronic HF is approximately $1000 \text{ pg}\cdot\text{mL}^{-1}$. With a quantification of NT-proBNP levels over a longer period of time, a rising pattern could be identified in an early stage and predict an imminent negative outcome [4]. Therefore, at-home monitoring of NT-proBNP concentration in blood for patients at risk could be highly beneficial both for prevention and monitoring of therapy progress [7, 8]. Primary prevention of HF would decrease the number of incidents, while the improvement of medical care would lead to an increased survival rate. The final aim is to reduce incidents, mortality and hospitalization [5].

For home monitoring, it is inevitable to have a minimal sample demand, no sample preparation and preferably no processing steps other than sample addition. It is proposed here that microfluidics combined with electrochemical detection fulfill these requirements and show an enormous potential for miniaturization and POC testing [9, 10]. With respect to optimizing the sensitivity afforded by simple electrochemical transducers like the here used screen-printed carbon electrode, many researchers use nanomaterials, such as metallic nanoparticles either as

surface coating for the electrode or as label. They have unique (electro)chemical, physical, and optical properties, because their high surface-to-volume ratio and the more exposed crystalline planes compared to the bulk material accelerate mass transport [11]. We have thus developed previously an electrochemical assay in which silver nanoparticles serve as label [12]. The detection sandwich is immobilized on the working electrode of a SPCE. After covering of the three-electrode area with potassium chloride the presence of AgNPs on the electrode surface is measured by a sequence of oxidation and reduction reactions followed by differential pulse voltammetry [13]. This method is superior to the galvanic exchange assay process demonstrated by the Crooks research group [3, 14, 15], because no gold coating of the working electrode is necessary and the process is less diffusion dependent.

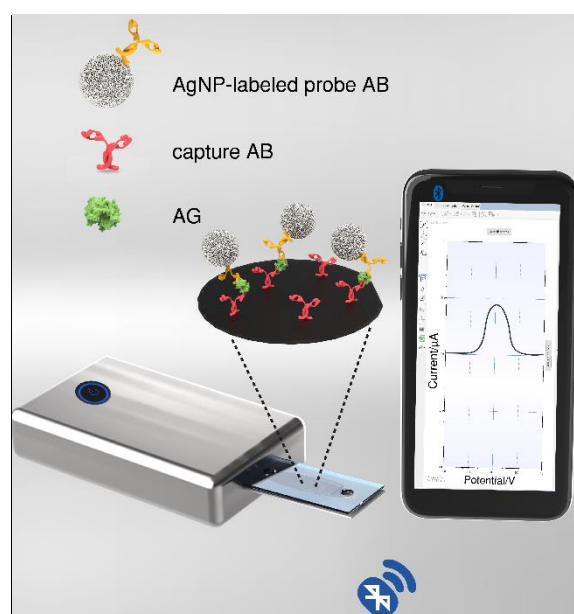


Figure 4.1. Schematic (not-to-scale) representation of the sandwich assay on the WE of a SPCE integrated in a microfluidic chip with AgNPs as label using a Bluetooth potentiostat and a smartphone for the measurement.

This assay showed high sensitivity and robustness, but the format was not suitable for point-of-care. Therefore, this assay principle [12] was combined with microfluidics (Figure 4.1) in order to automate and simplify the assay steps, and especially also to enable dry storage of all reagents, and increase sensitivity and reproducibility.

A prominent strategy of combining microfluidics and (electro)chemical analysis is the flow injection analysis (FIA), where a flow stream carries the analyte over the electrode surface [16]. FIA formats outperform the often time consuming and expensive standard analytical methods because they offer quantitative information with high precision, sensitivity and reliability.

Moreover, due to short analysis time and high sample throughput with minimal cost they are ideal for clinical analysis [11]. The here proposed simple microfluidic biosensor chip combines the LFA and FIA approaches with electrochemical detection and provides a strategy to include all reagents necessary in a dried format directly on chip (just as in an LFA) and apply the pumping regime of a FIA system. Our unique set-up enables in contrast to other published work the formation of the detection complex in flow right on the working electrode. In contrast, in competing methods using AgNPs as labels [3, 17], additional pipetting steps and/or wet chemicals are needed. In comparison to these others, our microfluidic assay can be used for home-monitoring, since it is simple to perform, *i.e.* no pipetting steps are necessary, and the chemicals can be stored in dry form over an extended time period. Of course, miniaturized pumps or strong capillary forces will in the future replace the pumps used within this work.

4.2 Experimental Section

4.2.1 Materials and Instruments

Biotinylated capture antibody (polyclonal proBNP sheep-IgG-biotin), antigen (NT-proBNP (1-76) amid) in buffer or human serum and probe antibody (monoclonal NTproBNP mouse-IgG) were provided by Roche Diagnostics GmbH, Mannheim, Germany. Citrate capped silver nanospheres ($d=50$ nm, 0.022 mg·mL⁻¹) were purchased from nanoComposix (www.nanocomposix.com). Sodium chloride (NaCl, *p.a.*), disodium hydrogen phosphate (Na₂HPO₄·2 H₂O, *p.a.*), sodium hydrogen carbonate (NaHCO₃, *p.a.*) and potassium dihydrogen phosphate (KH₂PO₄, *p.a.*) were ordered from Merck (www.merckmillipore.com). Bovine serum albumin (BSA, >96%), trehalose (D-(+)-trehalose dihydrate, ≥99%), L-ascorbic acid (AA, 99%) and Tween 20 (>97%) were supplied from Sigma Aldrich (www.sigmaaldrich.com). Potassium chloride (KCl, *p.a.*) was obtained from Roth (www.carlroth.com). 4-(2-hydroxyethyl)-1-piperazineethanesulfonic acid (HEPES, ≥99%) and sodium sulfite (Na₂SO₃, *p.a.*) were acquired from VWR (de.vwr.com) and sodium hydroxide (NaOH, 1 M) was bought from Labochem international (www.labochem.de). Polyethyleneterephthalat (PET) foil was ordered from GoodFellow (www.goodfellow.com). Double-sided adhesive tape (thickness=100 μm) was purchased from Roedel GmbH (www.roedel-gmbh.de), while PMMA (Plexiglas® XT) was supplied from Kunststoff Acryl Design GmbH (www.kad-group.de).

HEPES buffer consisted of 10 mM HEPES in ddH₂O and was adjusted to a pH of 7.4. HEPES blocking buffer was prepared by addition of 0.1% (w/v) BSA to this HEPES buffer. Phosphate buffered saline (PBS) consisted of 137 mM NaCl, 2.7 mM KCl, 38 mM Na₂HPO₄·2 H₂O and 12 mM KH₂PO₄ in ddH₂O with a pH of 7.4. For PBST washing buffer 0.05% (w/v) Tween 20 were added to this PBS. PBS blocking buffer consisted of PBS and 1% (w/v) BSA.

Electrochemical measurements were performed using screen-printed carbon electrodes, bare (DRP-110) or with streptavidin coated working electrode (DRP-110STR, both: Metrohm AG, www.dropsens.com) and an EmStat blue potentiostat with corresponding software (PalmSens, www.palmsens.com). For nanoparticle modification, the ThermoMixer comfort (Eppendorf, online-shop.eppendorf.de) was used. Flow chips were prepared using a laser cutter model VLS2.30 with CO₂ laser (30 W, λ=10.6 μm) from Universal Laser Systems, Arizona, USA. For plasma cleaning, the PlasmaFlecto 10 from Plasma Technology GmbH (Herrenberg, Germany) was used. The chip holder was manufactured in house and the LEGATO® 111 syringe pump, which was used for the microfluidic experiments, was purchase from kd Scientific (www.kdscientific.com).

4.2.2 Modification of Silver Nanoparticles

The silver nanoparticles were modified using a simple adsorption procedure, which was already optimized and the AB-AgNPs were characterized in a previous work [12]. Very briefly: a volume of 1 mL of AgNP solution (0.02 mg·mL⁻¹) was centrifuged for 10 min at 10,000 g. The supernatant was discarded and the pellet resuspended in 1 mL 10 mM HEPES (pH 7.4) with 10 μg probe antibody. After incubation at room temperature with gentle mixing (350 rpm) for 2 h in the dark, the nanoparticles were centrifuged once again for 10 min at 10,000 g. The supernatant was discarded and the pellet resuspended in 1 mL HEPES blocking buffer (10 mM HEPES+0.1% (w/v) BSA, pH 7.4).

4.2.3 Drying of Labeled Probe Antibody

Experiments with dried AB-AgNPs were performed using coated polymer disks. They were prepared by pipetting 20 μL of the respective solution on a PET support and drying for 1 h at 50 °C. For the disks without matrix, the AB-AgNP stock solution (20 μg·mL⁻¹ in 10 mM HEPES+0.1% (w/v) BSA, pH 7.4) was diluted 1:2 with 10 mM HEPES buffer (pH 7.4), while a 40% (w/v) trehalose solution (in 10 mM HEPES, pH 7.4) was used for the dilution for trehalose disks. To measure the electrochemical activity after several days of storage in the fridge, the

nanoparticles were rehydrated with 20 μL 10 mM HEPES buffer (pH 7.4) for 1 h at room temperature and 10 μL were dried on top of the WE of a DRP-110 at room temperature. Then, 50 μL 0.1 M KCl were added covering the three-electrode area and the electrochemical measurement was performed: after pretreatment with 1.25 V for 60 s and -0.8 V for 30 s, differential pulse voltammetry was performed from -0.25 V to 0.25 V with $t_{\text{puls}}=50$ ms, $E_{\text{step}}=10$ mV, $E_{\text{amplitude}}=80$ mV, scan rate= 20 mV \cdot s $^{-1}$.

The trehalose content and drying was optimized with respect to lower water content and higher reproducibility. For the following experiments, a 20% (w/v) trehalose solution (in 10 mM HEPES, pH 7.4) was used for dilution and the disks were dried overnight at 50 $^{\circ}\text{C}$. Then, the bioassay, which was described in a previous publication, was performed. Very briefly: the SPCEs (DRP-110STR) were washed three times with 50 μL 50 mM PBS buffer (pH 7.4). Then, 10 μL of the capture AB (25 $\mu\text{g}\cdot\text{mL}^{-1}$ in 50 mM PBS buffer, pH 7.4) were dropped onto the working electrode. For each step of the bioassay, incubation and washing were performed as follows: after incubation for 1 h at room temperature under water saturated atmosphere the solution was removed and the electrode washed three times with 50 μL PBST (50 mM PBS+0.05% (w/v) Tween 20, pH 7.4). After drying under nitrogen flow, blocking was performed using 10 μL PBS blocking buffer (50 mM PBS+1% (w/v) BSA, pH 7.4). In the third step, the antigen solution (100 $\text{ng}\cdot\text{mL}^{-1}$ in 50 mM PBS, pH 7.4) was added and the dry probe AB disk was set on top. After incubation and washing, the electrodes were washed additionally with 50 mM PBS (pH 7.4) and ddH $_2$ O. Directly prior to the electrochemical measurement, the electrode was dried under nitrogen flow.

Moreover, different oxygen scavengers were tested, which were added to the trehalose solution before drying of the disks (5 mM in 20% (w/v) trehalose solution), namely ascorbic acid, sodium sulfite and sodium hydrogen carbonate.

4.2.4 Fabrication of Flow Chips

The flow chips consisted of a DRP-110STR electrode as bottom and a PMMA piece with in- and outlet as top. Both parts were glued together by double-sided adhesive tape in which the channel layout was cut (Figure 4.2 a). The fabrication was done by a laser cutter with CO $_2$ laser (30 W, $\lambda=10.6$ μm , image density 5) according to a previously designed template (Figure 4.2 b). The channel layout (blue) was cut out of double-sided adhesive tape (100% power, 70% speed, 200 PPI) and glued to the SPCE after washing the electrode three times with 50 μL 50 mM PBS

(pH 7.4) and drying under nitrogen flow. Then, the capture AB immobilization was performed as described for the standard bioassay above. For the top, the outline, in- and outlet (black) were cut out of PMMA (100% power, 6.5% speed, 1000 PPI) and the cavity (grey) was engraved in the bottom side of the PMMA (40% power, 90% speed, 1000 PPI). The cavity was between 75 and 100 μm deep.

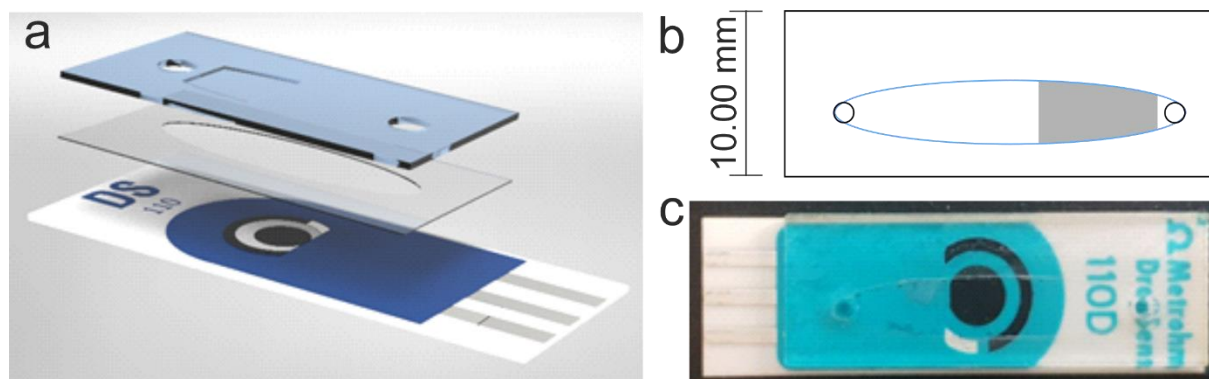


Figure 4.2. (a) Schematic representation of the three-layered flow chip with DRP-110STR as bottom layer, double-sided adhesive tape (transparent, 100 μm thickness, middle layer) and PMMA top (blue). (b) Template for the laser cutter, while black lines were cut out of PMMA (100% power, 6.5% speed, 1000 PPI), blue oval was cut out of double-sided adhesive tape (100% power, 70% speed, 200 PPI) and grey was engraved into PMMA (40% power, 90% speed, 1000 PPI) and (c) actual photograph of the finished microfluidic chip with scale bar representing 10.00 mm.

For first experiments, the top was glued together with the SPCE after capture AB immobilization. For microchips with dried AB-AgNPs, blocking with 20 μL PBS blocking buffer (50 mM PBS+1% (w/v) BSA, pH 7.4) was additionally performed with incubation and washing as described above for the bioassay and the electrodes were dried under nitrogen flow. Moreover, the PMMA tops were cleaned by plasma treatment for 1 min (0.2 bar, 75 W, 100% O_2) and 10 μL of 10% (w/v) trehalose in AB-AgNPs stock solution (in 10 mM HEPES+0.1% (w/v) BSA) were pipetted into the cavity on the bottom side of the PMMA top and dried overnight at 50 $^\circ\text{C}$. The top and bottom part were glued together to form the finished flow chip. All chips were sealed using tape and stored at 4 $^\circ\text{C}$ until further usage.

4.2.5 Microfluidic Experiments

As pretest, the AB-AgNP stock was diluted 1:2 with a 0.2 M KCl solution. Then, 50 μL of this mix were pipetted on a DRP-110 electrode, covering the three-electrode area, and the electrochemical measurement was performed: pretreatment with 1.25 V for 60 s and -0.8 V for 30 s, DPV from -0.25 V to 0.25 V with $t_{\text{puls}}=50$ ms, $E_{\text{step}}=10$ mV, $E_{\text{amplitude}}=80$ mV, scan rate=20 $\text{mV}\cdot\text{s}^{-1}$. As comparison, a DRP-110 was glued together with the channel top consisting

of structured double-sided adhesive tape and a PMMA piece with in- and outlet. The channel was filled with the mix ($0.01 \text{ mg}\cdot\text{mL}^{-1}$ AB-AgNP in 0.1 M KCl) via manual withdrawal of the solution out of an Eppendorf tube from the opposed side with a syringe and the electrochemical measurement was performed again.

First microfluidic experiments were performed using the setup shown in Figure S4.2 a, while the flow chips with dried AB-AgNPs were operated using a simplified version (Figure S4.2 b). The pumping strategy for microfluidic experiments with and without dried AB-AgNPs is shown in Figure S4.3. The system was kept bubble-free at any time and for the experiments with AB-AgNPs in solution (a), the AG was incubated with the AB-AgNP in a 1:1 ratio for 2 h prior to injection. For electrochemical detection, the channel was filled with 0.1 M KCl , removed from the chip holder and inserted into a bluetooth potentiostat. As pretreatment 1.18 V for 60 s and -0.8 V for 30 s were applied before DPV was performed from -0.25 V to 0.25 V with $t_{\text{puls}}=50 \text{ ms}$, $E_{\text{step}}=10 \text{ mV}$, $E_{\text{amplitude}}=80 \text{ mV}$, scan rate= $20 \text{ mV}\cdot\text{s}^{-1}$.

The bioassay was repeated over six months to test the stability of the dried reagents. For these measurements a 10% (w/v) trehalose with $10 \text{ mM Na}_2\text{SO}_3$ solution was used as matrix to dry the AB-AgNP solution ($20 \text{ }\mu\text{g}\cdot\text{mL}^{-1}$) overnight at $50 \text{ }^\circ\text{C}$.

4.3 Results and Discussion

4.3.1 Development of AB-AgNPs as Dry Reagent for Sensors and Microfluidic Chips

In previous work, a bioassay for NT-proBNP using AgNPs and SPCEs was developed as described in the introduction [12]. Here, detailed information on the electroanalytical principle for AgNP detection via DPV are described, as well as development and optimization of the bioassay and its corresponding parameters. Limits of detection of $4.0 \text{ ng}\cdot\text{mL}^{-1}$ were achieved, making the bioassay well-suited for NT-proBNP testing being just slightly above the $1 \text{ ng}\cdot\text{mL}^{-1}$ clinical threshold. However, the multiple assay steps, pipetting, and incubation periods as well as reproducibility, and the need for all liquid reagents, rendered this assay merely a proof-of-principle bioassay. Instead, we investigated here, how a general immuno sandwich assay for an important biomarker can be translated into a self-contained, miniaturized biosensor, focusing on a microfluidic format, which would allow FIA-like automation. The used antibodies (biotinylated polyclonal capture AB and monoclonal probe AB) are included in the commercially available NT-proBNP test by Roche Diagnostics [19]. Therefore, the specificity

and binding efficacy of this AB pair was adopted without further tests. Initial tests investigated the possibility of drying AgNP-labeled probe antibodies. Here, the functionality of the antibodies as well as the nanoparticle colloidal stability have to be maintained throughout the process of drying and redispersion. First, 20 μL AB-AgNPs were dried on a polymer support using different rehydration times (Figure S4.4 a). Using 20 μL HEPES, the optimum signal was achieved after incubation of the disk for 1 h. The redispersion was not complete after 30 min, while after 2 h, beginning oxidation of the AB-AgNPs by air oxygen decreased the signal again. When compared to control AB-AgNPs in solution (Figure S4.4 b), it was observed that drying has only minor influence on the electrochemical activity, suggesting that the rehydrated AB-AgNPs do not form clusters that would impeded in their electrochemical quantification. The increased signal variability is assumed to be caused by the larger number of steps taken prior to signal generation. However, storage of the dehydrated AB-AgNPs revealed instability over time (Figure 4.3 a), dropping to only 20% of the original peak area after one week due to oxidation of the silver by air oxygen. AB-AgNPs were therefore sought to be embedded in a matrix, which should dramatically decrease oxidation and hence increase long-term stability. For simple rehydration in microfluidic channel and to maintain the stability of the attached antibodies, main design criteria for the matrix were solubility in water/buffer, complete dehydration at $\leq 50\text{ }^\circ\text{C}$, and no interference with the NPs, antibodies or the electrochemical measurement. Thus, agarose as a hydrogel with large pore sizes was studied (0.1–0.5% (w/w) agarose in double-distilled water) with various drying procedures. The strong yellow color of all gels indicates that the AB-AgNPs do not aggregate upon drying. Less concentrated gels show a slight color shift to orange after several days, while the 0.5% (w/w) agarose gel stays yellow. Since the AgNPs turn orange/brownish upon oxidation [20], this refers to an increased stability against oxidation for higher concentrated agarose gels. However, it was not possible to recover the AB-AgNPs by passive diffusion independent of the agarose content used. It is assumed the pores are too small for the 50 nm NPs to migrate just based on diffusion. A second, promising approach is the use of sugars such as maltose and trehalose which are often employed in freeze-drying of proteins. Specifically, trehalose is well-known to stabilize biomaterials due to interactions of the sugar with polar head groups and glass formation [21]. While establishing a glass-like network upon drying, it completely dissolves by addition of water. Experiments showed that AB-AgNPs dissolved in trehalose solution and those first dehydrated in trehalose and then redispersed gave the same electrochemical response

(Figure S4.5). Furthermore, the electrochemical activity remained stable over a course of 7 days, after an initial drop of to 75% of the fresh AB-AgNP signal (Figure 4.3 b).

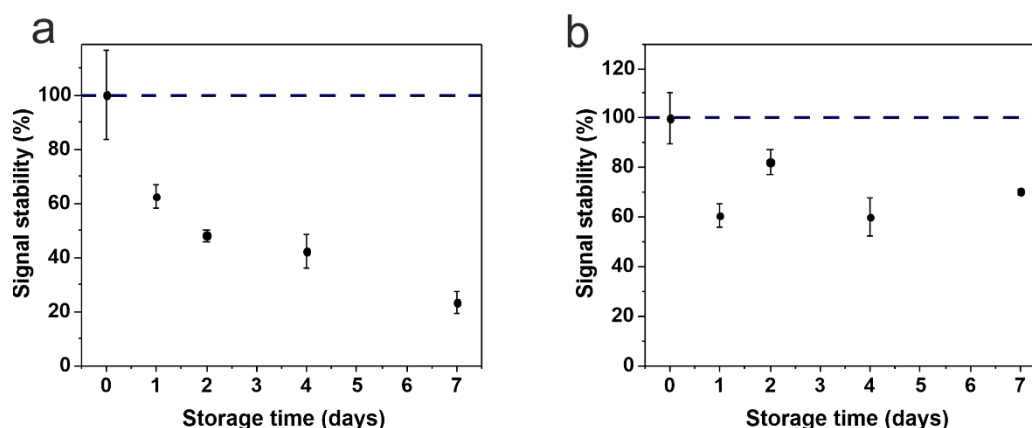


Figure 4.3. Signal stability of the dried AB-AgNPs (a) without matrix and (b) in 20% (w/v) trehalose over a week. Signal stability is calculated by normalizing the mean peak area of the respective day to the mean signal directly after drying. Standard deviations were calculated based on three parallel measurements of three separate disks. Error bars represent mean values $\pm 1\sigma$ ($n=3$).

It can be concluded that the matrix stabilizes the AB-AgNPs against oxidation and the stability in dry-form can be enhanced drastically by drying of the particles in trehalose matrix. In a final confirmation assay, it was determined, whether the antibodies remain stable and functional upon the dehydration in trehalose. The AB-AgNPs were dried in 10% (w/v) trehalose overnight at 50 °C in order to ensure a complete dehydration. As it is shown in Figure S4.6, the assay delivered a signal of $0.37 \pm 0.08 \text{ V} \cdot \mu\text{A}$ for $100 \text{ ng} \cdot \text{mL}^{-1}$ which is comparable to previous experiments and confirms that the antibodies are active after drying and rehydration and the dried AB-AgNPs in trehalose can be used in order to simplify the bioassay protocol.

4.3.2 Development of a Microfluidic Chip for NT-proBNP

Microfluidic chips with integrated electrochemical detection were chosen for the automation and miniaturization of the bioassay. This dramatically reduces any pipetting step and increases the efficiency of the assay. The portable SPCE was integrated into microchannels through adhesive tape and laser cutting processes. Various channel shapes (Figure S4.1) and heights were tested in order to avoid air bubble trapping and enable the wetting of the three-electrode area, while in the end the design shown in Figure 4.2 with a channel height, *i.e.* tape thickness, of 100 μm , showed superior performance. The overall functionality of the electrochemical detection strategy within microfluidic channels was proven by comparing the performance against a stand-alone SPCE electrode. The microdevice was filled manually with a 1:1 mixture

of AB-AgNP stock solution and 0.2 M KCl, and the same solution was dropped on the stand-alone SPCE. It was found that while the peak height varies greatly between $28 \pm 4 \mu\text{A}$ and $13 \pm 1 \mu\text{A}$, more importantly, the peak area is constant in the margin of the error ($0.8 \pm 0.1 \text{ V} \cdot \mu\text{A}$ vs. $0.7 \pm 0.1 \text{ V} \cdot \mu\text{A}$) (Figure 4.4). Consequently, the same amount of silver is converted in both systems, but the thin layer and the partial coverage of the three electrodes due to the channel layout on the chip results overall in slower reactions and an increased peak width.

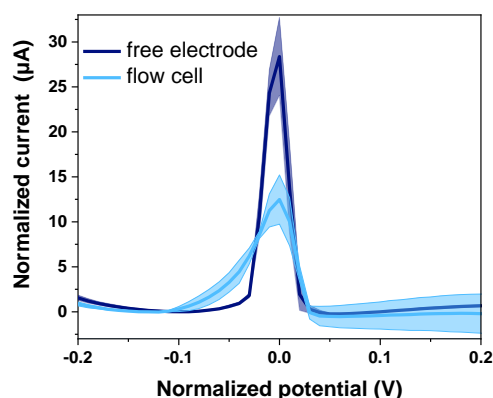


Figure 4.4. Differential pulse voltammograms of a 1:1 mixture of AB-AgNP stock and 0.2 M KCl on a free DRP-110 (dark blue) or in a microfluidic channel (light blue), normalized to the respective current at -0.12 V in y-direction and to the peak potential in x-direction. The colored area behind the curve represents $\pm 1\sigma$ with standard deviation calculated based on three parallel measurements with three different SPCEs ($n=3$).

The reduced counter electrode surface area within the microchannel with respect to the working electrode area resulted in suboptimal electrochemical conditions, *i.e.* gas evolution occurred during the oxidative pretreatment at 1.25 V. By lowering this oxidation potential to 1.18 V, bubble-free processes could be ensured, which is important for the reliability of the assay. It should be noted, that another strategy could be the design of a larger counter electrode to fit within the channel in the future. Using the current design and electrochemical strategy, a microfluidic chip bioassay was performed by immobilization of the capture AB in the flow chip and injection of preincubated AG/AB-AgNP mix resulting in a LOD 15x lower compared to the stand-alone sensor (Figure S4.7). We assume this is due to the lowered diffusion effects of the nanoparticles within the narrow confinement of the microchannels, and the more effective washing that can be done reducing non-specific binding. At the same time, the mean standard deviation is with 25% ($n \geq 4$) too high. Therefore, the trehalose drying procedure of AB-AgNPs was adapted from being an off-chip reagent to be directly deposited

within the microchannels. Since drying within the channel itself lead to clogging (Figure S4.1) a cavity was created in the PMMA top to still dry the AB-AgNP directly within the chip. Different depths (50-100 μm) and volumes of AB-AgNP trehalose mix (5 and 10 μL) were tested. The focus was on obtaining a deep enough cavity to assure penetrability of the microchannel with as much AB-AgNP trehalose mix as possible without it spreading over the PMMA top before drying. Also, to ensure complete dissolution of the AB-AgNPs, the cavity was kept as shallow as possible. With 40% laser power, which results in a cavity depth around 87 μm , reliable permeability was reached. Moreover, an oxygen plasma treatment (1 min, 75 W) was added to increase hydrophilicity of the PMMA and facilitate even spreading of the solution inside the cavity. Also, for the successful and reproducible release of the nanoparticle conjugates three washing buffers (PBST, PBST+0.1% (w/v) BSA and PBST+0.1 M KCl) and various incubation and washing velocities were investigated (Figure S4.8). The highest signal and also highest S/N was obtained by using 0.5 $\mu\text{L}\cdot\text{min}^{-1}$ for rehydration of the AB-AgNPs and incubation with the sample, and washing with 750 μL PBST at 50 $\mu\text{L}\cdot\text{min}^{-1}$.

4.3.3 Performance of the Microfluidic Bioassay

Finally, using the optimized conditions, dose-response curves for NT-proBNP were carried out both in buffer and undiluted human serum (Figure 4.5). For the measurements in buffer (a), a LOD comparable to the biochip with liquid AB-AgNP reagent was obtained (0.24 $\text{ng}\cdot\text{mL}^{-1}$) confirming the superiority of the miniaturized biosensor in comparison to the stand-alone bioassay with a LOD of 4.0 $\text{ng}\cdot\text{mL}^{-1}$. The optimized microchip assay is drastically simplified as only one pump is required. Thus, by having reduced assay steps, avoiding manual pipetting, and preventing non-specific interactions, this optimized microfluidic biosensor has only 9% error ($n\geq 3$) in contrast to the prior microchip without dried AB-AgNPs ($\bar{\sigma}=25\%$) and the stand-alone bioassay ($\bar{\sigma}=17\%$). This suggests that the assay is highly suitable for the automation in a flow injection setup, both in a POCT as well as a clinical lab system, which would further decrease the variability and increase parallelization and efficacy. Here, an in-line injection port for the sample and KCl solution could be used with washing buffer as flow stream, which will be the focus of future studies.

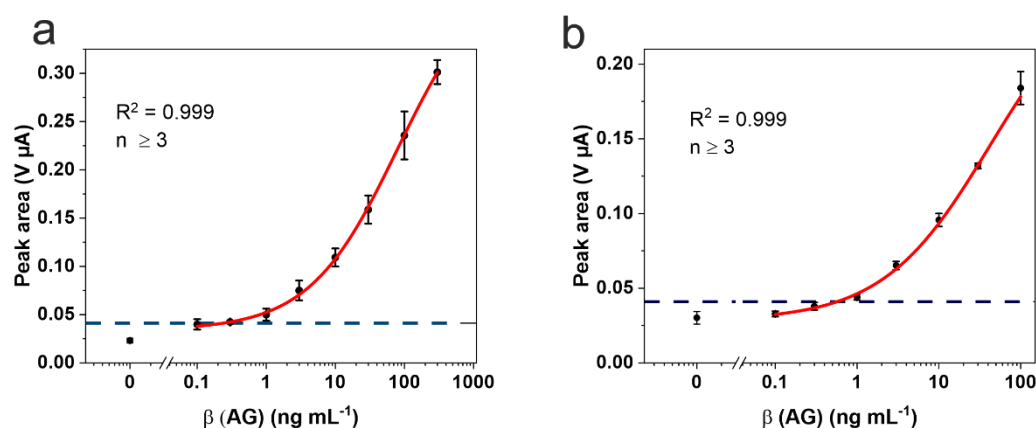


Figure 4.5. Plot of peak area against logarithm of antigen concentration in (a) PBS buffer (50 mM, pH 7.4) and (b) undiluted human serum with logistic fit (red line) and corresponding parameters. The blue dashed line indicates the LOD. Standard deviations were calculated based on four parallel measurements using four different flow chips, while outliers were removed after Q-test (confidence interval 95%). Error bars represent mean values $\pm 1\sigma$ ($n \geq 3$).

In spiked human serum (b), the course of the dose-response curve is analogous to experiments done in buffer, providing a LOD of $0.57 \text{ ng}\cdot\text{mL}^{-1}$ and a mean standard deviation of only 6% ($n \geq 3$). The slightly lower sensitivity was expected due to partial blocking of the electrode by serum protein adsorption. Overall, it can be concluded that this microchip biosensor is suitable for the analysis of NT-proBNP content in blood. To confirm the results obtained by our microfluidic assay, the spiked serum samples, which were obtained from Roche Diagnostics, were additionally analyzed with Roche's Elecsys[®]. The results with corresponding divergence between NT-proBNP spike concentration (β_{spike}) and actual concentration determined with the Elecsys system (β_{Elecsys}) are shown in Table 4.1.

Table 4.1. NT-proBNP spiked concentrations (β_{spike}) as obtained from Roche Diagnostics with respective NT-proBNP concentrations measured with Roche's Elecsys[®] (β_{Elecsys}) and divergence of both.

$\beta_{\text{spike}} \text{ (ng}\cdot\text{mL}^{-1})$	$\beta_{\text{Elecsys}} \text{ (ng}\cdot\text{mL}^{-1})$	Divergence
1.00	0.81	18.68%
3.00	2.32	22.56%
10.00	8.01	19.91%
30.00	27.50	8.30%
100.00	42.77	57.23%

The reason for the rather big divergence between spiked concentration and concentration found with the Elecsys[®] system is known to be the dissolution of the peptide out of the matrix.

This causes a decrease in peptide stock concentration. Taking this commercially available analysis as the gold standard and the real concentration of NT-proBNP, the data from the serum calibration can be fitted again (Figure S4.9) and a new LOD, which is even below the previously determined one, can be calculated. With a NT-proBNP concentration of $0.38 \text{ ng}\cdot\text{mL}^{-1}$, this LOD is only 37% higher than the one calculated in buffer. It can be concluded that the protein adsorption on the electrode has only minor influence on the assay and also the antibody binding is not changed.

Various NT-proBNP tests have been published in recent years, as further discussed in [22]. A recent study by Pollok *et al.* [3] is technologically closest to our microfluidic biosensor. Their reported LODs are similar, however our sensor includes a simpler working procedure and smaller sample volume (10 μL vs. 100 μL). Moreover, the developed method shows distinct advantages compared to the currently used methods in clinical settings such as the commercially available NT-proBNP tests from Roche Diagnostics. With the Cobas h 232 a portable point-of-care device with optical detection of AuNP labels is offered [19]. However, typical for lateral flow assays larger sample volumes are needed, which makes it impossible for use in home-monitoring. In contrast, the here developed microchip assay only needs 10 μL of sample volume, which can easily be obtained via a mere finger prick. Secondly, fleece and membrane fabrication for LFA test strips are prone to variations requiring a continuous fine-tuning of products made during the manufacturing process, so that other assay formats are highly desirable. The Cobas h 232 has a measuring range from $0.06\text{-}9 \text{ ng}\cdot\text{mL}^{-1}$ and a detection time of 12 min, which makes it superior with respect to analytical performance. However, the here presented assay is with its dynamic range of $0.6\text{-}100 \text{ ng}\cdot\text{mL}^{-1}$ sensitive in the necessary range for chronic heart failure and will most likely gain from better manufacturing strategies once designed for mass production, just as the Cobas system [4]. Another NT-proBNP detection device is Roche's Elecsys[®], which is designed for analytical laboratories [18]. Here, NT-proBNP in blood serum or plasma is detected via electrochemiluminescence. The immunoassay is performed with 15 μL sample volume in a disk or rack handling system. The analytical performance is with a measuring range of $5\text{-}35,000 \text{ ng}\cdot\text{L}^{-1}$ and 9-18 min assay time clearly superior. However, this detection system is a lab device, which is expensive, requires sample preparation and cannot be used at the point-of-care.

4.3.4 Stability Study

AgNPs are known to be easily oxidized under ambient conditions, leading to a perception of instability especially for long-term uses in the scientific literature [23]. However, we have previously demonstrated, that protein-coated AgNPs remain colloiddally stable over ten weeks and deliver a constant electrochemical signal for at least four weeks when stored at 4 °C, indicating that long-term stability is clearly achievable. The here developed trehalose-supported drying of AB-AgNPs also showed significantly improved performance (see Figure 4.3), however, when monitoring the trehalose disks over ten weeks (Figure 4.6 a), it is obvious that storage beyond 4 weeks is not feasible as the predictable oxidation of the AgNPs leads to unreliable and eventually only limited signal responses (*i.e.* drop to 50% of the original signal). To improve long-term stability of the dried AB-AgNPs, various oxygen scavengers were included in the trehalose matrix. Specifically, before drying, 5 mM AA, Na₂SO₃, NaHCO₃ were added to the trehalose mix, respectively. None of these substances showed a negative effect on the original electrochemical signal of the bioassay. After ten weeks, the assay was performed again to determine their protective power against oxidation (Figure 4.6 b). While ascorbic acid and NaHCO₃ showed no protective effect, Na₂SO₃ was highly effective in avoiding any oxidation of the AgNPs and hence a normalized signal of 100±23% was obtained. This indicates that Na₂SO₃ is indeed suitable to protect the AgNPs from oxygen, while having no negative influence on the bioassay itself.

Therefore, the AB-AgNPs were dried in trehalose with 10 mM Na₂SO₃ within the microchips. After assembly, the chips were sealed for storage at 4 °C, where a constant humidity in the channel could best ensure similar conditions for all dried AB-AgNPs. Finally, the signal stability over four months was investigated (Figure 4.6 c). Here, over a period of 18 weeks, the bioassay signal stays constant with a mean relative error of 10%. This is a key finding as it supports the general feasibility of dry storage of protein-coated AgNPs in air. Afterwards, the signal decreases rapidly and reaches 30% at six months.

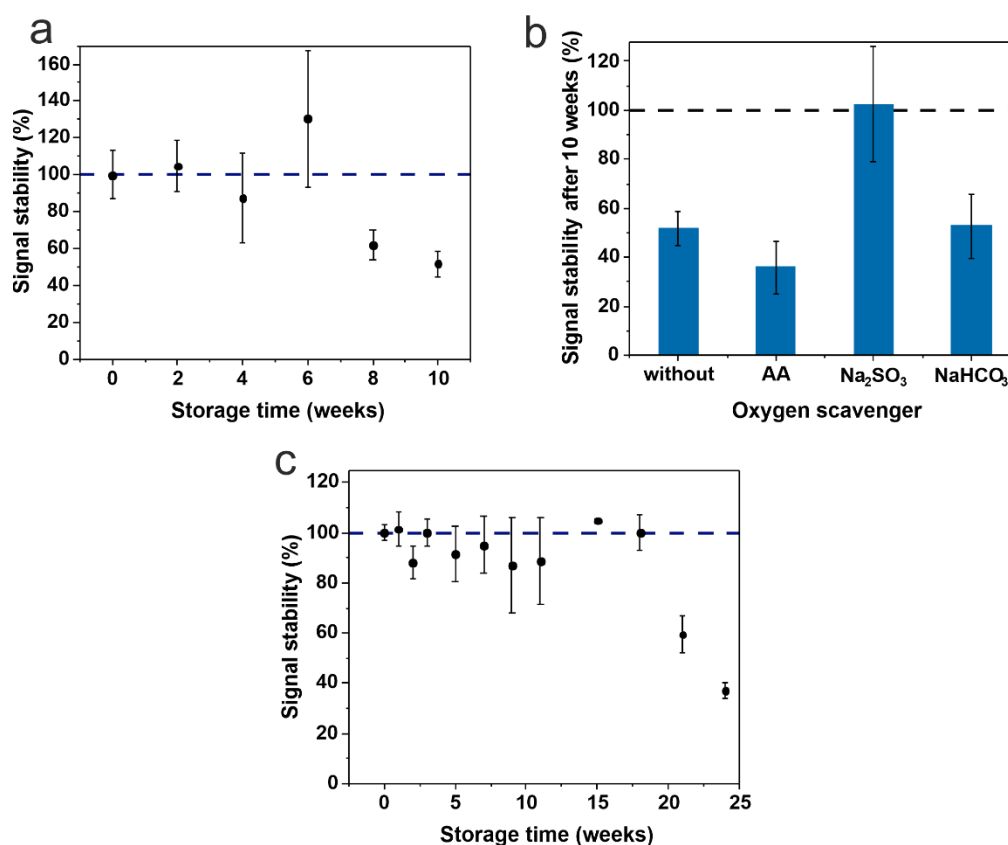


Figure 4.6. (a) Stability of the bioassay signal using the AB-AgNPs, dried in 10% (w/v) trehalose at 50 °C overnight, stored at 4 °C over ten weeks and (b) signal stability after ten weeks using none or different oxygen scavengers (5 mM, ascorbic acid, sodium sulfite and sodium hydrogen carbonate). Standard deviations were calculated based on five parallel measurements on five different SPCEs, while outliers were removed after Q-test (confidence interval 95%). Error bars represent mean values $\pm 1\sigma$ ($n \geq 4$). (c) Stability of the bioassay signal using the AB-AgNPs, dried in 10% (w/v) trehalose with 10 mM sodium sulfite at 50 °C overnight, stored at 4 °C over six months. Standard deviations were calculated based on four parallel measurements on four different flow chips, while outliers were removed after Q-test (confidence interval 95%). Error bars represent mean values $\pm 1\sigma$ ($n \geq 3$). In all cases, the bioassay was performed in the microfluidic flow chip using a constant AG concentration of $100 \text{ ng}\cdot\text{mL}^{-1}$ and signal stability means peak area normalized to the signal right after drying.

It is assumed, that this drop is due to the depletion of the oxygen scavenger. For an extension of the AB-AgNP stability in dry form, a higher oxygen scavenger concentration will simply be used in the trehalose matrix in the future. The high relative errors for weeks 9 and 11 of around 20% can be explained by handling errors and the small number of replicates of hand-made flow chips that were used.

4.4 Conclusion

Overall, we presented here a method for NT-proBNP detection ready for the challenges of the POC. The electrochemical detection via silver nanoparticle labels in a microfluidic chip provides the appropriate limit of detection, dynamic range and through the selection of antibodies also specificity needed for a point-of-care test system, where a finger prick sample volume must suffice. The most important design criteria were the reduction in sample volume needed and the one-step assay procedure as typically afforded by lateral flow assays. The former was accomplished through a microfluidic design that can provide reliable data using only 10 μL of sample volume. The latter was obtained through dry-storage of the electrochemical label, AgNPs, on chip. The decision to investigate microfluidic channel designs instead of a membrane-based system in LFAs stems from the unavoidable variability of membrane and fleece fabrication that is a ubiquitous challenge in the rapid test community. Furthermore, each LFA concept must use enough volume to saturate the membrane material which either requires two-step procedures or large sample volumes. We demonstrated here therefore the proof-of-principle that membrane-free systems can provide the analytical figures of merit necessary for sensitive NT-proBNP detection for the POC.

Moreover, the research demonstrated that AgNPs are not only colloidally stable, but can also be rendered highly durable against oxidation by dehydrated storage in the presence of an oxygen scavenger. This opens up further possibility for their use as label in a many other electrochemical and possibly also optical POCTs for clinical diagnostics of low-concentrated analytes that can currently not be served with standard LFA technology.

4.5 References

1. Savarese G, Lund LH. Global Public Health Burden of Heart Failure. *Cardiac Failure Review*. 2017;03:7. doi:10.15420/cfr.2016:25:2.
2. Hunt SA, Abraham WT, Chin MH, Feldman AM, Francis GS, Ganiats TG, et al. ACC/AHA 2005 Guideline Update for the Diagnosis and Management of Chronic Heart Failure in the Adult: a report of the American College of Cardiology/American Heart Association Task Force on Practice Guidelines (Writing Committee to Update the 2001 Guidelines for the Evaluation and Management of Heart Failure): developed in collaboration with the American College of Chest Physicians and the International Society for Heart and Lung Transplantation: endorsed by the Heart Rhythm Society. *Circulation*. 2005;112:e154-235. doi:10.1161/CIRCULATIONAHA.105.167586.
3. Pollok NE, Rabin C, Walgama CT, Smith L, Richards I, Crooks RM. Electrochemical Detection of NT-proBNP Using a Metalloimmunoassay on a Paper Electrode Platform. *ACS Sens*. 2020;5:853–60. doi:10.1021/acssensors.0c00167.
4. Kim H-N, Januzzi JL. Natriuretic peptide testing in heart failure. *Circulation*. 2011;123:2015–9. doi:10.1161/CIRCULATIONAHA.110.979500.
5. Roger VL. Epidemiology of heart failure. *Circ Res*. 2013;113:646–59. doi:10.1161/CIRCRESAHA.113.300268.
6. Mueller C, McDonald K, Boer RA de, Maisel A, Cleland JGF, Kozhuharov N, et al. Heart Failure Association of the European Society of Cardiology practical guidance on the use of natriuretic peptide concentrations. *Eur J Heart Fail*. 2019;21:715–31. doi:10.1002/ejhf.1494.
7. Song K-S, Nimse SB, Sonawane MD, Warkad SD, Kim T. Ultra-Sensitive NT-proBNP Quantification for Early Detection of Risk Factors Leading to Heart Failure. *Sensors (Basel)* 2017. doi:10.3390/s17092116.
8. Bellagambi FG, Petersen C, Salvo P, Ghimenti S, Franzini M, Biagini D, et al. Determination and stability of N-terminal pro-brain natriuretic peptide in saliva samples for monitoring heart failure. *Sci Rep*. 2021;11:13088. doi:10.1038/s41598-021-92488-2.
9. Pu Z, Zou C, Wang R, Lai X, Yu H, Xu K, Li D. A continuous glucose monitoring device by graphene modified electrochemical sensor in microfluidic system. *Biomicrofluidics*. 2016;10:11910. doi:10.1063/1.4942437.

10. Primiceri E, Chiriaco MS, Notarangelo FM, Crocamo A, Ardissino D, Cereda M, et al. Key Enabling Technologies for Point-of-Care Diagnostics. *Sensors (Basel)* 2018. doi:10.3390/s18113607.
11. Oliveira PRd, Oliveira MM, Zarbin AJG, Marcolino-Junior LH, Bergamini MF. Flow injection amperometric determination of isoniazid using a screen-printed carbon electrode modified with silver hexacyanoferrates nanoparticles. *Sensors and Actuators B: Chemical*. 2012;171-172:795–802. doi:10.1016/j.snb.2012.05.073.
12. Beck F, Horn C, Baeumner AJ. Ag nanoparticles outperform Au nanoparticles for the use as label in electrochemical point-of-care sensors. *Anal Bioanal Chem* 2021. doi:10.1007/s00216-021-03288-6.
13. Hao N, Li H, long Y, Zhang L, Zhao X, Xu D, Chen H-Y. An electrochemical immunosensing method based on silver nanoparticles. *Journal of Electroanalytical Chemistry*. 2011;656:50–4. doi:10.1016/j.jelechem.2011.01.029.
14. Cunningham JC, Kogan MR, Tsai Y-J, Luo L, Richards I, Crooks RM. Paper-Based Sensor for Electrochemical Detection of Silver Nanoparticle Labels by Galvanic Exchange. *ACS Sens*. 2016;1:40–7. doi:10.1021/acssensors.5b00051.
15. Walgama C, Nguyen MP, Boatner LM, Richards I, Crooks RM. Hybrid paper and 3D-printed microfluidic device for electrochemical detection of Ag nanoparticle labels. *Lab Chip*. 2020;20:1648–57. doi:10.1039/d0lc00276c.
16. Kanso H, Begoña González García M, Ma S, Ludwig R, Fanjul Bolado P, Hernández Santos D. Dual Biosensor for Simultaneous Monitoring of Lactate and Glucose Based on Thin-layer Flow Cell Screen-printed Electrode. *Electroanalysis*. 2017;29:87–92. doi:10.1002/elan.201600487.
17. Li X, Scida K, Crooks RM. Detection of hepatitis B virus DNA with a paper electrochemical sensor. *Anal Chem*. 2015;87:9009–15. doi:10.1021/acs.analchem.5b02210.
18. Roche Diagnostics AG. <https://diagnostics.roche.com/ch/de/products/params/electsys-nt-probnp.html#productSpecs>. Accessed 9 Apr 2021.
19. Bertsch T, Chapelle J-P, Dempfle C-E, Giannitsis E, Schwabs M, Zerback R. Multicentre analytical evaluation of a new point-of-care system for the determination of cardiac and thromboembolic markers. *Clin Lab*. 2010;56:37–49.
20. Gallardo OAD, Moiraghi R, Macchione MA, Godoy JA, Pérez MA, Coronado EA, Macagno VA. Silver oxide particles/silver nanoparticles interconversion: susceptibility of

forward/backward reactions to the chemical environment at room temperature. RSC Adv. 2012;2:2923. doi:10.1039/c2ra01044e.

21. Crowe LM, Reid DS, Crowe JH. Is trehalose special for preserving dry biomaterials? Biophys J. 1996;71:2087–93. doi:10.1016/S0006-3495(96)79407-9.
22. Colom G, Salvador J-P, Acosta G, Albericio F, Royo M, Marco M-P. Competitive ELISA for N-terminal pro-brain natriuretic peptide (NT-proBNP) determination in human plasma. Analyst. 2020;145:6719–27. doi:10.1039/d0an00650e.
23. Keast VJ, Myles TA, Shahcheraghi N, Cortie MB. Corrosion processes of triangular silver nanoparticles compared to bulk silver. J Nanopart Res. 2016;18:289. doi:10.1007/s11051-016-3354-9.

4.6 Supporting Information

Experimental Procedure for Microfluidic Experiments

Different designs were tested for the flow chips (Figure S4.1). The channel layout (blue) was cut out of double-sided adhesive tape (100% power, 70% speed, 200 PPI), the PMMA piece was glued on top and the outline, in- and outlet (black) were cut out (100% power, 6.5% speed, 1000 PPI).

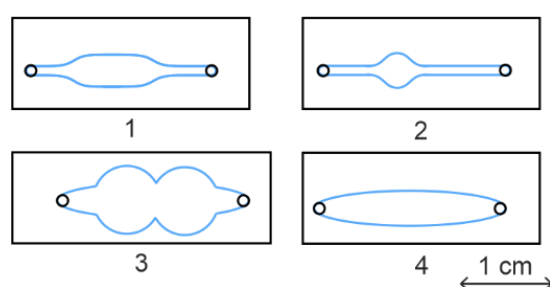


Figure S4.1. Template of microfluidic chips for the laser cutter, while black lines are cut out of PMMA (100% power, 6.5% speed, 1000 PPI), blue shapes are cut out of double-sided adhesive tape (100% power, 70% speed, 200 PPI) with scale bar representing 1 cm.

For the designs 1 and 2, bubbles were trapped in the channel and uniform filling of the channel with up to $50 \mu\text{L}\cdot\text{min}^{-1}$ injection speed was not possible. In case of design 3, two zones were defined for including the AB-AgNP directly into the chip. Here, zone A was used for drying of the AB-AgNP and zone B included the entire three-electrode area within the channel. However, after drying of AB-AgNP in trehalose matrix, the channel both with 100 and 200 μm channel height clogged and no flow-through process was feasible. Thus, design 4 was used to enable bubble-free solution flow and paired with a cavity in the chip's lid for dried AB-AgNPs (Figure 4.2). The tape thickness, *i.e.* channel height, was chosen to be 100 μm to ensure smallest channel dimensions possible over the three-electrode area.

For the first flow chips, a DRP-110STR electrode was washed three times with 50 μL PBS and incubated with 10 μL capture AB ($25 \mu\text{g}\cdot\text{mL}^{-1}$ in 50 mM PBS, pH 7.4) for 1 h at room temperature. Afterwards, it was washed three times with 50 μL PBST (50 mM PBS+0.05% (w/v) Tween 20, pH 7.4) and the channel top was attached to this electrode forming the flow chip.

The first microfluidic setup (Figure S4.2 a) consisted of two syringe pumps (LEGATO[®] 111 syringe pump, kd Scientific), one for washing buffer (A1) and one for KCl (A2). Both lines were connected by a T-piece (B) and led into the chip holder (C), and then into the waste or buffer

reservoir (D). The simplified setup used for experiments with dried AB-AgNPs (Figure S4.2 b) consisted of a syringe pump (A), a T-piece (B), which connected the main line to a dead end, which was used as bubble trap (C), a chip holder with in- and outlet (D), and a waste or buffer reservoir (E). The flow chip was inserted into the chip holder as shown in the magnification. The tubing was attached to in- and outlet via self-casted PDMS seals, which were pressed on the in- and outlet by the chip holder.

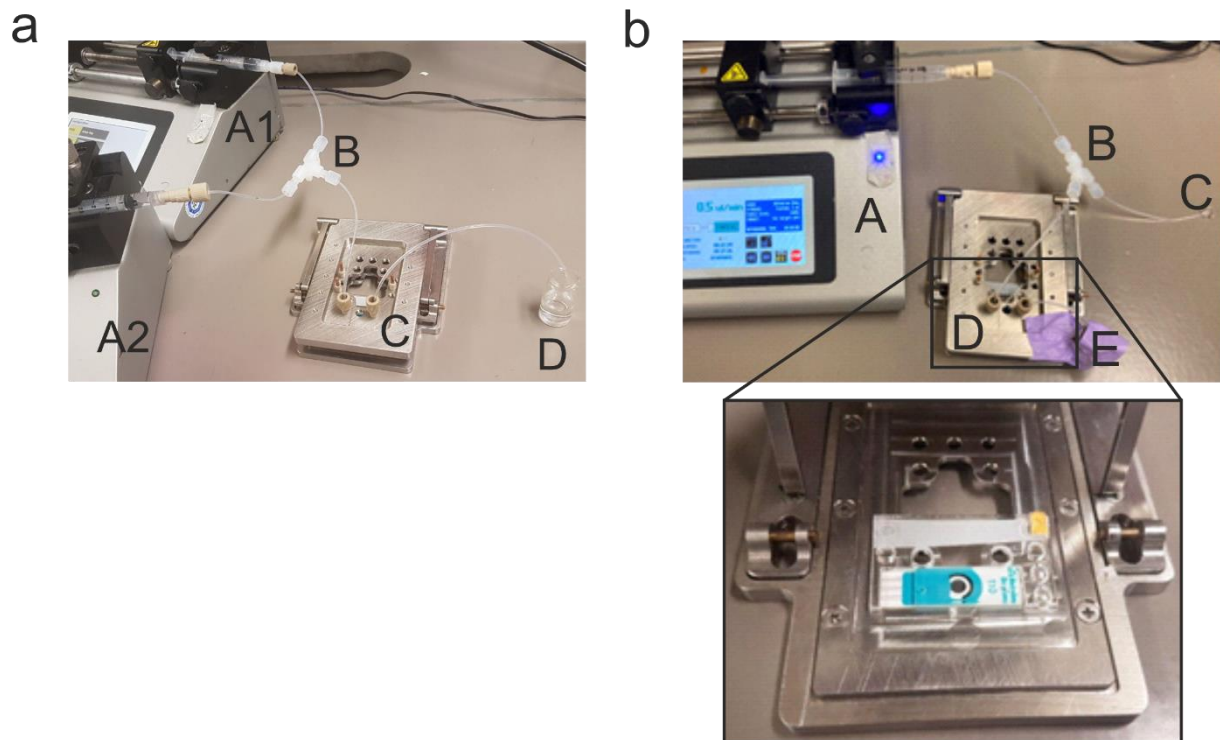


Figure S4.2. Photograph (a) of the microfluidic setup used with liquid AB-AgNP with syringe pump for washing buffer (A1) and KCl (A2), T-piece (B), chip holder (C) and buffer reservoir/ waste (D) and (b) of the microfluidic setup used with dried AB-AgNPs with syringe pump (A), T-piece (B), bubble trap (C), chip holder (D) and buffer reservoir/ waste (E) with a close-up on the chip holder with inserted flow chip.

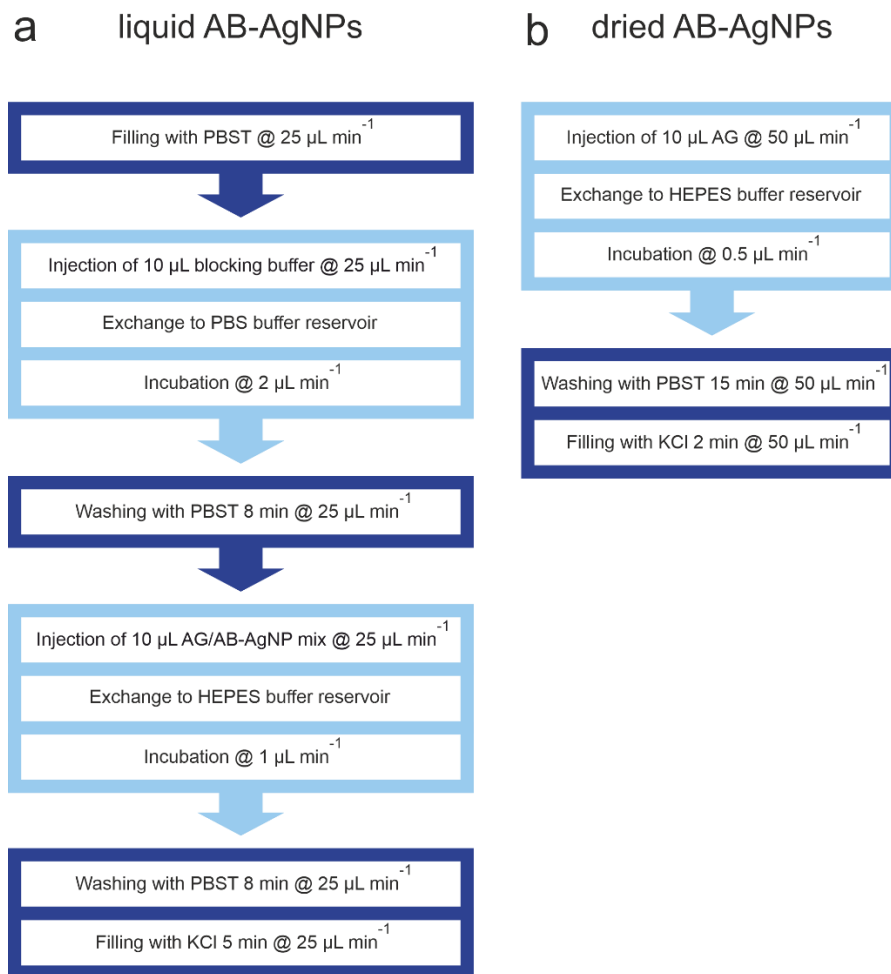


Figure S4.3. Pumping strategy for the microfluidic experiments (a) without and (b) with dried AB-AgNPs, for dark blue steps the pump was operated in injection mode, while light blue indicates withdrawal mode. AG/AB-AgNP mix was incubated in a 1:1 ratio for 2 h prior to injection, 0.1 M KCl was used for filling of the microchannel.

Pretests for Drying of the AgNPs

AB-AgNP stock solution ($20 \mu\text{g}\cdot\text{mL}^{-1}$ in 10 mM HEPES+0.1% (w/v) BSA, pH 7.4) was diluted 1:5 with 10 mM HEPES buffer (pH 7.4) and $50 \mu\text{L}$ of this mixture were pipetted onto polymer disks. After drying for 1 h at $50 \text{ }^\circ\text{C}$, the NPs were rehydrated with $20 \mu\text{L}$ 10 mM HEPES (pH 7.4) for varying amounts of time. A volume of $10 \mu\text{L}$ of this mixture was then pipetted on the WE of a DRP-110 SPCE and left to dry at room temperature for electrochemical measurement: after pretreatment with 1.25 V for 60 s and -0.8 V for 30 s, differential pulse voltammetry was performed from -0.25 V to 0.25 V with $t_{\text{puls}}=50 \text{ ms}$, $E_{\text{step}}=10 \text{ mV}$, $E_{\text{amplitude}}=80 \text{ mV}$, scan rate= $20 \text{ mV}\cdot\text{s}^{-1}$ (Figure S4.4 a). Next, the dried AB-AgNPs were compared to pure 10 mM HEPES buffer (pH 7.4) dried on the support (blind) and AB-AgNPs ($20 \mu\text{g}\cdot\text{mL}^{-1}$ in 10 mM HEPES+0.1% (w/v) BSA, pH 7.4) diluted 1:2 in 10 mM HEPES buffer (pH 7.4) without drying (control). For all three samples, the electrochemical activity was measured as described above (Figure S4.4 b).

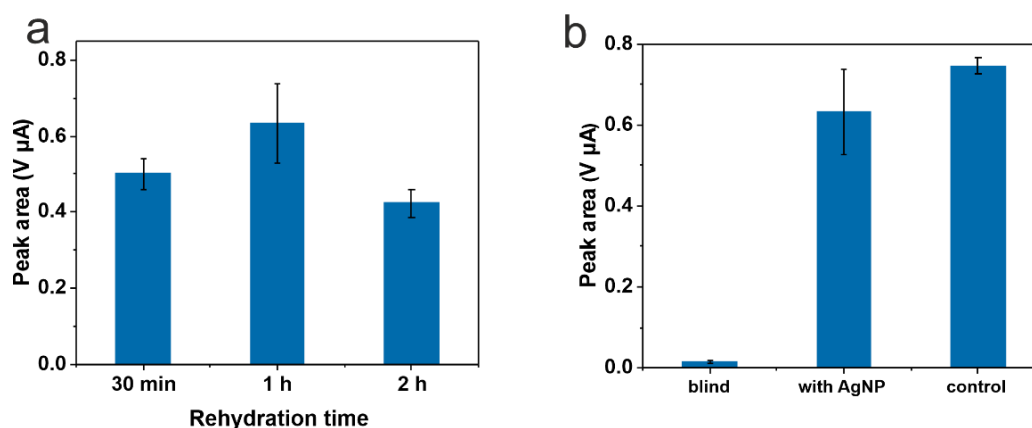


Figure S4.4. Electrochemical activity of (a) $50 \mu\text{L}$ 1:5 diluted AB-AgNP stock ($4 \mu\text{g}\cdot\text{mL}^{-1}$ in 10 mM HEPES, pH 7.4) dried for 1 h at $50 \text{ }^\circ\text{C}$ after rehydration with $20 \mu\text{L}$ 10 mM HEPES (pH 7.4) at room temperature for a different amount of time and of (b) $50 \mu\text{L}$ 10 mM HEPES (pH 7.4, blind) and $50 \mu\text{L}$ 1:5 diluted AB-AgNP stock ($4 \mu\text{g}\cdot\text{mL}^{-1}$ in 10 mM HEPES, pH 7.4, with AgNP) dried for 1 h at $50 \text{ }^\circ\text{C}$ after rehydration with $20 \mu\text{L}$ 10 mM HEPES (pH 7.4) for 1 h at room temperature, with 1:2 diluted AB-AgNPs ($10 \mu\text{g}\cdot\text{mL}^{-1}$ in 10 mM HEPES, pH 7.4) without drying as control. Standard deviations were calculated based on three parallel measurements on three different SPCEs ($n=3$). Error bars represent mean values $\pm 1\sigma$.

In Figure S4.5, a comparison of trehalose disks (20% (w/v) trehalose in 10 mM HEPES, pH 7.4 without (blind) or with 1:2 diluted AB-AgNPs ($10 \mu\text{g}\cdot\text{mL}^{-1}$ in 10 mM HEPES, pH 7.4) (with AgNP)) with AB-AgNPs 1:2 diluted in 20% (w/v) trehalose (control) in solution is shown. The dried NPs were redispersed in $20 \mu\text{L}$ 10 mM HEPES buffer (pH 7.4) for 1 h at room temperature. The electrochemical activity was measured as described above.

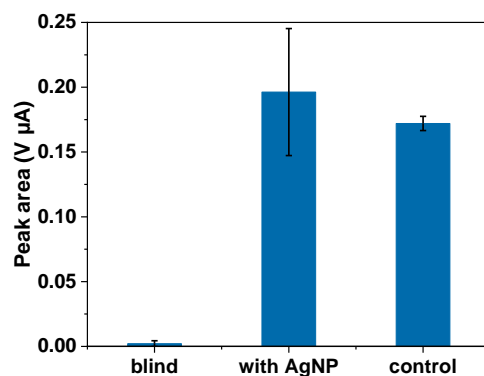


Figure S4.5. Electrochemical activity of 20 μL 20% (w/v) trehalose (blind) and 20 μL 1:2 diluted AB-AgNP stock in 20% (w/v) trehalose (with AgNP) dried for 1 h at 50 $^{\circ}\text{C}$ after rehydration with 20 μL HEPES for 1 h at room temperature, with 1:2 diluted AB-AgNPs in 20% (w/v) trehalose without drying as control. Standard deviations were calculated based on three parallel measurements on three different SPCEs ($n=3$). Error bars represent mean values $\pm 1\sigma$.

The bioassay was performed using 0 and 100 $\text{ng}\cdot\text{mL}^{-1}$ AG in 50 mM PBS (pH 7.4) and AB-AgNP (20 $\mu\text{g}\cdot\text{mL}^{-1}$ in 10 mM HEPES+0.1% (w/v) BSA+10% (w/v) trehalose, pH 7.4) dried overnight at 50 $^{\circ}\text{C}$. Rehydration of the AB-AgNPs and incubation with AG was performed directly on the electrode in one step. Exemplary differential pulse voltammograms are shown in Figure S4.6.

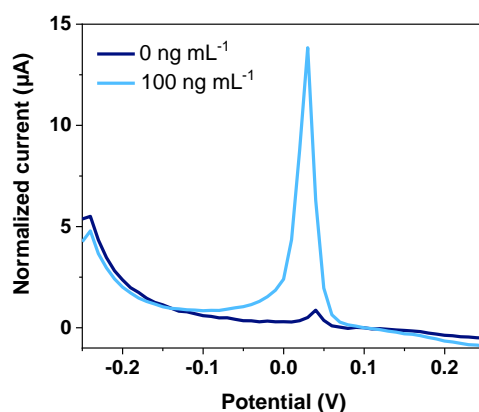


Figure S4.6. Exemplary differential pulse voltammograms of pure 50 mM PBS (pH 7.4, dark blue) or 100 $\text{ng}\cdot\text{mL}^{-1}$ AG (in 50 mM PBS, pH 7.4, light blue), bioassay performed with AB-AgNPs (20 $\mu\text{g}\cdot\text{mL}^{-1}$ in 10 mM HEPES+0.1% (w/v) BSA+10% (w/v) trehalose, pH 7.4) dried at 50 $^{\circ}\text{C}$ overnight, normalized to the respective current at 0.1 V.

Measurements with Preincubation

For microfluidic experiments with preincubation, 5 μL AG solution (in 50 mM PBS, pH 7.4) was incubated with 5 μL AB-AgNP stock ($20 \mu\text{g}\cdot\text{mL}^{-1}$ in 10 mM HEPES+0.1% (w/v) BSA, pH 7.4) for 2 h at room temperature. Then, the microfluidic experiments were performed following the flow chart shown in Figure S4.3 a. The assay was performed with AG concentrations from 0 to $300 \text{ ng}\cdot\text{mL}^{-1}$ (concentrations given as injected in the microfluidic system). The results are shown in Figure S4.7. The calculated LOD is $0.27 \text{ ng}\cdot\text{mL}^{-1}$ with a mean error of 25% ($n \geq 4$).

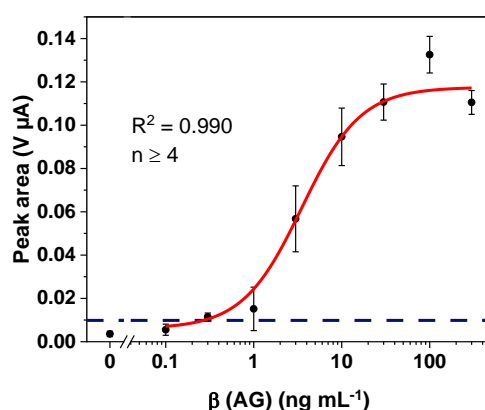


Figure S4.7. Plot of peak area against logarithm of injected antigen concentration after preincubation with AB-AgNPs with logistic fit (red line) and corresponding parameters. The blue dashed line indicates the LOD. Standard deviations were calculated based on five parallel measurements using five different flow chips, while outliers were removed after Q-test (confidence interval 95%). Error bars represent mean values $\pm 1\sigma$ ($n \geq 4$).

Incubation and Washing Speeds for Optimized Microfluidic Setup

The incubation and washing procedure was optimized for the microfluidic setup with dried AB-AgNPs. To find a valid starting point for the optimizations, some calculations were performed first. For the WE in the microfluidic channel a volume of around $1.25 \mu\text{L}$ was calculated based on the dimensions of the channel ($h=100 \mu\text{m}$) and the working electrode ($d=4 \text{ mm}$). For the incubation speed optimizations, the residence time of sample on the working electrode was calculated using the effective volume ($1.25 \mu\text{L}$) and the incubation speed of 0.25, 0.5 or $1 \mu\text{L}\cdot\text{min}^{-1}$, which resulted in 45, 23 or 11 min respectively. As starting point for the incubation speed optimizations, the 60 min hybridization time of the standard assay [12] were used. Due to a lower diffusion distance (from the center to the surface) within the small confinements of the microfluidic channel ($50 \mu\text{m}$ vs. 3.5 mm in 96-well microtiter plates), a smaller residence time was expected to be sufficient for an effective capture of the antigen. To

test this theory, the signal of $100 \text{ ng}\cdot\text{mL}^{-1}$ AG (in 50 mM PBS, pH 7.4) is shown for different incubation velocities (Figure S4.8 a). The maximum signal with lowest error is received for $0.50 \text{ }\mu\text{L}\cdot\text{min}^{-1}$. Indeed, the tests confirmed that 23 min hybridization time was optimal for 10 μL of sample under these conditions. For the washing velocity, the same approach was used. The effective washing time for the volume on the WE ($1.25 \text{ }\mu\text{L}$) was 10 min for $250 \text{ }\mu\text{L}$ @ $25 \text{ }\mu\text{L}\cdot\text{min}^{-1}$, 5 min for $250 \text{ }\mu\text{L}$ @ $50 \text{ }\mu\text{L}\cdot\text{min}^{-1}$ or 15 min for $750 \text{ }\mu\text{L}$ @ $50 \text{ }\mu\text{L}\cdot\text{min}^{-1}$, respectively. The S/N between the signals for 100 and $0 \text{ ng}\cdot\text{mL}^{-1}$ AG (in 50 mM PBS, pH 7.4) is plotted in Figure S4.8 b. An increase of washing speed with same volume keeps the S/N constant. A drastic increase of the S/N was achieved by an additional increase of volume. The signal stayed constant, which means that no detection complex is washed off the surface, while the background signal decreases. This shows that 15 min washing with a high velocity is the optimal compromise between duration and effective washing. In the end, an incubation speed of $0.5 \text{ }\mu\text{L}\cdot\text{min}^{-1}$ and washing with $750 \text{ }\mu\text{L}$ at $50 \text{ }\mu\text{L}\cdot\text{min}^{-1}$ was used for the final assay.

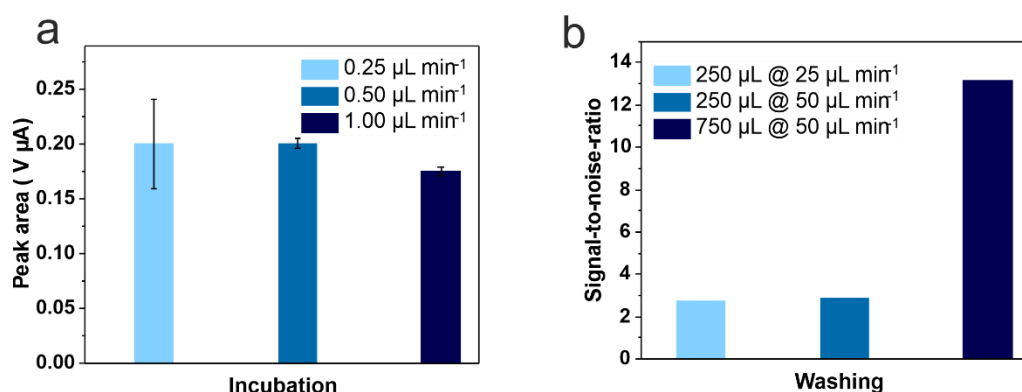


Figure S4.8. (a) Peak area of the assay performed with $100 \text{ ng}\cdot\text{mL}^{-1}$ AG concentration (in 50 mM PBS, pH 7.4) in the flow cells with dried AB-AgNPs with different incubation speed ($n=2$), while washing with $750 \text{ }\mu\text{L}$ at $50 \text{ }\mu\text{L}\cdot\text{min}^{-1}$ and (b) signal-to-noise ratio for $100 \text{ ng}\cdot\text{mL}^{-1}$ AG concentration (in 50 mM PBS, pH 7.4) in the flow cells with dried AB-AgNPs with different washing speed and volume ($n=1$), with incubation at $0.5 \text{ }\mu\text{L}\cdot\text{min}^{-1}$.

Serum Calibration with NT-proBNP Concentrations Measured by Roche's Elecsys

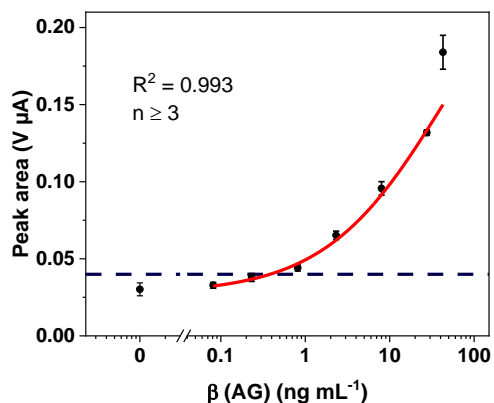
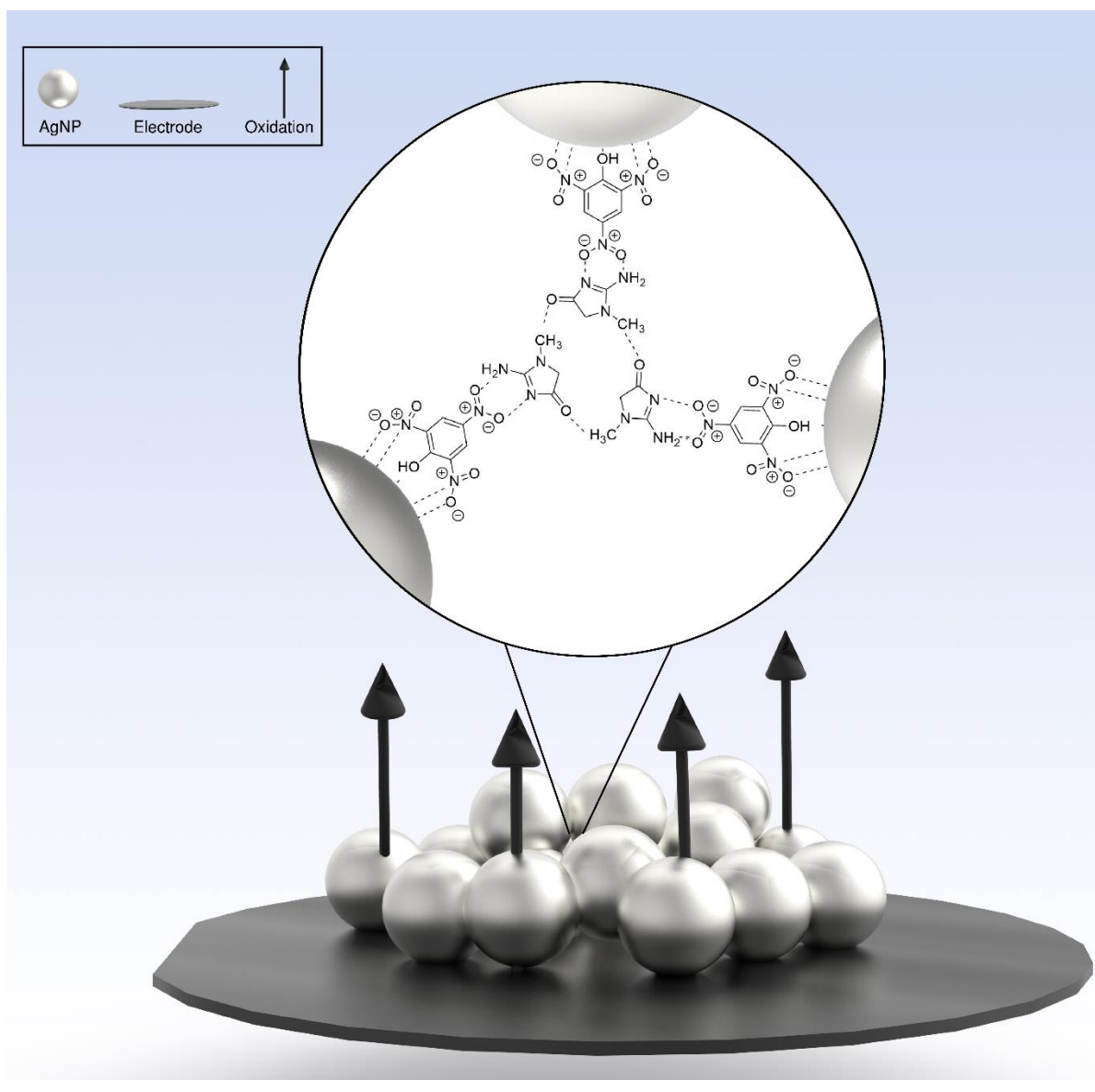


Figure S4.9. Plot of peak area against logarithm of antigen concentration in undiluted human serum as measured with Roche's Elecsys[®] (Table 4.1) with logistic fit (red line) and corresponding parameters. The blue dashed line indicates the LOD. Standard deviations were calculated based on four parallel measurements using four different flow chips, while outliers were removed after Q-test (confidence interval 95%). Error bars represent mean values $\pm 1\sigma$ ($n \geq 3$).

5 Easy Electrochemical Aggregation Assay for Quantification of Creatinine at the Point-of-Care

Graphical Abstract



This chapter is part of a manuscript intended for publication.

Abstract

The creatinine content in blood or urine is a commonly used clinical parameter to assess problems with the renal function of patients. Here, an easy and fast electrochemical aggregation assay was developed to quantify creatinine based on the specific interaction of picric acid modified silver nanoparticles with creatinine. It was found out that 10 nm AgNPs modified with 10 μ M PA are ideal for electrochemical detection and show effective aggregation. An all-dried procedure was developed without any loss of performance to make the assay accessible to point-of-care strategies. Moreover, the sensitivity of this assay type can be controlled by the ratio of PA-AgNP to sample, which makes it easily adjustable to different matrices with various analyte concentration ranges. With a 2:3 ratio of PA-AgNPs to sample, a LOD of 76 μ M was reached with a mean standard deviation of 12% in buffer was reached. The aggregation assay was then applied for the detection of creatinine in 1:10 diluted synthetic urine and a clear dependence of the electrochemical peak area to creatinine content was found between 0.4 and 2 mM (4-20 mM creatinine in undiluted urine). Thus, this proof-of-principle already covers the majority of the physiological range without PA-AgNP-sample ratio adjustments.

Keywords

electrochemical biosensor, silver nanoparticle, aggregation, blood analysis, differential pulse voltammetry

5.1 Introduction

Point of care testing is defined as clinical laboratory testing conducted close to the site of patient care, which can be in the hospital laboratory as well as right on the patient's bed. Clinical personnel or patients themselves can perform the tests, while latter is referred to as self-testing. Advantages over conventional testing methods include ease of handling, rapidness, and cost-efficiency [1]. This sparked a rising interest of the research community since the year 2000, which can be seen in numbers of publications regarding POCT. Nowadays, POCT devices are found in various medicinal fields, like endocrinology/diabetes, cardiology, nephrology, critical care, fertility, hematology/coagulation, infectious disease, microbiology, and general health screening. A variety of formats including LFAs or microfluidics are employed and commercially available. However, still new solutions, especially for self-testing, are sought after with high accuracy, high sensitivity, low sample volume demand and quantitative determination.

There are many examples found in literature, which show the use of a silver nanoparticle aggregation assay. Most of them use an optical or colorimetric detection based on the local surface plasmon resonance of AgNPs. Upon aggregation, the localized surface plasmons of individual particles are coupled and the resonance wavelength shifts [2]. These assays are easy to perform, fast and were employed for various analytes including biothiols [3, 4], DNA [5] or adenosine [6], in a multitude of sample matrices. Due to the inherent instability of AgNP dispersions, suitable surface modifications are necessary to render these assays truly useful and thorough selectivity studies are needed.

Creatinine in urine or serum is a commonly used clinical marker for renal function. Since the creatinine content is more independent of the diet, it is a better measure for renal glomerular filtration rate than urea or nitrogen residues. Although the concentration of creatinine in the plasma or serum of healthy adults ranges between 44 and 150 μM , it can be considerably decreased in children or patients with various diseases (27-44 μM) [7]. In urine, the creatinine concentration found by a spot test varies strongly between 30 and 300 mg/dL (2.65-26.5 mM) depending inter aliae on gender and comorbidities [8]. Due to this varying amount of creatinine in individuals, a self-testing device for patients at-risk or during treatment of a kidney disease would be highly useful to detect changes in an early stage. The Jaffe reaction [9], which is the reaction of creatinine with picric acid in alkaline solution to form a strongly colored compound,

is traditionally used for clinical creatinine detection via photometric measurements. The reaction is highly sensitive with a limit of detection of $9 \mu\text{M}$ [10], and it meets modern analytical performance requirements for routine use. However, the reaction is influenced by various metabolites and this accounts for significant positive errors especially in low concentration regions. Modifications of this reaction are available, but they make the reaction more time-consuming and difficult to automate [7]. Therefore, other approaches are sought after. Parmar *et al.* developed an aggregation assay based on the interaction of AgNPs modified with picric acid (Figure 5.1 b) and creatinine in neutral or slightly acidic media [11]. The basis for this highly specific interaction is the tautomeric form of creatinine (Figure 5.1 c). They extensively characterized this system and investigated the selectivity against a multitude of biomolecules and further influencing factors. While the system was proven to be highly selective and sensitive, it still suffers from common drawbacks of optical transduction methods. In order to ensure a sufficient path length, sample volume demand is rather high, usually in the range of several hundreds of μL to a few mL. The turbidity and color of the sample are further limiting factors. Therefore, blood samples have to be pretreated via centrifugation or dilution. This makes quantitative self-testing for the patient difficult. An electrochemical aggregation assay combines the advantages of this method with higher miniaturization potential, lower sample/reagent volume demand and low-cost instrumentation. The aggregation of AgNPs in presence of the analyte is detected by the change of DPV signal of the silver oxidation (Figure 5.1 a). Silver is an ideal electrochemical tag due to the inherent instability, which enables easy-to-perform, interference-free detection at low potential [12].

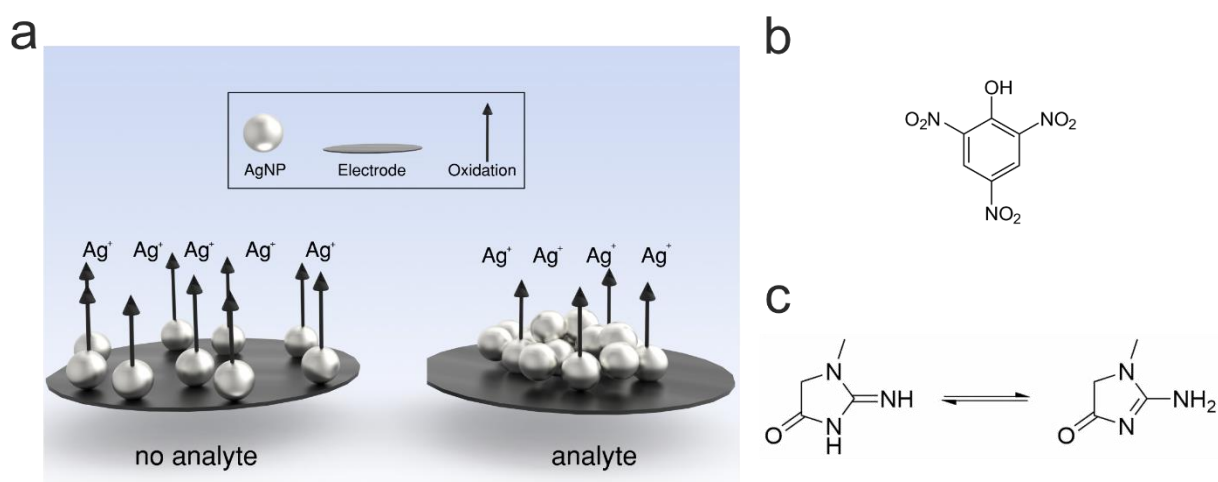


Figure 5.1. (a) Schematic representation of the electrochemical detection of the aggregation upon presence of the analyte and structures of (b) picric acid and (c) the tautomeric form of creatinine.

Up to date, not much has been done regarding the electrochemical detection of AgNP aggregation. Hu *et al.* compared optical and electrochemical detection of the AgNP aggregation in presence of biothiols [13]. However, since unmodified AgNPs were used, the aggregation is not selective, and it can be seen rather as a proof-of-principle. In the present work, homocysteine (HCy) was also used as model analyte in combination with unmodified AgNPs for basic investigations regarding the electrochemical detection and aggregation. Other researchers employed dissolved organic matter-capped AgNPs on a glassy carbon electrode for the detection of atrazine induced aggregation [14]. However, this procedure is based on a composite electrode, which makes it considerably different to the homogeneous approach employed in our studies. Since the analyte-surface modification combination utilized here was previously published, characterization of this system and the aggregation was not performed again. This work focuses on the electrochemical detection of the AgNP aggregation and the facilitation of the procedure to ultimately receive an easy POC self-testing device.

5.2 Experimental Section

5.2.1 Materials and Instruments

Citrate capped silver nanospheres ($d=10-100$ nm, 0.02 mg·mL⁻¹) were purchased from nanoComposix (www.nanocomposix.com). Disodium hydrogen phosphate ($\text{Na}_2\text{HPO}_4 \cdot 2 \text{H}_2\text{O}$, *p.a.*), potassium hydrogen phosphate ($\text{K}_2\text{HPO}_4 \cdot 3\text{H}_2\text{O}$, *p.a.*) and sodium dihydrogen phosphate ($\text{NaH}_2\text{PO}_4 \cdot \text{H}_2\text{O}$, *p.a.*) were ordered from Merck (www.merckmillipore.com). Trehalose (D-(+)-trehalose dihydrate, $\geq 99\%$) and Sigmatrix urine diluent (surin) were supplied from Sigma Aldrich (www.sigmaaldrich.com). Potassium chloride (KCl, *p.a.*) and sodium dodecyl sulfate (SDS, 99%) were obtained from Roth (www.carlroth.com). Sodium hydroxide (NaOH, 1 M) was bought from Labochem international (www.labochem.de). Picric acid (PA, saturated aqueous) was purchased from Morphisto GmbH (www.morphisto.de).

Phosphate buffer (10 mM, pH 7) consisted of 5.8 mM $\text{Na}_2\text{HPO}_4 \cdot 2 \text{H}_2\text{O}$ and 4.2 mM $\text{NaH}_2\text{PO}_4 \cdot \text{H}_2\text{O}$ in ddH₂O with a pH of 7.

Alkaline phosphate buffer (300 mM, pH 12) consisted of 300 mM $\text{K}_2\text{HPO}_4 \cdot 3\text{H}_2\text{O}$ and 2 g·L⁻¹ SDS in ddH₂O and the pH was adjusted to 12.7 using 1 M NaOH.

Electrochemical measurements were performed using screen-printed carbon electrodes (DRP-110, Metrohm AG, www.dropsens.com) and an EmStat blue potentiostat with corresponding software (PalmSens, www.palmsens.com). For nanoparticle modification, the ThermoMixer comfort (Eppendorf, online-shop.eppendorf.de) and Amicon® Ultra-2 mL centrifugal filters (Ultracel®-3K) from Merck (www.merckmillipore.com) were used in combination with a Rotina 380R centrifuge from Hettich (www.hettichlab.com).

5.2.2 Modification of Silver Nanoparticles

The silver nanoparticles were modified using a simple adsorption procedure, which was optimized and adjusted from [11]. For size comparison, 1.5 mL of 10 and 30 nm AgNPs were centrifuged for 30 min at 17,000 g and 10 min at 10,000 g, respectively. After removal of 1.35 mL supernatant, the precipitate was resuspended with 300 μ L picric acid (1 μ M PA in ddH₂O) and incubated under shaking at 350 rpm for 2 h at room temperature. For further modifications, centrifugation filters were used to increase the AgNP (d=10 nm) concentration by a factor of 10. Then, the concentrated AgNPs were incubated in a ratio of 1:2 with PA (1, 10, 100 μ M PA in ddH₂O) for 2 h under shaking at 350 rpm at rt.

5.2.3 Aggregation Assay

For every experiment, KCl was dried on the three-electrode area to reach a final concentration in the solution on the electrode of 0.01 M (denoted as KCl electrode). For size dependence, PA-AgNPs (10-30 nm with 1 μ M PA) were mixed with creatinine (0, 0.1, 1, 10 mM in 10 mM phosphate buffer, pH 7) in a 1:1 ratio and incubated for 1 h at rt. Afterwards, they were added to the prepared KCl electrodes and DPV was performed from -0.2 V to 0.2 V with $t_{\text{puls}}=50$ ms, $E_{\text{step}}=10$ mV, $E_{\text{amplitude}}=80$ mV and scan rate= 20 mV \cdot s⁻¹. For all further experiments, a mixing ratio PA-AgNPs to creatinine of 2:3 was used. The differently modified PA-AgNPs (10 nm with 1, 10, 100 μ M PA) were tested each with 0, 100 and 1000 μ M creatinine in 10 mM phosphate buffer (pH 7) upon incubation for 1 h at rt.

5.2.4 Development of a Dry Testing Procedure

For a dry procedure, 20 μ L of PA-AgNPs (10 nm with 10 μ M PA) in 5% (w/v) trehalose were dried in an Eppendorf tube at 65 °C for 3 h or 50 °C overnight. The electrodes were prepared by drying 30 μ L of KCl on the three-electrode area. For KCl concentration optimization, 0.01, 0.05 and 0.1 M KCl were used, while 0.01 M KCl was utilized for all other experiments. For the performance of the assay, 30 μ L creatinine in 10 mM phosphate buffer (pH 7) were added to

the Eppendorf tube and the PA-AgNPs were resolubilized. Different incubation times from 5 min to 1 h were tested with 0 and 100 μ M creatinine, while an incubation of 1 h was used for all other measurements in buffer.

5.2.5 Detection of Creatinine in Urine Samples

For reference quantification of creatinine in synthetic urine, a kinetic colorimetric method (Cromatest) based on a modified Jaffe's reaction from Linear Chemicals was utilized. A short description can be found in the supporting information. For creatinine detection, the surin was diluted 1:10 with ddH₂O and spiked with varying amount of creatinine resulting in 0.4, 0.6, 1, 2, and 4 mM creatinine in 1:10 diluted surin. The dry testing procedure was performed as described in section 5.2.4., only the incubation time was shortened to 10 min.

5.3 Results and Discussion

The electrochemical measurement and general aggregation parameters were optimized using homocysteine as model analyte with unmodified AgNPs in order to minimize further influences due to AgNP surface modification. First, the influence of a dissolving pretreatment (1.25 V for 60 s, -0.8 V for 30 s) before performance of DPV was investigated (Figure S5.1 a). While the signal intensity is higher in comparison to the measurement without pretreatment, no signal difference especially in the low concentration range was seen. The same concentration shows a signal change of approximately 70% after removal of the pretreatment. This can be explained with the theory for the electrochemical detection. Due to the high overpotential at the oxidation potential of 1.25 V, the tunneling distance of the electrons increases [15]. Therefore, individual particles and small aggregates, formed with a low analyte concentration, are oxidized completely. However, if the analyte concentration is high enough to form huge aggregates, even with pretreatment a signal change is measured. On the contrary, for a fast DPV sweep, the different amount of AgNPs in direct contact with the electrode surface results in a change of the oxidation around 0 V (vs. Ag/AgCl RE). The electrochemical measurement of aggregation (Figure 5.1 a) is therefore a kinetic effect and for highly sensitive detection, only a DPV scan is necessary. Next, two different measurement procedures were tested using the same system (Figure S5.1 b). For the dried procedure, the AgNP solution is dried on the electrode after incubation with HCy and then resolubilized with KCl for the DPV measurement. Here, no signal change is seen in the low concentration range. However, a fluid measurement, meaning the

AgNP solution is dropped onto an electrode, where KCl was previously dried on (KCl electrode), shows a big signal change, even at small concentrations. The reason is probably, that drying of the AgNPs covers the electrode surface completely, which renders the system insensitive for the aggregation grade. Further experiments were performed using the fluid procedure without pretreatment. As an additional advantage, these findings accelerate the measurements significantly.

5.3.1 Optimization of AgNP Modification

The size of AgNPs had a significant influence on the aggregation behavior. Nanoparticle diameters between 10 and 100 nm were tested previously with the model analyte HCy (Figure S5.2). Due to decreasing surface-to-volume ratio, the electrochemical signal decreases with increasing AgNP diameter. However, the aggregation results in higher signal changes for bigger nanoparticles, especially for low HCy concentrations, because the distance to the electrode increases more significantly for aggregation of bigger nanoparticles. However, only smaller nanoparticles are tested for the creatinine detection to ensure a measurable signal. For Figure 5.2, 10 (a) and 30 nm PA-AgNPs (b) were incubated with differently concentrated creatinine solutions. Due to different concentrations after the modification, the absolute peak areas cannot be taken into account. However, the 10 nm particles seem to be more sensitive and show higher signal change for low concentrations. The reason could be that with the low PA concentration of 1 μM , the density of PA on the bigger nanoparticle's surface is not high enough to cause effective aggregation at low analyte concentrations. This effect seems to prevail the just described higher electrochemical signal change for bigger NPs. Therefore, 10 nm particles are used for all following experiments, which combined high electrochemical signal with effective aggregation. Since precipitation by centrifugation is not complete for 10 nm particles, centrifugation filters were used in the following for increase of the NP concentration and buffer exchange.

Next, different amounts of PA (1, 10, 100 μM) in the modification were tested. These PA-AgNPs were incubated with differently concentrated creatinine solutions. Figure 5.2 c shows the signal normalized to the respective blind signal, denoted as signal change.

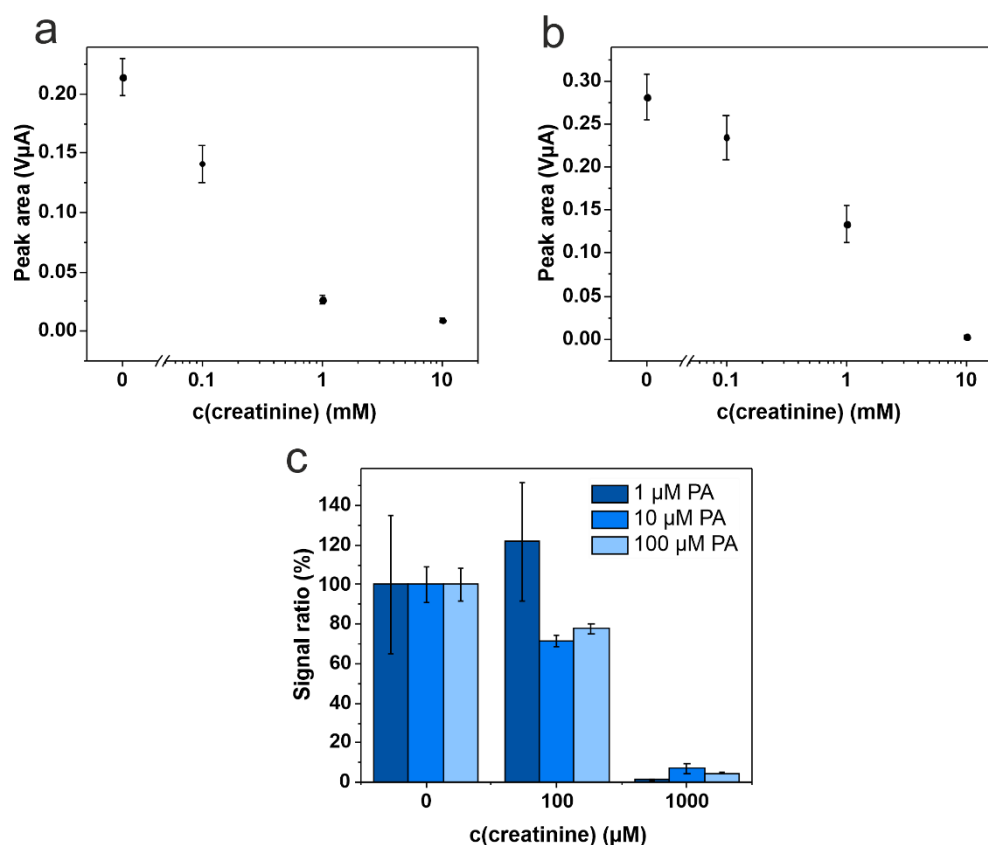


Figure 5.2. DPV peak area for PA-AgNPs (1 μM PA) with (a) 10 and (b) 30 nm diameter after incubation with differently concentrated creatinine solutions (0-10 mM in 10 mM phosphate buffer, pH 7) and (c) DPV peak area of AgNPs (10 nm) modified with 1-100 μM PA incubated with differently concentrated creatinine solutions (0, 100, 1000 μM in 10 mM phosphate buffer, pH 7) normalized to the respective blind signal. Standard deviations were calculated based on three parallel measurements on three separate SPCEs. Error bars represent mean values $\pm 1\sigma$ ($n=3$).

Especially in the low creatinine concentration regime, 10 μM PA seems to be ideal. Since a concentration of 1 μM PA is not sufficient for effective AgNP coverage, it does not show a signal change for low creatinine concentrations and high errors. Using a concentration of 100 μM PA shows similar but slightly worse results to 10 μM , probably due to free picric acid, which binds the creatinine and thus inhibits the aggregation of PA-AgNPs. Therefore, 10 μM PA was used in the modification for all following experiments.

5.3.2 Development and Optimization of a Dry Testing Procedure

To make this principle better applicable for the point-of-care, drying of the PA-AgNPs was investigated next. First tests show that ideal results are achieved by separating the PA-AgNPs from KCl during incubation, probably due to oxidation of the silver by air oxygen. Therefore, AgNPs were dried for 3 h at 65 $^{\circ}\text{C}$ in a 5% (w/v) trehalose matrix in an Eppendorf tube. The trehalose builds a glass-like network upon drying, which enables drying and redispersion

without aggregation or excessive oxidation of AgNPs, and inclusion of an oxygen scavenger for long-time storage [16]. The trehalose content for the aggregation assay was also optimized using the model analyte Hcy and unmodified AgNPs (Figure S5.3). The presence of trehalose in the investigated concentration range does not seem to have any influence on the aggregation of the AgNPs and a minimum of 5% (w/v) is necessary to stabilize the particles upon drying and enable a sensitive detection. A further increase of the trehalose content impairs the results probably due to partial inhibition of the aggregation. Using this optimized matrix, the sensor response for different creatinine concentration was compared to the earlier used wet procedure, *i.e.* incubation of creatinine with PA-AgNP solution (Figure 5.3).

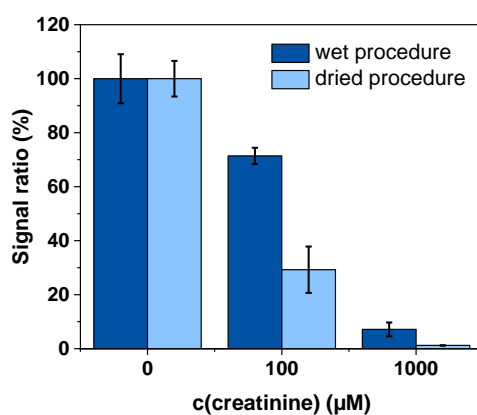


Figure 5.3. DPV peak area normalized to the respective blind signal for different creatinine concentrations (0, 100, 1000 µM in 10 mM phosphate buffer, pH 7) using wet (dark blue) and dried procedure (light blue), wet: incubation of PA-AgNPs with creatinine in a 1:2 ratio for 1 h, dried: drying of 20 µL PA-AgNPs in 5% (w/v) trehalose for 3 h at 65 °C, incubation with 30 µL creatinine for 1 h. Standard deviations were calculated based on three parallel measurements on three separate SPCEs. Error bars represent mean values $\pm 1\sigma$ (n=3).

A clear increase in signal change is seen for the dried procedure throughout the creatinine concentrations. The reason lies presumably in the higher PA-AgNP concentration during incubation, which enables more effective aggregation. Moreover, the mean relative error is slightly reduced from 16% to 12%.

For the dried procedure, the KCl content in the measurement solution (Figure 5.4 a) and the incubation time of creatinine with PA-AgNPs (Figure 5.4 b) were optimized. It shows clearly that the blind signal decreases considerably with increasing KCl concentration, while the 100 µM creatinine signal stays rather constant. Small KCl concentrations show a higher signal change and are therefore needed for a highly sensitive detection. The reason could be that

AgNPs get oxidized quickly in contact with high concentrations of KCl by air oxygen or that the chemical equilibrium of the aggregation is shifted to the educt side in high ionic strength media. Due to the fluid procedure (*i.e.* PA-AgNP-creatinine solution dropped onto KCl electrode), the KCl concentration in contact with the PA-AgNPs is higher, right when the nanoparticle solution is pipetted onto the electrode. Thus, a low dried concentration of 0.01 M KCl was used for all measurements.

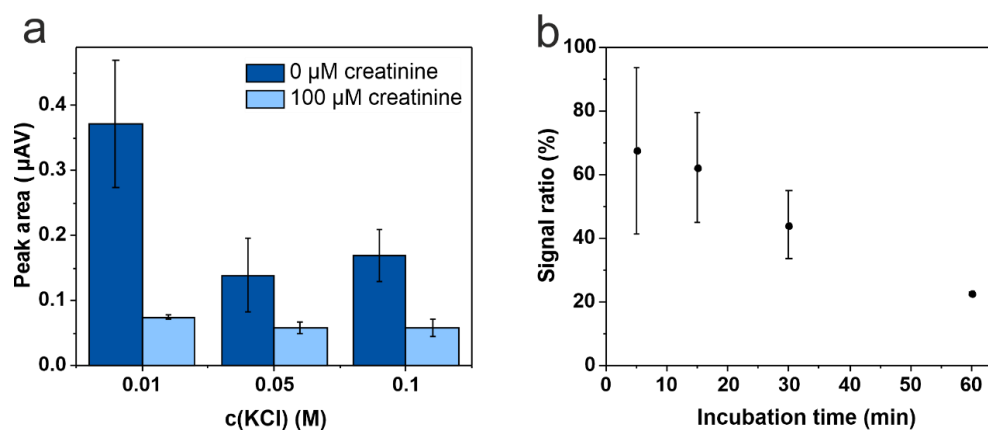


Figure 5.4. (a) DPV peak area after incubation of dried PA-AgNPs (10 nm, 10 µM PA) with 0 and 100 µM creatinine (in 10 mM phosphate buffer, pH 7) measured on SPCEs with different KCl concentrations (0.01, 0.05, 0.1 M) dried on the three-electrode area and (b) DPV peak area normalized to the respective blind signal after different incubation times of dried PA-AgNPs (10 nm, 10 µM PA) with 100 µM creatinine (in 10 mM phosphate buffer, pH 7). Standard deviations were calculated based on three parallel measurements on three separate SPCEs. Error bars represent mean values $\pm 1\sigma$ ($n=3$).

An incubation for 1 h is necessary in the current format, because the aggregation kinetic in buffer solution is rather slow. It can be seen clearly that the SD decreases enormously and the signal ratio to the blind reaches 20% for 100 µM. The incubation time, however, can be shortened considerably for samples with high creatinine concentrations, for example urine.

5.3.3 Dose-Response-Curves in Buffer

Usually, aggregation of silver nanoparticles is measured through the optical shift of the plasmonic band due to coupling of the electron oscillation. The strong color change from yellow to red around 100 µM can even be seen with the naked eye (Figure 5.5 a). However, this optical detection suffers from disadvantages especially for the measurements of strongly colored or turbid samples, *e.g.* whole blood, and requires more complicated and bigger hardware in comparison to electrochemical detection.

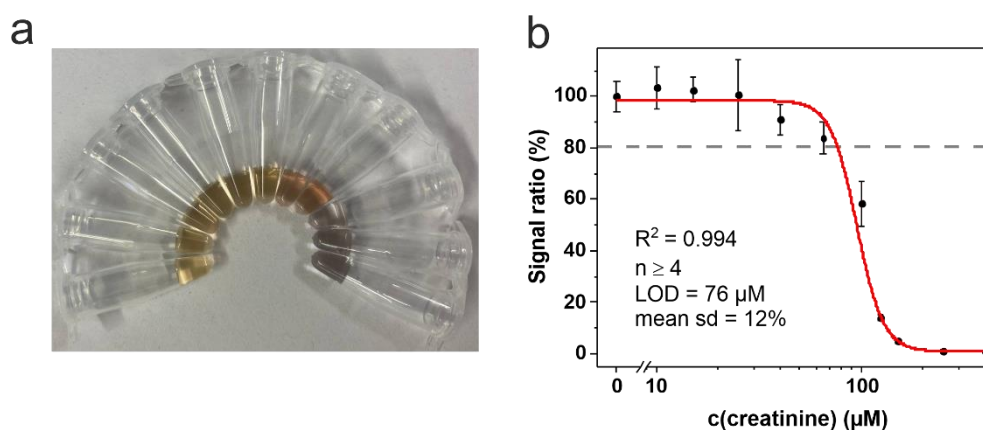


Figure 5.5. (a) Color change of PA-AgNPs with increasing creatinine concentration from left to right (0, 10, 15, 25, 40, 65, 100, 125, 150, 250, 400 μM in 10 mM phosphate buffer, pH 7) after 60 min and (b) DPV peak area normalized to the blind signal for different creatinine concentrations (0–400 μM in 10 mM phosphate buffer, pH 7) measured via the dried procedure with 0.01 M KCl and 1 h incubation. Red line indicates the logistic fit, the grey dotted line represents the LOD. Standard deviations were calculated based on five parallel measurements on five separate SPCEs, while outliers were removed after Q-Test (confidence interval 95%). Error bars represent mean values $\pm 1\sigma$ ($n \geq 4$).

In Figure 5.5 b, a dose-response curve covering the μM concentration range is shown. A sigmoidal curve shape can be seen with a linear concentration range between 60 and 150 μM , a limit of detection of 76 μM and mean error of 12%. The LOD is calculated based on the fit parameter for the lower border A_1 and the standard deviation of the blind $sd(\text{blind})$ according to equation 5.1.

$$LOD = A_1 - 3 \cdot sd(\text{blind}) \quad (5.1)$$

The sensitivity of these aggregation assays can be easily adjusted via changes in the sample to PA-AgNP ratio as shown previously for the model analyte HCy (Figure S5.4). It is seen, that 30 and 100 μL AgNPs, both with 20 μL HCy, show different sensitive ranges. While a ratio of sample to NPs of 1:5 seems to be sensitive in the high concentration range, a 2:3 ratio, shows bigger signal change in the low concentration range. The reason is that the more AgNPs are present, the more analyte is needed for an effective, measurable aggregation. The deviations from the sigmoidal fit can be explained by the single-use electrodes and irregular coating and dissolution of KCl. Using an industrially roll-to-roll fabricated electrode system, these errors should be considerably reduced.

5.3.4 Application for Urine Samples

Parmar *et al.* applied this system for the analysis of serum and other blood samples [11]. Creatinine can be detected in blood as well as urine. Since kidney problems quickly lead to

changes of the creatinine concentration in blood, these measurements are typically used in the emergency room upon suspicion of acute kidney failure. However, for at-home monitoring of chronic renal problems or medical treatment of such, urine is the ideal matrix. It is easily obtained, non-invasive and creatinine is present in high concentrations (2.65-26.5 mM [8]). Therefore, the creatinine quantification was next tested in synthetic urine matrix. Since no exact information about the creatinine content in the purchased synthetic urine is available, a modification of the clinically used Jaffe's reaction is employed to quantify the creatinine and provide an external reference measurement. The amount of creatinine in the 1:50 diluted sample (surin) is calculated over comparison of the absorbance values (Table S5.1) at 510 nm after 30 s (A_1) and after 90 s (A_2) to a creatinine standard (177 μ M) according to equation 5.2.

$$\frac{(A_2 - A_1)_{sample}}{(A_2 - A_1)_{standard}} \cdot c_{standard} \cdot 50 = 4 \pm 1 \text{ mM} \quad (5.2)$$

In first aggregation tests, a strong matrix effect was seen: probably caused by the high ion concentrations in urine, especially chloride (usually 20-40 mM [17]), the aggregation is either hindered or the electrochemical measurement somehow impaired. However, also the change of color, which is an optical indication for aggregation, only takes place for concentrations around 1 mM (Figure 5.6 a). This allows the conclusion, that the aggregation itself is affected rather or at least to a bigger extent than the electrochemical measurement. Therefore, the creatinine content in urine samples cannot be quantified comparing to the buffer calibration, but a new calibration curve has to be recorded using standard addition method. Since this should only be a proof-of-principle, experimental parameters were not varied to find the exact PA-AgNP-sample ratio for the physiological range, the surin was rather diluted 1:10 to fit into the current dynamic range. Solely the incubation time was adjusted to 10 min after it was seen that the AgNPs aggregate considerably faster than in buffer. The reason is probably that less diffusion time is necessary for collisions between the analyte and the PA-AgNPs in higher concentrated solutions. After spiking of the 1:10 diluted surin ($c_0(\text{creatinine})=0.4$ mM) to receive further concentrations (0.6, 1, 2, 4 mM in 1:10 diluted surin), the aggregation assay was performed. In high ionic strength solutions, the PA-AgNP solutions look more colorless, but the color change can still clearly be noticed in the investigated concentration region (Figure 5.6 a).

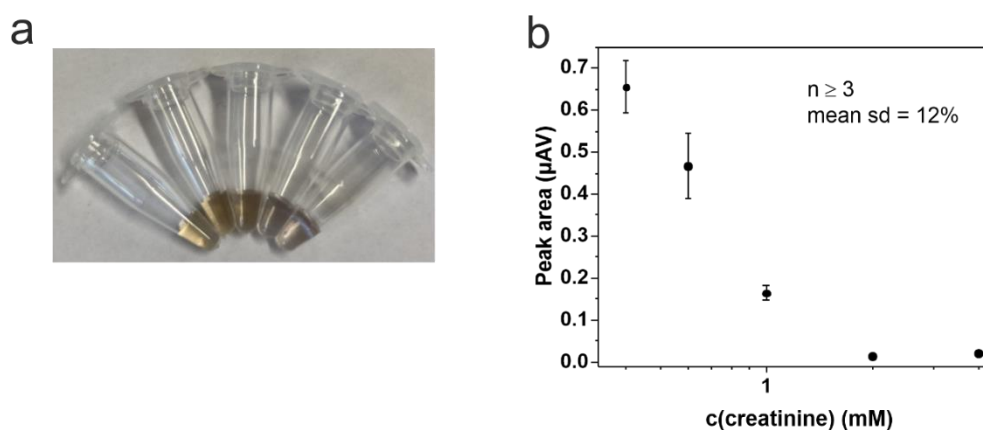


Figure 5.6. (a) Color change of PA-AgNPs dried in 5% (w/v) trehalose with increasing creatinine concentration from left to right (0.4, 0.6, 1, 2, 4 mM in 1:10 diluted surin) after 5 min and (b) DPV peak area for different creatinine concentrations (0.4–4 mM in 1:10 diluted surin) measured via the dried procedure with 0.01 M KCl and 10 min incubation. Standard deviations were calculated based on four parallel measurements on four separate SPCEs, while outliers were removed after Q-test (confidence interval 95%). Error bars represent mean values $\pm 1\sigma$ ($n \geq 3$).

The corresponding DPV peak area is plotted in Figure 5.6 b. A dependence of the peak area on the concentration of creatinine can be seen from 0.4–2 mM. With this, the unmodified dry procedure aggregation assay covers already the majority of the physiological range (4–20 mM in undiluted urine). Although the lower region of the sigmoidal curve could not be monitored and fitting of the data is impossible, the curve shows a similar course to the dose-response curve in buffer. This shows that the aggregation assay of PA-AgNPs for creatinine can in principle be used for urine analysis. After adjustment of the PA-AgNP-analyte ratio, a measurement in undiluted urine should be also possible. As expected, the signal is slightly higher for the same creatinine content (Figure S5.5), but the PA-AgNPs are definitely aggregated as proven by color change.

5.4 Conclusion

Aggregation assays are a very easy and effective way of analyte detection, when combined with a selective AgNP-surface modification. Both, the optical, as well as the electrochemical detection show similar sensitive ranges. However, the electrochemical detection offers higher miniaturization potential and needs fewer and low-cost hardware. In an earlier publication PA-AgNPs showed to be highly selective for creatinine. Here, it was shown that the principle is also applicable as POC strategy due to the ability to dry all needed reagents without loss of performance. Since this assay should be applied for home-monitoring of disease or medication

progress, PA-AgNPs were employed for the quantification of creatinine in urine matrix. No additional sample preparation besides easy 1:10 dilution is necessary, and the proof-of-principle assay already covered the majority of the physiological range. For future development, the ratio of PA-AgNP to sample amount should be adjusted to fit the physiological range in undiluted urine. Moreover, the PA-AgNPs in stabilizing matrix could be dried on a roll-to-roll fabricated capillary-driven flow chip with integrated electrodes to develop an actual POC self-testing prototype device. The storage stability of this device would have to be confirmed. However, dried AgNPs in trehalose matrix with oxygen scavenger were proven to be highly stable over several months in water-sealed atmosphere before. Overall, this aggregation assay combines the ease of handling with suitable sensitivity, speed of detection and low apparatus requirements and is highly promising for future development of self-testing devices.

5.5 References

1. Lippa PB. POCT - Patientennahe Labordiagnostik. 2nd ed. Berlin, Heidelberg: Springer Berlin / Heidelberg; 2012.
2. Guo X. Surface plasmon resonance based biosensor technique: a review. *J Biophotonics*. 2012;5:483–501. doi:10.1002/jbio.201200015.
3. Vaishnav SK, Patel K, Chandraker K, Korram J, Nagwanshi R, Ghosh KK, Satnami ML. Surface plasmon resonance based spectrophotometric determination of medically important thiol compounds using unmodified silver nanoparticles. *Spectrochim Acta A Mol Biomol Spectrosc*. 2017;179:155–62. doi:10.1016/j.saa.2017.02.040.
4. Thomas A, Sivasankaran U, Kumar KG. Biothiols induced colour change of silver nanoparticles: A colorimetric sensing strategy. *Spectrochim Acta A Mol Biomol Spectrosc*. 2018;188:113–9. doi:10.1016/j.saa.2017.06.040.
5. Ma X, Miao P. Silver nanoparticle@DNA tetrahedron-based colorimetric detection of HIV-related DNA with cascade strand displacement amplification. *J Mater Chem B*. 2019;7:2608–12. doi:10.1039/c9tb00274j.
6. Yousefi S, Saraji M. Optical aptasensor based on silver nanoparticles for the colorimetric detection of adenosine. *Spectrochim Acta A Mol Biomol Spectrosc*. 2019;213:1–5. doi:10.1016/j.saa.2019.01.036.

7. Benkert A, Scheller F, Schössler W, Hentschel C, Micheel B, Behrsing O, et al. Development of a creatinine ELISA and an amperometric antibody-based creatine sensor with a detection limit in the nanomolar range. *Anal Chem.* 2000;72:916–21. doi:10.1021/ac9909047.
8. Barr DB, Wilder LC, Caudill SP, Gonzalez AJ, Needham LL, Pirkle JL. Urinary creatinine concentrations in the U.S. population: implications for urinary biologic monitoring measurements. *Environ Health Perspect.* 2005;113:192–200. doi:10.1289/ehp.7337.
9. Jaffe M. Ueber den Niederschlag, welchen Pikrinsäure in normalem Harn erzeugt und über eine neue Reaction des Kreatinins. *Zeitschrift für Physiologische Chemie.* 1886:391–400.
10. Küme T, Sağlam B, Ergon C, Sisman AR. Evaluation and comparison of Abbott Jaffe and enzymatic creatinine methods: Could the old method meet the new requirements? *J Clin Lab Anal* 2018. doi:10.1002/jcla.22168.
11. Parmar AK, Valand NN, Solanki KB, Menon SK. Picric acid capped silver nanoparticles as a probe for colorimetric sensing of creatinine in human blood and cerebrospinal fluid samples. *Analyst.* 2016;141:1488–98. doi:10.1039/c5an02303c.
12. Beck F, Horn C, Baeumner AJ. Ag nanoparticles outperform Au nanoparticles for the use as label in electrochemical point-of-care sensors. *Anal Bioanal Chem.* 2022;414:475–83. doi:10.1007/s00216-021-03288-6.
13. Hu L, Hu S, Guo L, Tang T, Yang M. Optical and electrochemical detection of biothiols based on aggregation of silver nanoparticles. *Anal. Methods.* 2016;8:4903–7. doi:10.1039/c6ay01295g.
14. Zahran M, Khalifa Z, Zahran MA-H, Abdel Azzem M. Dissolved Organic Matter-Capped Silver Nanoparticles for Electrochemical Aggregation Sensing of Atrazine in Aqueous Systems. *ACS Appl. Nano Mater.* 2020;3:3868–75. doi:10.1021/acsanm.0c00597.
15. Ma W, Ma H, Yang Z-Y, Long Y-T. Single Ag Nanoparticle Electro-oxidation: Potential-Dependent Current Traces and Potential-Independent Electron Transfer Kinetic. *J Phys Chem Lett.* 2018;9:1429–33. doi:10.1021/acs.jpcclett.8b00386.
16. Beck F, Horn C, Baeumner AJ. Dry-reagent microfluidic biosensor for simple detection of NT-proBNP via Ag nanoparticles. *Anal Chim Acta.* 2022;1191:339375. doi:10.1016/j.aca.2021.339375.
17. Ronco C, Kellum JA, Bellomo R, Ricci Z, editors. *Critical care nephrology.* Philadelphia, PA: Elsevier Inc; 2018.

5.6 Supporting Information

Optimization of the Measurement Procedure with HCy

The differently concentrated homocysteine solutions (0, 10, 100 μM in ddH₂O) were incubated in a 1:10 ratio with AgNPs ($d=30$ nm) for 30 min at rt. For the different procedures (Figure S5.1 b), 30 μL of this mixture were either dried on the SPCE and 0.01 or 0.1 M KCl added before the measurement (dried, orange) or dropped onto a KCl electrode (fluid, blue). Then, DPV was performed from -0.2 V to 0.2 V with $t_{\text{puls}}=50$ ms, $E_{\text{step}}=10$ mV, $E_{\text{amplitude}}=80$ mV and scan rate= 20 $\text{mV}\cdot\text{s}^{-1}$. To investigate different settings (Figure S5.1 a), 30 μL of the mixture were pipetted on top of a KCl electrode and the electrochemical measurement was performed with (light blue) and without (dark blue) pretreating the electrodes at 1.25 V for 60 s and -0.8 V for 30 s.

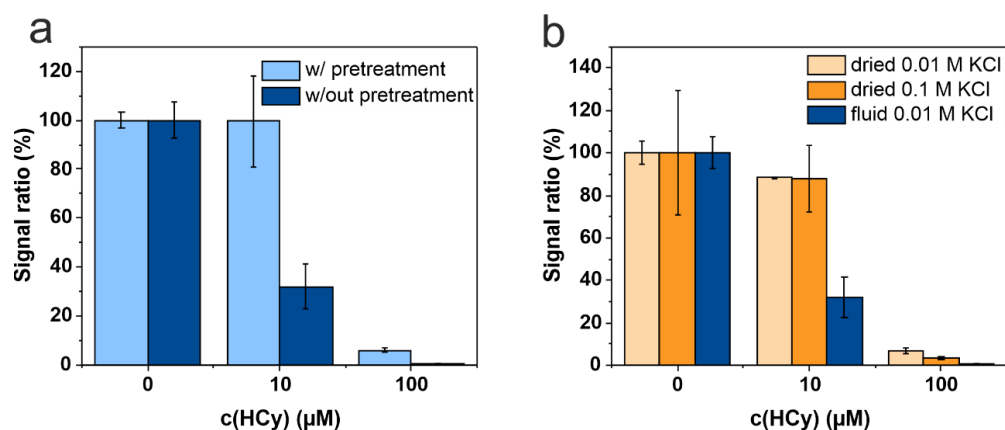


Figure S5.1. DPV peak area normalized to peak area of the blind (0 μM HCy), denoted as signal ratio, against concentration of HCy for (a) different measurement settings and (b) different procedures. Settings: with (light blue) and without (dark blue) oxidation, reduction pretreatment, measured with fluid procedure. Procedures: dried AgNPs (orange), redispersed with KCl (0.01 M KCl, light orange; 0.1 M KCl, dark orange) or dried 0.01 M KCl, redispersed with liquid AgNPs (dark blue), measured without pretreatment. Standard deviations were calculated based on three parallel measurements on three separate SPCEs. Error bars represent mean values $\pm 1\sigma$ ($n=3$).

Size Dependence of the Electrochemical Signal with HCy

The differently concentrated HCy solutions (0, 10, 100 μM in ddH₂O) were incubated in a 1:10 ratio with AgNPs (d=10, 30, 50, 80, 100 nm) at rt overnight to ensure complete aggregation. Afterwards, 30 μL were measured on a KCl electrode electrochemically without pretreatment (Figure S5.2). The graphs a and b show differential pulse voltammograms of AgNPs with diameters of (a) 10 nm and (b) 80 nm after incubation with differently concentrated HCy solutions. The plots c and d are different presentations of the same data, showing (c) the mean peak area for each tested diameter or (d) the peak area normalized to the respective blind signal, denoted as signal ratio.

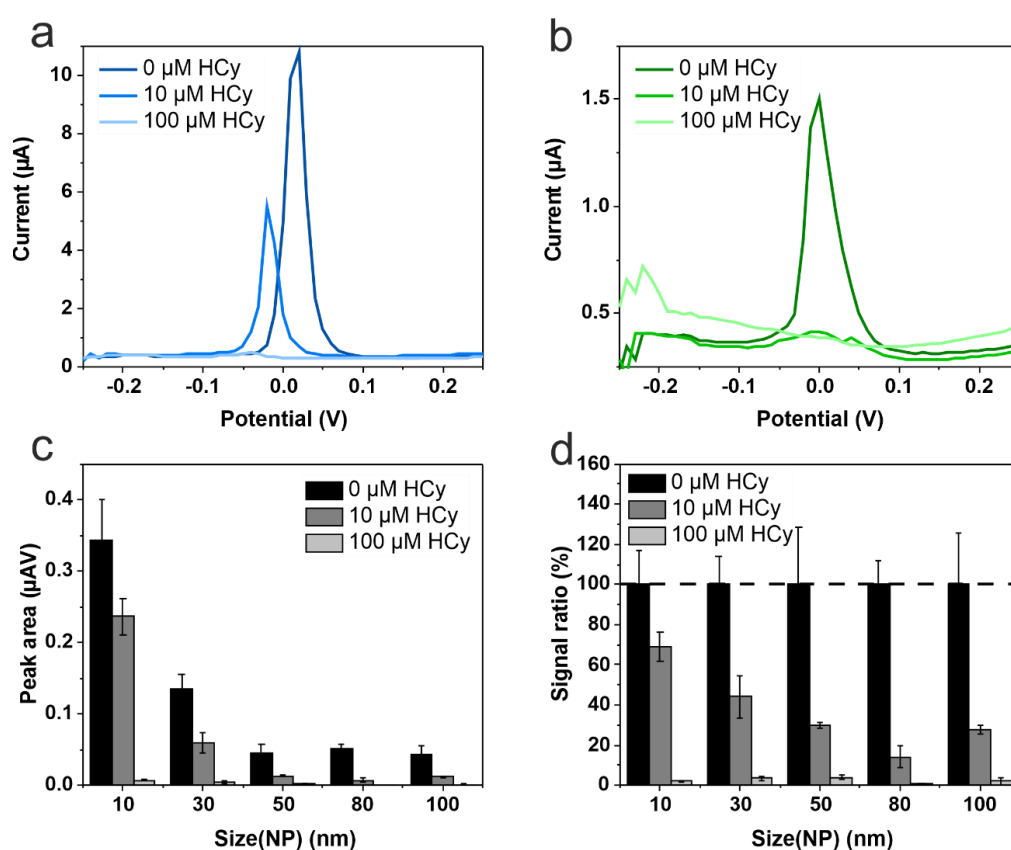


Figure S5.2. Exemplary differential pulse voltammograms of (a) 10 nm and (b) 80 nm diameter AgNPs after incubation with increasing HCy concentration (from dark to light colored). (c) Peak area for the tested AgNP diameters (in nm) after incubation with increasing HCy concentration (from dark to light colored). (d) DPV peak area after incubation with increasing HCy concentration (from dark to light colored) normalized to peak area of the blind (0 μM HCy) of the respective size, denoted as signal ratio, against diameter of AgNPs. Standard deviations were calculated based on three parallel measurements on three separate SPCEs. Error bars represent mean values $\pm 1\sigma$ ($n=3$).

Optimizations of Dry Procedure with HCy

In the course of the optimizations of the dried procedure, different trehalose contents were tested. For this, a 1, 5, 10% (w/v) trehalose in AgNPs (d=30 nm) stock solution with 0.01 M KCl was prepared. Then, 100 μL of this solution was dried on the SPCE overnight at 50 $^{\circ}\text{C}$. For the measurement, 20 μL HCy (0, 10, 100 μM in ddH₂O) and 10 μL ddH₂O were added and incubated for 1 h at rt. Afterwards, the electrochemical measurement without pretreatment was performed (Figure S5.3).

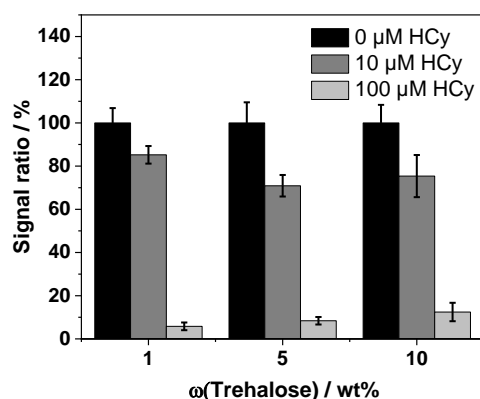


Figure S5.3. DPV peak area normalized to the respective blind signal measured in electrodes with 100 μL of AgNP mix with different trehalose content $\omega(\text{Trehalose})$ (0.01 M KCl in AgNP (d=30 nm)) dried at 50 $^{\circ}\text{C}$ overnight incubated with 20 μL of differently concentrated HCy solutions (lighter color indicates higher concentration). Standard deviations were calculated based on three parallel measurements on three separate SPCEs. Error bars represent mean values $\pm 1\sigma$ (n=3).

Next, different volumes (30, 50, 100 μL) of the 10% (w/v) trehalose in AgNP (d=30 nm) stock solution with 0.01 M KCl were dried on the SPCE at 50 $^{\circ}\text{C}$ overnight. The measurement was performed as just described (Figure S5.4).

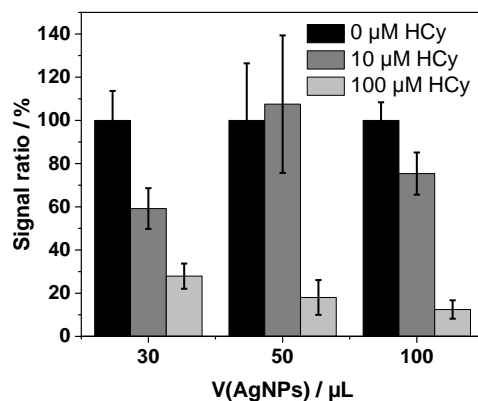


Figure S5.4. DPV peak area normalized to the respective blind signal measured in differently produced chips with different volumes of AgNP mix V(AgNPs) (10% (w/w) trehalose, 0.01 M KCl in AgNP (d=30 nm)) dried at 50 $^{\circ}\text{C}$ overnight incubated with 20 μL of differently concentrated HCy solutions (lighter color indicates higher concentration). Standard deviations were calculated based on three parallel measurements on three separate SPCEs. Error bars represent mean values $\pm 1\sigma$ (n=3).

Kinetic Colorimetric Creatinine Quantification via modified Jaffe's Reaction (Cromatest by Linear Chemicals)

To form the working reagent, picric acid (25 mM in ddH₂O) was mixed in a 1:1 ratio with alkaline buffer (300 mM phosphate buffer, pH 12.7+2 g·L⁻¹ SDS). A creatinine solution (177 μM in 10 mM phosphate buffer, pH 7) was used as standard and a 1:50 diluted synthetic urine in ddH₂O as sample. All three solutions were preincubated at 37 °C. Then, 1.0 mL of working reagent was mixed with 100 μL sample or standard in a 10 mm PMMA cuvette and the absorbance was measured against ddH₂O after 30 s (A₁) and after 90 s (A₂) at 510 nm using a Cary50 Bio UV Visible spectrophotometer from Varian. The absorbance values can be found in Table S5.1.

Table S5.1. Absorbance values measured after 30 s (A₁) and 90 s (A₂) for the standard (177 μM creatinine in 10 mM phosphate buffer, pH 7) and sample (1:50 diluted surin in ddH₂O), threefold determination each.

	A ₁ (a.u.)	A ₂ (a.u.)
standard	0.0623	0.0766
	0.0594	0.0725
	0.0594	0.0709
sample	0.0684	0.0727
	0.0673	0.0737
	0.0580	0.0635

Additional Creatinine Measurement in Undiluted Surin

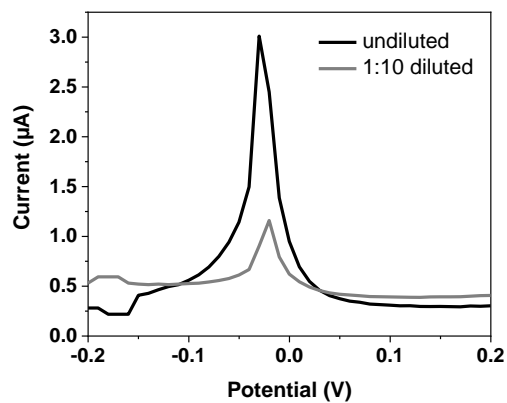


Figure S5.5. Exemplary differential pulse voltammograms of PA-AgNPs after incubation with 4 mM creatinine in undiluted surin (black) and 1:10 diluted surin (grey) for 10 min.

6 Conclusions and Future Perspectives

This thesis discusses the development of electrochemical biosensors for clinical analysis employing silver nanoparticles as signal amplification tags. It was shown that AgNPs are highly versatile and can be used in optical, as well as electrochemical sensing, as marker or surface modifier. However, up to date these techniques are rarely applied for clinical analytes at the point-of-care due to toxicity and stability concerns. To show their real benefit as signal amplification tags in electrochemical applications, AgNPs were compared to the more commonly used gold nanoparticles in a simple model immunoassay. Silver is less noble than gold and therefore possesses higher instability. This leads to (i) a higher electrochemical activity and with that better signal amplification ability. Thus, the LOD of the model bioassay is improved by a factor of 6.5 by switching from gold to silver. Moreover, (ii) redox reactions take place at lower potentials (25 vs. 250 mV), which renders the detection less sensitive to interferences, especially in biological matrices, and expand the range of possible electrode materials. AgNPs are already the most abundant commercialized nanocompound [1] due to their various applications based on their biocidal properties. This makes them easily obtainable and relatively low-cost, which are ideal conditions for their extended use in biosensors. Current advances in research with respect to surface modifications or different stabilizing matrices, as done in this thesis, enable long-term stability of the AgNPs. With this, they can lead the future development of electrochemical biosensors.

The most common POC self-testing format is the lateral flow assay. LFAs enable simple one-step assays and usually, include optical detection. Lately, also electrochemical LFAs were developed [2], which combine the ease of handling with high miniaturization potential and low-cost hardware. However, membrane-based systems suffer from the unavoidable variability of membrane and fleece fabrication. Furthermore, each LFA concept must use enough volume to saturate the membrane material, which either requires two-step procedures or large sample volumes, which excludes finger prick samples. Therefore, other test formats are employed by now, as the here presented microfluidic approach. Especially for self-testing, simple execution of the testing procedure is key. The development of miniaturized microfluidic pumps and further equipment enables the use at the POC. Generally, microfluidic systems are utilized frequently in clinical analysis with high sensitivity and reproducibility and they have been thoroughly investigated. After further miniaturization, the here developed microfluidic

approach with its simple production, procedure and high stability of all-dried reagents is strongly suited for self-testing.

However, the additional equipment renders the self-testing device more expensive and washing on the chip is difficult to perform in this setting. Therefore, an aggregation assay was employed as a different membrane-free format. A suitable surface modification-analyte combination is essential for the selectivity of this technique due to the colloidal instability of AgNPs. The electrochemical detection is simple and fast with only minimal hardware requirements. Moreover, the principle can be used flexibly for different analytes, as long as they are able to induce selective nanoparticle aggregation. Via changing of the sample to AgNP ratio, the assay can be adjusted to various concentration ranges depending on the chosen analyte. The stability of the reagents in dry form enables long-time storage of the self-testing device and easy performance by the user. After simple addition of the sample and incubation, no washing is needed, and the electrochemical measurement can be performed directly. The scope of this aggregation assay can be easily extended further to different analytes and matrices.

For both, the immunoassay and the aggregation assay, the standard deviations are not yet in the acceptable range for clinical sensing. Therefore, next steps should include further miniaturization and prototyping in order to improve the reproducibility by automated production. Moreover, the screen-printed carbon electrodes should be replaced by roll-to-roll fabricated carbon electrodes, produced in-house at Roche. This would cancel out the variability of the externally purchased screen-printed carbon electrodes, reduce the cost of the final clinical self-testing devices and ease the production of microfluidic chips due to its flexible substrate. The principal of electrochemical sensing developed in this thesis using AgNPs as label is highly promising for future POC applications and can potentially replace the nowadays commonly used AuNPs due to their versatile and highly sensitive use in clinical sensing. There is still development necessary and important in the AgNP as well as in the POC field. Understanding the toxicity and processes connected to AgNPs is still pending. Moreover, most research focuses mainly on lowering of the limit of detection or developing and employing new materials or detection techniques, while the research in the POC field stagnated in the last years. However, decreasing the sample volume, cost and time demand as well as increasing the ease of handling and selectivity should be just as important in further investigations to

make the newest research successes also accessible to the POC field. The COVID-19 pandemic taught us, that versatile, reliable, and sensitive POC testing is and will be crucial looking into the future. Therefore, it is inevitable that the advances in research, for example the increased stability of AgNPs, are used to design and develop new, superior POC strategies.

References

1. Flores-López LZ, Espinoza-Gómez H, Somanathan R. Silver nanoparticles: Electron transfer, reactive oxygen species, oxidative stress, beneficial and toxicological effects. Mini review. *J Appl Toxicol*. 2019;39:16–26. doi:10.1002/jat.3654.
2. Perju A, Wongkaew N. Integrating high-performing electrochemical transducers in lateral flow assay. *Anal Bioanal Chem*. 2021;413:5535–49. doi:10.1007/s00216-021-03301-y.

Curriculum Vitae

Persönliche Daten

Franziska Beck | Maria-Herbert-Straße 11 | 93051 Regensburg | franziska2.beck@ur.de

Geburtsdatum: 19.09.1995 | Geburtsort: Landshut | Staatsangehörigkeit: Deutsch

Ausbildung

- 11/2018 – 05/2022** **Promotionsstudium**, Chemie – Universität Regensburg
- Dissertation: „Development of electrochemical biosensors for clinical analysis“
- Institut für Analytische Chemie, Chemo- und Biosensorik
Roche Diagnostics, Mannheim
- (Prof. Dr. Antje J. Bäumner)
- 10/2016 – 09/2018** **Master of Science**, Chemie – Universität Regensburg
- Masterarbeit: „Development of a sensitive and selective electrochemical immunoassay with nanoparticle mediated signal amplification“
- Institut für Analytische Chemie, Chemo- und Biosensorik
- (Prof. Dr. Antje J. Bäumner)
- 10/2013 – 11/2016** **Bachelor of Science**, Chemie – Universität Regensburg
- Bachelorarbeit: „Investigation of the doping ratio of lanthanide ions in NaYF₄(Yb,Tm) nanoparticles on the upconversion luminescence“
- Institut für Analytische Chemie, Chemo- und Biosensorik
- (Dr. Thomas Hirsch, Prof. Dr. Antje J. Bäumner)
- 09/2005 – 06/2013** **Allgemeine Hochschulreife** – Hans-Carossa-Gymnasium Landshut

Auszeichnungen

- | | |
|---------|--|
| 03/2019 | Posterpreis

4. Münchner Point-of-care Testing Symposium, München, Deutschland |
| 06/2019 | Studienpreis Analytische Chemie

Fachgruppe Analytische Chemie in der Gesellschaft Deutscher Chemiker |
| 10/2020 | Posterpreis „Sensor 100 trophy“

Sensors in Medicine 2020, online |

Sonstige Qualifikationen und Fortbildungen

- 1. Sachkundenachweis**
nach §5 in Verbindung mit §2 der Chemikalien-Verbotsverordnung durch erfolgreiche Teilnahme an der Lehrveranstaltung „Rechtskunde und Toxikologie“, Regensburg
SoSe 2016
- 2. Mentoren-Schulung**
hochschuldidaktische Schulung zu verschiedenen Themenbereichen wie Motivation und Kommunikation, Regensburg
WiSe 2016/2017
- 3. 8. „Frühjahrsschule Industrielle Analytische Chemie“**
Fachgruppe Analytische Chemie in der Gesellschaft Deutscher Chemiker, Leipzig,
03/2018
- 4. „Summer School: Commercializing Biosensors“**
In Zusammenhang mit dem „31st Anniversary World Congress on Biosensors“, online,
07/2021
- 5. „Qualitätsmanagement in der Analytischen Chemie“ – Kurs**

Dr. Robert Schupfner, Universität Regensburg, SoSe 2022
- 6. Mitglied der Graduiertenschule ChemPharm**

List of Publications

Journal Publications

1. Cornelia A. Hermann, Michael Mayer, Christian Griesche, **Franziska Beck**, and Antje J. Baeumner, *Analyst* **2021**, 146, 997 – 1003. DOI: <https://doi.org/10.1039/D0AN02027C>
2. **Franziska Beck**, Carina Horn, and Antje J. Baeumner, *Anal. Bioanal. Chem.* **2022**, 414, 475 - 483. DOI: <https://doi.org/10.1007/s00216-021-03288-6>.
3. **Franziska Beck**, Carina Horn, and Antje J. Baeumner, *Anal. Chim. Acta.* **2022**, 1191, 339375. DOI: <https://doi.org/10.1016/j.aca.2021.339375>.

Patent

Franziska Beck, and Antje J. Baeumner, Carina Horn, **2022**, WO2022063847A1, European Patent Office, <https://worldwide.espacenet.com/patent/search/family/072644018/publication/WO2022063847A1?q=pn%3DWO2022063847A1>

Presentations

Oral Presentations

03/2021 Virtual Pittcon 2021, Pittsburgh Conference & Exposition on Analytical Chemistry and Applied Spectroscopy, online

07/2021 31st Anniversary World Congress on Biosensors, online

Poster Presentations

03/2019 4. Münchner Point-of-care Testing Symposium, Munich, Germany

10/2020 Sensors in Medicine 2020, online

05/2022 Roche R&D Fair, online

Eidesstattliche Erklärung

Ich erkläre hiermit an Eides statt, dass ich die vorliegende Arbeit ohne unzulässige Hilfe Dritter und ohne Benutzung anderer als der angegebenen Hilfsmittel angefertigt habe; die aus anderen Quellen direkt oder indirekt übernommenen Daten und Konzepte sind unter Angabe des Literaturzitats gekennzeichnet.

Weitere Personen waren an der inhaltlich-materiellen Herstellung der vorliegenden Arbeit nicht beteiligt. Insbesondere habe ich hierfür nicht die entgeltliche Hilfe eines Promotionsberaters oder anderer Personen in Anspruch genommen. Niemand hat von mir weder unmittelbar noch mittelbar geldwerte Leistungen für Arbeiten erhalten, die im Zusammenhang mit dem Inhalt der vorgelegten Dissertation stehen.

Die Arbeit wurde bisher weder im In- noch im Ausland in gleicher oder ähnlicher Form einer anderen Prüfungsbehörde vorgelegt.

Regensburg, den 31.05.2022

Ort, Datum

Unterschrift